

# Thiophene-*S,S*-dioxidized Indophenine for Use in Organic Field-effect Transistors

by

Jackson Ellard

A thesis  
presented to the University of Waterloo  
in fulfillment of the  
thesis requirement for the degree of  
Master of Applied Sciences  
in  
Chemical Engineering (Nanotechnology)

Waterloo, Ontario, Canada, 2016

©Jackson Ellard 2016

## **AUTHOR'S DECLARATION**

I hereby declare that I am the sole author of this thesis. This is a true copy of the thesis, including any required final revisions, as accepted by my examiners.

I understand that my thesis may be made electronically available to the public.

## Abstract

To address the need for better n-type organic semiconductors, thiophene-*S,S*-dioxidized indophenine (IDTO) was developed. IDTO is a planar quinoidal molecule with deep energy levels which facilitate stable and efficient electron transport. IDTO is a promising material in the design and fabrication of high performance n-type organic field-effect transistors because it offers simple synthesis, as well as excellent processability and good performance. The work presented in this thesis follows the development of IDTO and its various uses in organic field-effect transistors. Firstly, the synthetic method for IDTO was systematically improved. Two important factors were improved, safety was improved by replacing the solvent, benzene, with the much less hazardous toluene and the yield of the synthesis was increased from less than 10% to ~40%. Next, IDTO and two derivatives (5-bromo-IDTO and 6-bromo-IDTO) were synthesized and evaluated as new n-type small molecule organic semiconductors. The three compounds all exhibited unipolar n-type characteristics in the range of  $10^{-2}$  to  $10^{-1}$   $\text{cm}^2\text{V}^{-1}\text{s}^{-1}$ . The highest electron mobility of  $0.11 \text{ cm}^2\text{V}^{-1}\text{s}^{-1}$  was measured for 6-bromo-IDTO. IDTO was then utilized as an electron accepting building block for the synthesis of two donor-acceptor polymers: PIDTOBT and PIDTOBTz. Both polymers showed unipolar n-type performance with electron mobilities on the order of  $10^{-2}$  to  $10^{-1}$   $\text{cm}^2\text{V}^{-1}\text{s}^{-1}$ . PIDTOBT had the highest electron mobility of  $0.18 \text{ cm}^2\text{V}^{-1}\text{s}^{-1}$  after annealing at  $200 \text{ }^\circ\text{C}$ . From the small molecule and polymer results, it is clear that IDTO is a promising material for unipolar n-type organic semiconductors. Since IDTO has a strong electron accepting feature, it was thought that IDTO would have another use as an electron trap. By blending IDTO with an ambipolar polymer that has a LUMO energy level above that of IDTO; electron transport could be suppressed under the correct conditions. The three small molecule IDTO compounds were blended with PINDFBT (TT) and PINDFBT (HH) to investigate the electron trapping ability of IDTO. Complete suppression of electron transport was not observed but the overall trend agreed with the theory. 6-bromo-IDTO having the lowest LUMO energy level showed the strongest electron trapping effect while IDTO had the weakest effect due to its higher LUMO energy level. This thesis provides a comprehensive study of the development and application of the novel material, IDTO.

## **Acknowledgements**

I would like to thank my supervisor, Dr. Yuning Li, for all of the guidance he has provided me. I have learned so much and gained invaluable skills under Dr. Li's supervision.

Thank you to all of the members of Dr. Li's group who have assisted me in my work and studies: Dr. Chang Guo, Dr. Yunfeng Deng, Dr. Bin Sun, Yinghui He and Jesse Quinn. Their training and advice were very helpful in my development. Special thanks to Jesse Quinn for performing some of the characterization measurements for me such as TGA, DSC, MS, GPC, XRD, AFM and DFT.

I express special appreciation to my amazing family and friends for their continuous support.

## Table of Contents

AUTHOR'S DECLARATION .....	ii
Abstract .....	iii
Acknowledgements .....	iv
Table of Contents .....	v
List of Figures .....	viii
List of Tables.....	x
List of Abbreviations.....	xi
List of Symbols .....	xiii
Chapter 1 Introduction and Background .....	1
1.1 Historic Background.....	1
1.2 Principles of Organic Field-Effect Transistors .....	2
1.3 Organic Semiconductors .....	4
1.3.1 Theoretical Background .....	4
1.3.2 Chemical Structure .....	8
1.4 Characterization.....	10
1.4.1 Chemical Composition .....	10
1.4.2 Material Properties .....	12
1.4.3 Solid State Properties .....	15
1.5 Fabrication and Evaluation.....	17
1.5.1 Fabrication.....	17
1.5.2 Evaluation.....	18
1.6 Objective and Scope of Work.....	21
1.6.1 Research Problem.....	21
1.6.2 Scope of Work.....	22
Chapter 2 Thiophene-S,S-dioxidized Indophenine.....	23
2.1 Introduction .....	23
2.2 IDTO Synthesis Improvement.....	24
2.2.1 Experimental Details .....	24
2.2.2 Results and Discussion.....	28
2.2.3 Conclusions .....	30
Chapter 3 IDTO as a Small Molecule N-type Organic Semiconductor .....	31

3.1 Experimental Details.....	31
3.1.1 Synthesis of IDTO .....	31
3.1.2 Characterization .....	32
3.2 Results and Discussion .....	33
3.2.1 DFT: Theoretical Calculations.....	33
3.2.2 TGA and DSC: Thermal Properties.....	34
3.2.3 UV-Vis and CV: Optical and Electrochemical Properties .....	35
3.2.4 XRD and AFM: Solid State Properties .....	37
3.2.5 OFET Evaluation .....	38
3.3 Conclusions.....	41
Chapter 4 IDTO as a Polymeric N-type Organic Semiconductor.....	43
4.1 Experimental Details.....	43
4.1.1 Synthesis .....	43
4.1.2 Characterization .....	44
4.2 Results and Discussion .....	45
4.2.1 DFT: Theoretical Calculation .....	45
4.2.2 TGA and DSC: Thermal Properties .....	46
4.2.3 UV-Vis and CV: Optical and Electrochemical Properties .....	46
4.2.4 XRD and AFM: Solid State Properties .....	48
4.2.5 OFET Evaluation .....	49
4.3 Conclusions.....	51
Chapter 5 IDTO Additive Blended with Ambipolar Polymer .....	52
5.1 Introduction.....	52
5.2 Experimental Details.....	56
5.3 Results and Discussion .....	56
5.4 Conclusions.....	62
Chapter 6 Summary and Future Directions.....	64
6.1 Summary .....	64
6.2 Future Directions .....	65
Bibliography .....	67
Appendix A List of Chemicals .....	75
Appendix B NMR and MS Data for Small Molecule IDTO Compounds .....	76

Appendix C NMR Data for IDTO Polymers .....	79
Appendix D PINDFBT (HH) Blend Comparison Graphs .....	81

## List of Figures

Figure 1.1: OFET Configurations: a) bottom gate bottom contact, b) bottom contact top gate, c) top contact bottom gate and d) top contact top gate.....	3
Figure 1.2: Operation modes: a) linear mode, b) pinch off and c) saturation mode. ....	4
Figure 1.3: Orbitals and bonding. ....	5
Figure 1.4: Molecular orbital energy level splitting.....	6
Figure 1.5: Examples of donating and accepting moieties. ....	9
Figure 1.6: X-ray diffraction diagram.....	16
Figure 1.7: Output graphs of a) hole and b) electron as well as transfer graphs for c) hole and d) electron.....	19
Figure 1.8: Obtaining mobility and $V_T$ from the graph.....	20
Figure 2.1: Chemical structures for the six isomers of indophenine.....	24
Figure 2.2: Original reaction scheme for IDTO.....	25
Figure 3.1: General reaction scheme for IDTO compounds. ....	32
Figure 3.2: A) Chemical structures, B) optimized geometries and C) electron density distributions obtained from DFT calculations for the IDTO compounds. ....	34
Figure 3.3: TGA (top) and DSC (bottom) for the IDTO compounds. ....	35
Figure 3.4: UV-Vis spectra for the IDTO compounds in solution (left) and thin film (right). ....	36
Figure 3.5: CV measurements and energy level diagrams for the IDTO compounds. ....	37
Figure 3.6: XRD (right) and AFM (left) results for the IDTO compounds. Inset of 6-bromo-IDTO XRD is an enlarged view of non-annealed. ....	38
Figure 3.7: Output (A, C and E) and transfer (B, D and F) graphs of IDTO (A and B), 5-bromo-IDTO (C and D) and 5-bromo-IDTO (E and F). ....	40
Figure 4.1: General reaction scheme for IDTO polymers <i>via</i> Stille-coupling polymerization.....	44
Figure 4.2: A) Chemical structures, B) optimized geometries and C) electron density distributions obtained from DFT calculations for the IDTO polymers.....	45
Figure 4.3: TGA (top) and DSC (bottom) for the IDTO polymers.....	46
Figure 4.4: UV-Vis spectra for the IDTO polymers in solution (left) and thin film (right). ....	47
Figure 4.5: CV measurements and energy level diagrams for the IDTO polymers.....	48
Figure 4.6: XRD (right) and AFM (left) results for the IDTO polymers.....	49
Figure 4.7: Output (A and C) and transfer (B and D) graphs of PIDTOBT (A and B) and PIDTOBTz (C and D). ....	50

Figure 5.1: LUMO energy level diagram for the selection of suitable polymers.....	54
Figure 5.2: Reaction scheme for PINDFBT (TT) and PINDFBT (HH).....	55
Figure 5.3: Comparison of 2% blends with PINDFBT (TT).....	58
Figure 5.4: Comparison of 5% blends with PINDFBT (TT).....	59
Figure 5.5: Comparison of 10% blends with PINDFBT (TT).....	59
Figure 5.6: Comparison of IDTO blends with PINDFBT (TT). ....	60
Figure 5.7: Comparison of 5-Br-IDTO blends with PINDFBT (TT).....	60
Figure 5.8: Comparison of 6-Br-IDTO blends with PINDFBT (TT).....	61

## List of Tables

Table 2.1: IDTO Synthesis Improvement Results .....	27
Table 3.1: UV-Vis absorption properties of IDTO compounds.....	36
Table 3.2: OFET performance parameters for IDTO compounds. ....	41
Table 4.1: UV-Vis absorption properties of IDTO polymers. ....	47
Table 4.2: OFET performance parameters for IDTO polymers.....	51
Table 5.1: OFET performance parameters for PINDFBT (TT) / IDTO compound blends. ....	56
Table 5.2: OFET performance parameters for PINDFBT (HH) / IDTO compound blends. ....	62

## List of Abbreviations

AFM	Atomic force microscopy
AgCl	Silver chloride
BT	Bithiophene
BTz	Bithiazole
CMOS	Complementary metal-oxide-semiconductor
CV	Cyclic voltammetry
D-A	Donor-acceptor
DCM	Dichloromethane
DDTS	Dodecyltrichlorosilane
DFT	Density functional theory
DI	Deionized
DMF	N,N'-dimethylformamide
DSC	Differential scanning calorimetry
GPC	Gel permeation chromatography
HMDS	Hexamethyldisilazane
HOMO	Highest occupied molecular orbital
IDTO	Thiophene-S,S-dioxidized indophenine
IPA	Isopropyl alcohol
K <sub>2</sub> CO <sub>3</sub>	Potassium carbonate
LUMO	Lowest unoccupied molecular orbital
m-CPBA	3-chloroperoxybenzoic acid
MgSO <sub>4</sub>	Magnesium sulfate
MS	Mass spectroscopy
n-Bu <sub>4</sub> NPF <sub>6</sub>	Tetrabutylammonium hexafluorophosphate
Na <sub>2</sub> CO <sub>3</sub>	Sodium carbonate
NMR	Nuclear magnetic resonance
OFET	Organic field-effect transistor
OLED	Organic light-emitting diode
OPV	Organic photovoltaic
p-TsOH	p-toluenesulfonic acid

PDI	Poly dispersity index
PMMA	Poly(methyl methacrylate)
TCE	Tetrachloroethane
TFA	Trifluoroacetic acid
TGA	Thermogravimetric analysis
UV-Vis	Ultraviolet-Visible spectroscopy
XRD	X-ray diffraction

## List of Symbols

A	Absorbance
$C_i$	Capacitance of insulator
c	Concentration
c	Speed of light
$E_g^{\text{opt}}$	Optical band gap
e	Energy of electron
h	Plank's constant
I	Current
$I_D$	Drain current
L	Length of channel
l	Path length
$M_n$	Number average molecular weight
$M_m$	Weight average molecular weight
$M_z$	Size average molecular weight
$M_v$	Viscosity average molecular weight
$V_g$	Gate voltage
$V_d$	Drain voltage
$V_t$	Threshold voltage
$V_{\text{red}}$	Reduction potential onset
$V_{\text{ox}}$	Oxidation potential onset
v/v	Volume to volume
W	Width of channel
$\lambda$	Wavelength
$\theta$	Angle
$\mu$	Mobility



# Chapter 1

## Introduction and Background

### 1.1 Historic Background

Organic electronics is a multidisciplinary field of study under the categories of material science and electrical engineering. The field of organic electronics did not have much meaning until the successful synthesis of the conductive polymer polyacetylene through halogen doping by MacDiarmid, Heeger and Shirakawa<sup>1</sup>. Since that discovery, the research and interest in organic electronics has increased significantly to the point where commercial products are beginning to come out on the market that incorporates some organic electronics such as curved/flexible displays.

Organic electronics requires both knowledge from organic chemistry and solid-state physics to design, synthesize, and apply electrically conductive organic compounds known as organic semiconductors. There are three electrical components that constitute the major of the organic electronic field: organic photovoltaics (OPVs), organic light-emitting diodes (OLEDs) and organic field-effect transistors (OFETs). OPVs are the organic equivalent of silicon solar cells in which electromagnetic radiation is absorbed by the active layers and converted to usable electricity. OLEDs produce light of various colors when an electric current is passed through. OFETs are devices that leverage an electric field to control the current through the device. OFETs can be used as electrical signal amplifiers or on/off switches in electronic devices. The work presented in this document focuses on OFETs and thus, only OFETs will be discussed in further detail.

The first example of an organic field-effect transistor was presented in 1983 by Ebisawa et al. when they fabricated an OFET using polyacetylene as the semiconductor<sup>2</sup>. Several years after, more successful OFETs were reported using polythiophene<sup>3</sup> and lutetium bisphthalocyanine<sup>4</sup>. These very early OFETs had very low charge carrier mobilities on the order of  $10^{-5}$  to  $10^{-4}$   $\text{cm}^2\text{V}^{-1}\text{s}^{-1}$ . Meaningful progress for OFETs was realized in 1990 when a flexible device with high mobility of  $0.43$   $\text{cm}^2\text{V}^{-1}\text{s}^{-1}$  was reported in a "soft" all organic field-effect transistor<sup>5</sup>. The device was fabricated on a polymer film made from poly(parabanic acid) resin, the dielectric was cyanoethylpullan and the active semiconducting layer was a film of  $\alpha$ -sexithiophene. The only non-organic component of the device was the contacts for which gold was used. This demonstrated the possibility that practical organic electronics could be realized with mobilities on par with amorphous silicon ( $0.1$  to  $1$   $\text{cm}^2\text{V}^{-1}\text{s}^{-1}$ ). Since then, research on OFETs has continued to grow and many improvements have been reported. To date,

hole mobilities as high as  $40 \text{ cm}^2\text{V}^{-1}\text{s}^{-1}$  have been reported using a rubrene-based OFET<sup>6</sup> and electron mobilities close to  $7 \text{ cm}^2\text{V}^{-1}\text{s}^{-1}$  have been reported for 6,13-Bis(triisopropylsilylethynyl)pentacene<sup>7</sup> and naphthalene diimides<sup>8</sup>. There is still so much more improvement that can be realized by continued research. Molecular design and device optimization are just a few strategies being investigated.

## 1.2 Principles of Organic Field-Effect Transistors

Organic field-effect transistors are made up of five components: source, drain, gate, dielectric and organic semiconductor. These five components can be arranged in four different configurations to form the transistor. The four configurations are: a) bottom gate-bottom contact, b) top gate-bottom contact, c) bottom gate-top contact and d) top gate-top contact<sup>9</sup>. Figure 1.1 details the arrangement of components in each of the four configurations. The source, drain and gate are the three contacts of the device. The source and drain are typically made of a conductive metal such as gold or aluminum, whereas the gate can be a conductive metal or part of a conductive substrate (in bottom gate configurations). The dielectric layer serves as an insulator to isolate the gate from the rest of the device. Dielectrics are usually a thermally grown silicon dioxide layer or an insulating polymer such as poly(methyl methacrylate) (PMMA). The organic semiconductor is the active layer of the device where a conductive channel is formed. The organic semiconductor is the objective of the majority of research and can consist of small molecules, polymers, metal organic complexes and even blends of two or more materials.

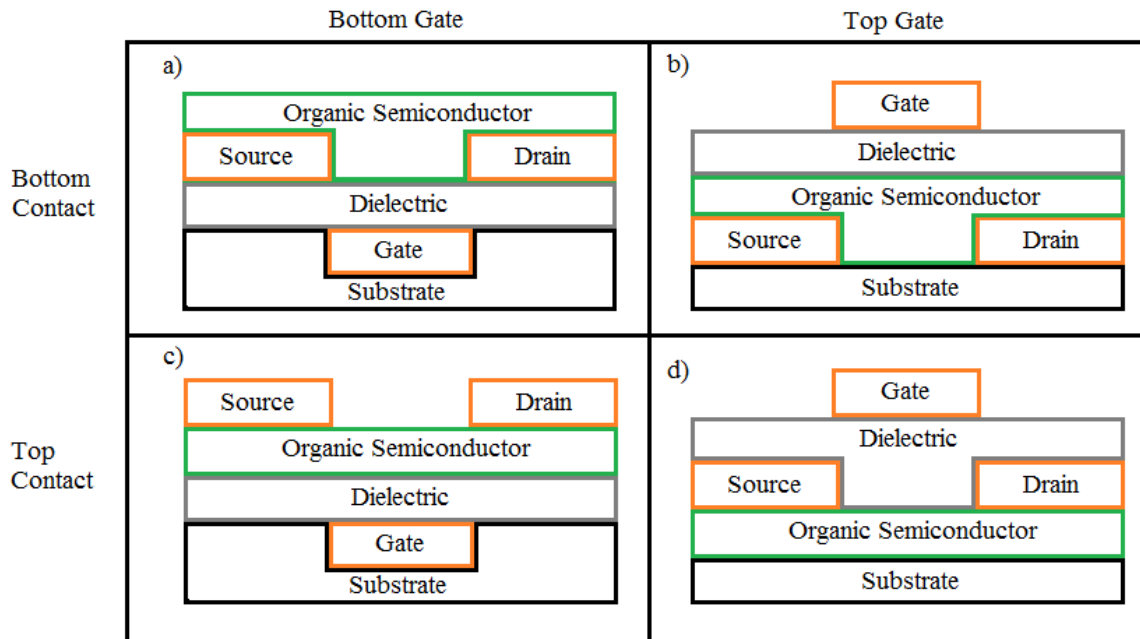


**Figure 1.1: OFET Configurations: a) bottom gate bottom contact, b) bottom contact top gate, c) top contact bottom gate and d) top contact top gate.**

The operation of an OFET can be analogous to that of a tap. In a tap, water flows from the inlet to the outlet and the amount of water that flows through is controlled by a valve. Similarly, current flows from the source to the drain of an OFET and the current is controlled by the gate. In actuality, a voltage applied to the gate electrode (referred to as gate voltage,  $V_g$ ) causes mobile charges in the semiconductor to redistribute such that a layer of charge forms at the semiconductor-dielectric interface. This creates the channel for which current can flow through the semiconductor when a voltage bias is applied between the source and drain (referred to as drain voltage,  $V_d$ ). The amount of current that can flow through the device is influenced by both the gate voltage and the drain voltage. Firstly, the gate voltage needs to be larger than a minimum voltage (referred to as the threshold voltage,  $V_t$ ) at which point the electric field is strong enough to move a sufficient amount of the mobile charges forming the channel. Increasing the gate voltage further, increases the size of the channel and hence the maximum amount of current that can flow through the channel. Increasing the gate voltage too high will result in the dielectric breaking down and current will flow to the gate. Secondly, drain voltage is the driving force for current to flow through the channel. When the drain voltage is much less than the gate voltage, the device is operating in a linear mode, i.e. the current is

proportional to the drain voltage. Increasing the drain voltage creates an asymmetrical change in the shape of the channel. The maximum current flow for a given gate voltage is reached when the channel is "pinched off" due to the large change in the channel shape. At this point, the device is in saturation mode. Further increase in drain voltage will not produce a significant change in the current<sup>10</sup>. Figure 1.2 shows the simplified representation of the channel at different operating modes for a bottom gate bottom contact device.

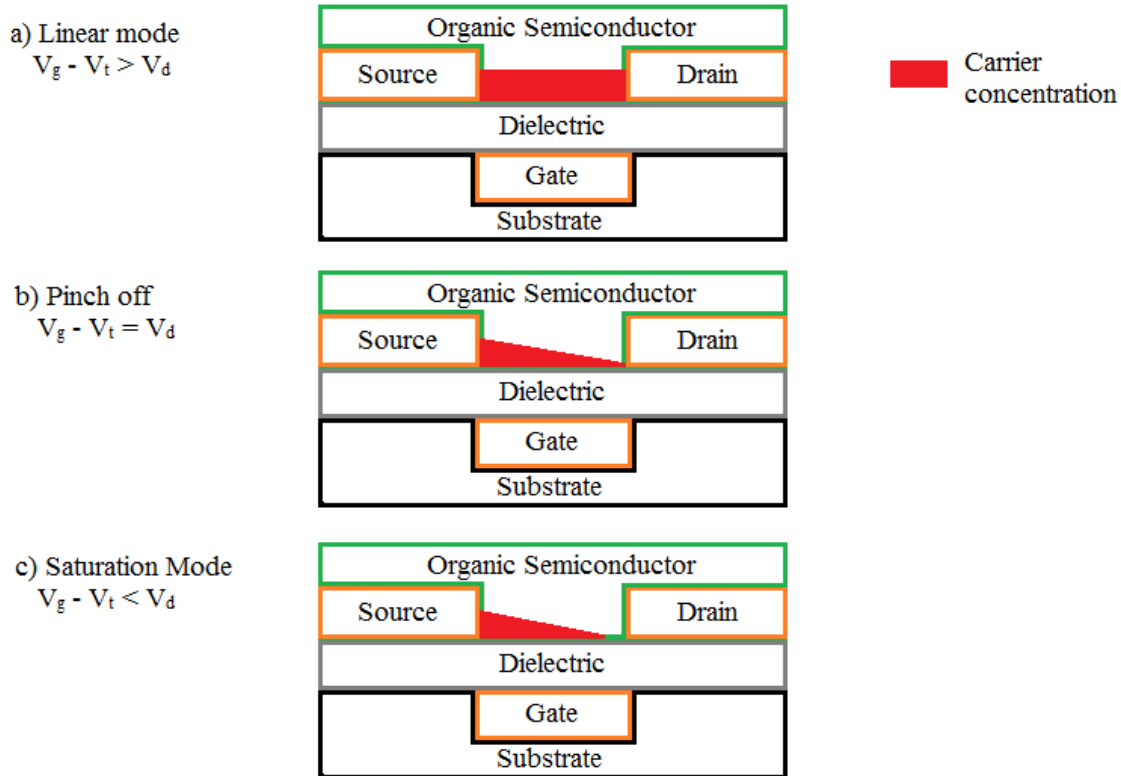


**Figure 1.2: Operation modes: a) linear mode, b) pinch off and c) saturation mode.**

## 1.3 Organic Semiconductors

### 1.3.1 Theoretical Background

Atoms are made up of protons, neutrons and electrons. The protons and neutrons make up the nucleus of the atoms. The electrons form orbitals around the nucleus of the atom. The orbitals are denoted in order as 1s, 2s, 2p<sub>x</sub>, 2p<sub>y</sub>, 2p<sub>z</sub>, 3s, 3p<sub>x</sub> and so on. Each orbital can hold two electrons and are filled from lowest number first (i.e. left to right)<sup>11</sup>. When atoms are covalently bonded together, the atoms share their outermost electrons by overlapping orbitals. The outermost electrons, called valence

electrons, form hybridized orbitals upon bonding<sup>12</sup>. Depending on the bonding arrangement, hybridization will differ. In the case of carbon atoms, there are six electrons and four of which are valence electrons. The four valence electrons can form a maximum of four bonds. When all four bonds are single bonds, the atomic orbitals undergo  $sp^3$  hybridization. In  $sp^3$  hybridization for carbon, the 2s and the three 2p orbitals interact forming four identical  $sp^3$  orbitals. Hybridized orbitals form  $\sigma$ -bonds which are in-plane overlapping of orbitals. When a double bond is present, carbon's atomic orbitals undergo  $sp^2$  hybridization.  $sp^2$  differs from  $sp^3$  in that only two 2p orbitals interact with the 2s orbital. This leaves one of the 2p orbitals to form a  $\pi$ -bond.  $\pi$ -bonds are out-of-plane overlapping of adjacent 2p orbitals. Lastly, in the case of a triple bond or two double bonds,  $sp$  hybridization occurs. This time only one 2p orbital interacts with the 2s orbital, leaving two 2p orbitals. Figure 1.3 gives a graphical representation of atomic orbitals and bonding.

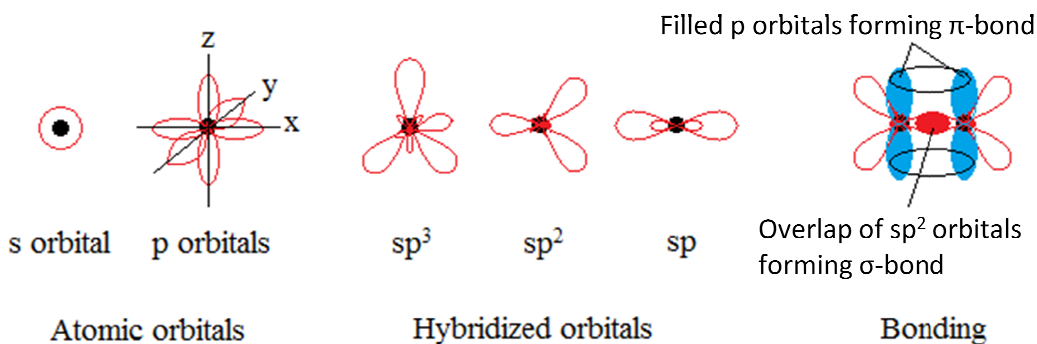


**Figure 1.3: Orbitals and bonding.**

In addition to atomic orbitals, there are molecular orbitals which are described as the combination of atomic orbitals across an entire molecule<sup>13</sup>. The molecular orbitals are split into bonding and anti-bonding orbitals, each with their own energy levels. The energy of the bonding orbitals are always lower than the energy of the individual atomic orbitals making up the molecular orbital. In contrast, the energy of the anti-bonding orbitals is always higher. The number of molecular orbitals in a molecule is equal to the number of atomic orbitals of the atoms that form the molecule. Electrons occupy the lowest energy levels first as they fill up the many orbitals<sup>14</sup>. Figure 1.4 demonstrates the orbital energy splitting using two carbon atoms as an example. The highest occupied molecular orbital (HOMO) energy level and the lowest unoccupied molecular orbital (LUMO) energy level are referred to as the frontier orbitals<sup>15</sup>. The frontier orbitals are important in predicting how the molecule will interact with its environment. The HOMO energy level is equal to the molecule's

ionization potential, i.e. how much energy is required to remove the most loosely bound electron in the ground state. The LUMO energy level is roughly the electron affinity of the molecule, i.e. how much energy is released when you add one electron to the ground state of the molecule. The difference in energy of the HOMO and LUMO energy levels is called the band gap. The band gap is the lowest amount of energy required to excite an electron from a bound state in the HOMO to a free state in the LUMO. The band gap is a crucial factor for the optical properties and electrical conductivity of a molecule. Optically, the band gap can be used to determine the longest wavelength of light that the molecule can absorb. Electrically, the size of the band gap influences whether the molecule is a conductor, semiconductor or insulator. When there is a very small band gap or no band gap at all electrons can easily enter free states and the molecule is conductive. On the other hand, a large band gap prevents electrons from becoming free and thus the molecule is insulating. In general, a molecule is considered a semiconductor if the band gap is less than 3 eV but not small enough to be conductive<sup>16</sup>. In an OFET, charge carriers are not produced within the organic semiconductor but rather injected from the source-drain electrodes. Electrons move through the LUMO orbitals and prefer lower energy levels. In contrast, holes travel through the HOMO orbitals and prefer higher energy levels. Therefore, it is more important, for conductivity, that the organic semiconductor be able to stabilize charge carriers and facilitate easy charge transport rather than having a smaller band gap.

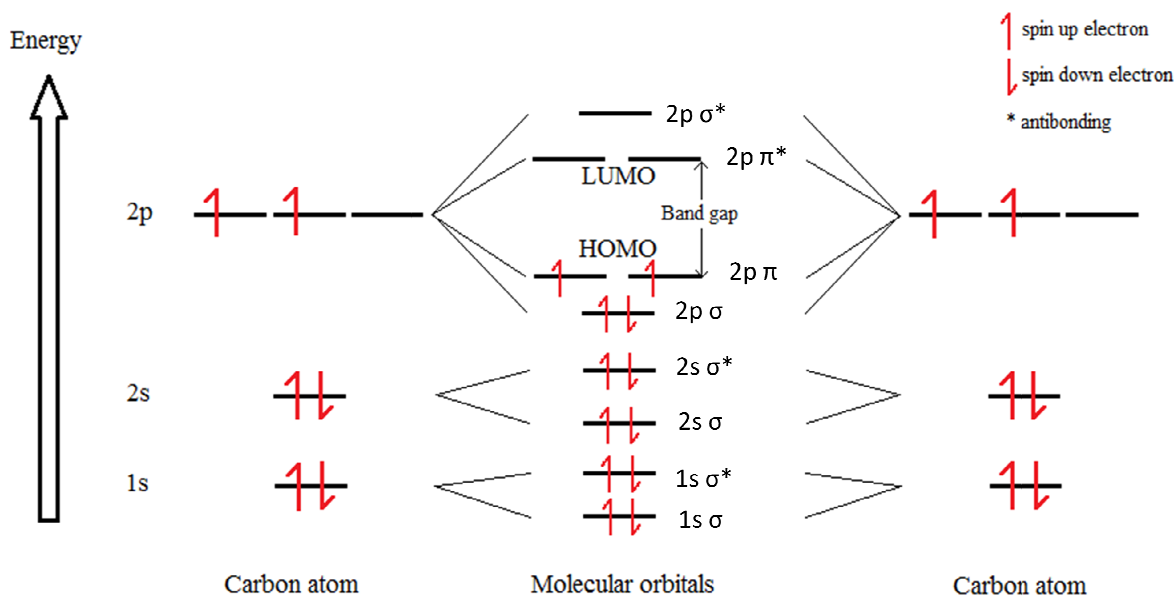


**Figure 1.4: Molecular orbital energy level splitting.**

Charge transport in organic semiconductors is much different than that of traditional inorganic semiconductors. Inorganic semiconductors typically use what is called band transport due to the well ordered structures that allow for large delocalized conduction bands. Instead, organic semiconductors tend to have charge carriers delocalized on much smaller entities such as single conjugated polymer molecules. For the charge carriers to be transported throughout the entire semiconductor film, charge hopping must occur from one molecule to the next<sup>17</sup>. Charge hopping is a process of thermally assisted tunneling as the charges move from one localized site to the next. The hopping process occurs when a charge is able to overcome an activation energy. This activation energy depends on the temperature, applied electric field and the hopping distance<sup>18</sup>. Increased temperature and electric fields would result in faster charge transport but in practice, these factors are restricted based on realistic application. Therefore, most research for increasing charge transport is focused on decreasing the hopping distance. The hopping distance in organic semiconductor films is equal to the intermolecular distance between two adjacent molecules. The intermolecular distance is decreased by increasing intermolecular forces and by creating efficient and well ordered packing of molecules. The chemical structure of the organic semiconductor has a large influence on the intermolecular distance. Chemical structure will be discussed in more detail in the next section. It should be noted that purity and uniformity of the film is also important since impurities, isomers and defects impede the packing and can introduce charge traps. Charge traps are deep energy wells where charge carriers can move to but they cannot move away from.

Organic semiconductors can be divided into three categories based on which charge carriers can be transported through the semiconductor. The first category is p-type semiconductors which facilitate only hole transport. The second category is n-type semiconductors which facilitate only electron transport. Lastly, the third category is ambipolar semiconductors which facilitate both hole and electron transport. The semiconductor type is influenced by 1) the ability to stabilize electrons and/or hole and 2) the ease of injection of charge carriers from the device electrodes. In both cases, the HOMO and LUMO energy levels of the semiconductor play a big role. A high HOMO energy level typically favors the transport of holes whereas a low LUMO energy level favors the transport of electrons. It is also important to look at the work function of the source and drain electrodes as well since charge carrier injection is energetically between the work function of the electrodes and the HOMO/LUMO energy levels of the semiconductor<sup>19,20</sup>. The difference in energy of the work function and HOMO/LUMO energy levels is defined as the injection barrier. As the injection barrier increases,

the injection of charge carriers becomes more and more difficult. The HOMO/LUMO energy levels can be tuned by chemical structure design which is discussed in the following section.

### 1.3.2 Chemical Structure

Organic molecules are a class of molecule that consists of mostly carbon and hydrogen. Within the class of organic molecules there is a subclass called organic semiconductors. Organic semiconductors have alternating single and double bonds throughout the molecule. These compounds are considered to have conjugated systems, meaning there are overlapping p-orbitals that allow delocalization of electrons across the entire system<sup>21</sup>. Electron lone pairs, radicals and carbenium ions may also partake in the conjugation as long as each atom in the system has an available p-orbital. It is important to note that alignment of the p-orbitals is crucial for overlap. Twisting of the molecule along the conjugated system can cause the p-orbitals to misalign and thus break the conjugation. Therefore, highly planar organic semiconductors are desirable. An additional benefit to highly planar molecules is more effective molecular stacking which decreases intermolecular distance and thus increases charge transport. Organic semiconductors can be separated into either small molecules or polymers as long as they maintain the basic criteria such as being fully conjugated and planar. Small molecules have the advantage of easier synthesis and little to no structural variation while polymers form more uniform films.

As mentioned before, HOMO/LUMO energy levels can be tuned by the inclusion of specific moieties into the chemical structure of the organic semiconductor. Electron deficient/electron accepting moieties decrease the energy levels of the semiconductor. In contrast, electron rich/electron donating moieties increase the energy levels<sup>22</sup>. A popular application of these moieties is the design and synthesis of donor-acceptor (D-A) polymers<sup>23</sup>. D-A polymers have backbones which are comprised of alternating electron donating and electron accepting moieties. D-A polymers have the advantage of shortening the intermolecular distance and therefore providing more efficient charge transport. The intermolecular distance is shortened by the attraction between donor and acceptor moieties of adjacent molecules. In general, electron donating moieties tend to contain thiophene groups and electron accepting moieties have nitrogen containing groups. Figure 1.5 gives the chemical structure of some of the electron donating and accepting moieties that have been used in the past<sup>24</sup>.

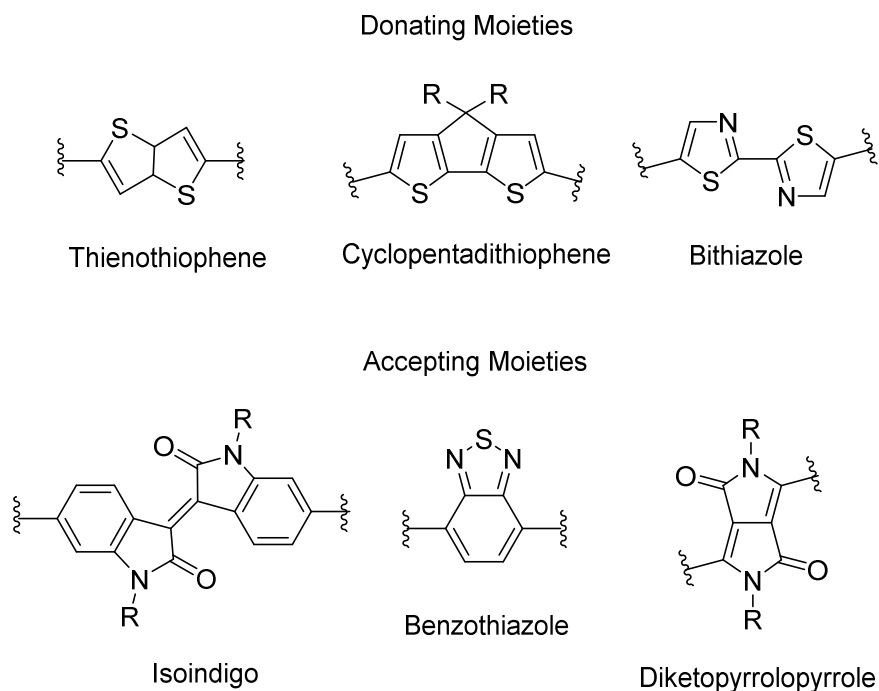


**Figure 1.5: Examples of donating and accepting moieties.**

An issue with the majority of organic semiconductors is their insolubility. Since the core structure of an organic semiconductor needs to be planar and there are strong intermolecular interactions, it is difficult for most solvents to interact with the semiconductor and thus the semiconductors are insoluble in most solvents. Solubility is important when considering that solution processability is one of the major selling points of organic electronics. Therefore, being able to dissolve the organic semiconductor is a very useful trait. To improve solubility, the interaction between solvent and solute must be increased<sup>25</sup>. This is done by increasing the temperature of the system, using a "stronger" solvent, modifying the chemical structure of the semiconductor or a combination of the three. The first method is simple but is not always effective and higher temperatures may not be practical for some applications. A stronger solvent refers to the polarity of the solvent. As the saying goes, like dissolves like, i.e. polar solvents dissolve polar compounds and non-polar solvents dissolve non-polar compounds. A stronger solvent is one that is closer in polarity to the solute. There is a limitation however; it is more practical to use "common" solvents as they make processing much simpler. Common solvents typically have low boiling points and relatively lower toxicity such as acetone, hexane, dichloromethane, etc. The most effective method to improve solubility is by chemical modification. This modification to the chemical structure of organic

semiconductors is the addition of side chains. These side chains are usually either straight or slightly branched alkyl chains. The alkyl chains are non-polar and thus decrease the overall polarity of the entire molecule. As well, the alkyl chains present more, easily accessible areas for solvent interaction. Similar to the other methods, there are a few drawbacks to the addition of side chains. Chemical modification increases the complexity of the molecule and the synthesis required. This increases costs and changes how the molecules react/interact. Careful design of side chain modification can ideally improve solubility without altering the optical/electronic properties of the molecule. Special consideration should be taken so that the side chains do not obstruct the packing of the molecules in the solid film.

## **1.4 Characterization**

In all scientific work, creating new and useful materials is not the only focus. It is also important to investigate and understand the properties of these new materials. To accomplish this, there are many characterization techniques that give insight into the unseen details which help to explain and prove the results that are obtained. The techniques used for the work presented here can be divided into three different functions: 1) determination of chemical composition, 2) measure material properties and 3) examine the properties of the solid state film. Each technique is describe in terms of how, what and why.

### **1.4.1 Chemical Composition**

The most immediate method of characterizing the chemical composition of organic molecules is nuclear magnetic resonance (NMR) spectroscopy<sup>26</sup>. The technique does not require exhaustive sample preparation, the instrument is easy to use and it takes minutes to a few hours (depending on the atoms of interest) to obtain the results. NMR is used to gather information on one specific atom at a time. For example, <sup>1</sup>H NMR is used to obtain information on just hydrogen atoms present in the compound while <sup>13</sup>C NMR gathers information on just carbon atoms present. NMR utilizes the interaction of an external magnetic field with that of the small magnetic field generated by a spinning nucleus. The spinning nuclei, known as NMR active nuclei must be introduced into the sample before a NMR spectrum can be measured. NMR active nuclei are an isotope of the atom of interest. These isotopes are introduced by atomic exchange with a molecule containing the isotope. The interaction of magnetic fields between the external field and that of the isotope causes an excitation of energy which is picked up by the instrument as a resonance signal. The resonance signal of one nucleus will differ

from another based on the immediate environment surrounding said nucleus. The resonance signals are counted and assigned a chemical shift, in ppm, relative to a reference (typically tetramethylsilane, 0 ppm) to give an NMR spectrum. Analyzing the NMR spectrum can give insight into the chemical structure of the sample by comparing obtained chemical shifts with that of known chemical shifts<sup>27</sup>. Integrating the NMR spectrum can give the number of atoms that share the same resonance signal. If the sample should be of a known compound, NMR can be used to confirm the sample and determine the purity of the sample. NMR data used in this work were recorded with a Bruker DPX 300 MHz spectrometer.

Mass spectroscopy (MS) is another technique that we use to determine the chemical composition of organic semiconductors. Molecules are ionized, usually by the bombardment of high energy electrons, which are then separated based on a mass-to-charge ratio by acceleration through electric or magnetic fields. The output of MS is a spectrum of relative abundance as a function of mass-to-charge ratio. High energy bombardment can cause some molecules to become fragmented which give additional peaks in the spectrum. Correlating known masses with the identified masses can be used to determine the chemical composition of the sample<sup>28</sup>. Again, MS can be used to confirm the sample and determine the purity of the sample. High resolution MS data in this work were obtained using a Thermo Scientific Q-Exactive Orbitrap.

A final characterization technique we use for chemical composition is applied to polymers exclusively. The technique is gel permeation chromatography (GPC) which separates molecules based on their size<sup>29</sup>. Polymer solutions are rarely monodispersed (of a single length) when they are synthesized and therefore, polymer solutions are a mixture of many polymers of different length. GPC can be used to determine the number average molecular weight ( $M_n$ ), weight average molecular weight ( $M_w$ ), size average molecular weight ( $M_z$ ), viscosity average molecular weight ( $M_v$ ) and polydispersity index (PDI) of a polymer sample. I.e. GPC is used to determine the average length of the polymers and how varied the lengths of the polymers are. In practice,  $M_n$ ,  $M_w$  and PDI are the most important values. A porous gel is packed into a column and the sample is flowed through one end and comes out the other end. The size of the molecule influences how long it takes to exit the column. Molecules with smaller hydrodynamic volumes can enter the pores of the gel and therefore spends more time in the column. The eluent coming out of the column is collected in portions according to their retention time (how long it stayed in the column). A detector at the end of the instrument system measures properties of the individual portions. Properties measured could include

viscosity and chemical composition for more information about the portions but concentration must always be measured. By comparing the retention times of the portions with a calibration curve (monodispersed polystyrene standards are used to make the calibration curve), the molecular weights of the portions can be determined. The weight distribution curve of the sample can be obtained by plotting the concentration vs. molecular weight of each portion. Analysis of the weight distribution curve gives the molecular weight values such as  $M_n$  and  $M_w$ . PDI is calculated by  $M_w/M_n$  and is a measure of how dispersed the molecular weight distribution is for a given polymer solution. Large PDI values indicate that there are many polymers of different length while PDI of one indicates a monodispersed solution. GPC measurements in this work were measured on a Malvern HT-GPC with polystyrene as the standards. High temperature GPC is used to increase the solubility of the polymer to reduce or eliminate any aggregation of the molecules and to ensure the polymer remains dissolved. Aggregation and/or precipitation during GPC results in additional molecular weight peaks that are false and the results obtained will not correctly represent the actual molecular weight of the polymer.

#### **1.4.2 Material Properties**

Thermogravimetric analysis (TGA) is a characterization technique which examines the change in physical and chemical properties of a material as the sample is heated. TGA measures the mass of a sample as a function of increasing temperature (with a constant heating rate). The change in mass of an organic semiconductor material can provide details about the decomposition mechanism, temperature of evaporation and whether the material undergoes oxidation at elevated temperatures<sup>30</sup>. TGA is used in this work to determine the thermal stability of a compound and the maximum temperature the material can be subjected to without observable decomposition. TGA in this work were taken on a TA Instruments SDT 2960 at  $10\text{ }^\circ\text{C min}^{-1}$  under nitrogen.

Differential scanning calorimetry (DSC) is another thermoanalytical characterization technique that is used to determine phase transition temperatures<sup>31</sup>. In DSC, a sample is placed in a sample holder beside an identical reference holder. Both holders are heated and the heat flux vs. temperature is measured. Peaks appear in the resulting graph when the sample absorbs or releases more heat as a result of a change in heat capacity of the sample. A sample will undergo a change in heat capacity when a physical change occurs such as melting. DSC can also identify the glass transition temperatures of polymeric samples. These temperatures of physical change are useful for the annealing step of device fabrication. Ideally, annealing allows movement of the semiconductor within the solid state film without the film melting to permit efficient rearrangement of the molecules

and thereby increase the crystallinity of the film. This requires heating of the film up to or close to the glass transition temperature of the semiconductor. Annealing temperatures should not exceed the melting temperature of the semiconductor to avoid reflowing of the film which can lead to loss of material in the device channel. DSC in this work were measured on a Perkin-Elmer DSC 7 at 10 °C min<sup>-1</sup> under nitrogen.

To measure the optical properties of an organic semiconductor, Ultraviolet-visible spectroscopy (UV-Vis) is used. A dilute solution or thin semi-transparent film on quartz of the semiconductor is subjected to varying wavelengths of light in the UV-Vis range (325 - 1100 nm). The amount of light absorbed at specific wavelengths by the sample is measured to produce a graph of absorbance vs. wavelength. The graph can be used to determine the wavelength of maximum absorbance ( $\lambda_{\max}$ ) and the onset absorption ( $\lambda_{\text{onset}}$ ).  $\lambda_{\max}$  is characteristic of the extent of delocalization of the electrons within the organic semiconductor.  $\lambda_{\max}$  at longer wavelengths generally indicate larger delocalization.  $\lambda_{\text{onset}}$  is used to determine the optical bandgap of the semiconductor<sup>32,33</sup>. The energy ( $E_g^{\text{opt}}$ ) corresponding to the  $\lambda_{\text{onset}}$ , using equation 1:

$$E_g^{\text{opt}} = \frac{h \times c}{\lambda_{\text{onset}}} \times e \quad (1)$$

where h is Planck's constant, c is the speed of light and e is the energy of an electron, is the minimum amount of energy (in eV) required for a photon to excite an electron from the HOMO energy level to the LUMO energy level (which is equivalent to the optical bandgap). Typically, the absorbance of a sample is measured for both a solution and a film to observe the shift in  $\lambda_{\max}$ . A red shift (shift to longer wavelengths) of the  $\lambda_{\max}$  is normally observed in the film absorbance compared to that of the solution absorbance because molecules aggregate in the solid state. This aggregation allows the overlap of  $\pi$ -orbitals which leads to increased delocalization of electrons and hence a red shift in  $\lambda_{\max}$ . The final property that can be obtained from the UV-Vis technique is the molar extinction coefficient of the semiconductor at  $\lambda_{\max}$ . The molar extinction coefficient is a parameter indicating how strongly the semiconductor can absorb light. Using the Beer-Lambert law, equation 2:

$$A = \epsilon c l \quad (2)$$

where A is absorbance,  $\epsilon$  is the molar extinction coefficient, c is concentration and l is the path length that the light travels through the sample (typically 1 cm), the molar extinction coefficient can be calculated from the solution absorbance spectrum if the path length of absorption and the

concentration of the solution is known. The molar extinction coefficient is most important for semiconductors used in OPVs and photodetectors but nevertheless is occasionally calculated for other organic semiconductor applications as well. UV-Vis measurements in this work were recorded on a Thermo Scientific Genesys 10 UV instrument.

Cyclic voltammetry (CV) is a characterization technique that is used to determine the electrochemical properties of an organic semiconductor. To perform a CV measurement, a working electrode, a counter electrode and a reference electrode are placed in an electrolyte solution. In this work, the working and counter electrodes are platinum disk electrodes, the reference is an Ag/AgCl electrode and the electrolyte solution is 0.1 M n-Bu<sub>4</sub>NPF<sub>6</sub> in dry acetonitrile. The analyte can either be dissolved in the solution or deposited as a thin film covering the working electrode. The potential of the working electrode against the reference is ramped linearly with time and the current between the working and counter electrodes is monitored. When the maximum voltage is reached (set by user), the potential is ramped in the opposite direction until a set minimum is reached. The cycle is repeated as many times as needed. The current vs. voltage is plotted to observe peaks caused by the oxidation and reduction of the analyte. The onset potentials of the oxidation and reduction peaks are compared to a reference compound of known HOMO and LUMO energy levels to obtain the HOMO and LUMO energy levels of the analyte. The reference compound used in this work is ferrocene which shows an oxidation onset potential at 0 V using the setup described above. This corresponds to the known HOMO energy of -4.8 eV for ferrocene<sup>34</sup>. To obtain the energy levels of the analyte, equations 3 and 4:

$$HOMO (eV) = -4.8 - V_{ox} \quad (3)$$

$$LUMO (eV) = -4.8 - V_{red} \quad (4)$$

where  $V_{ox}$  is the onset potential of the oxidation peak and  $V_{red}$  is the onset potential of the reduction peak, are used. The electrochemical band gap is then calculated from the difference in energy of the LUMO to HOMO energy level. This electrochemical band gap is generally larger than the optical band gap due to the absence of electron-hole pair interaction and is more representative of the band gap seen by charge carriers moving through the semiconductor. CV data in this work were measured using a CHI600E Electrochemical Analyser.

The final characterization technique for investigating material properties of an organic semiconductor is density functional theory (DFT). DFT is a computational quantum mechanical

modeling technique based on the chemical structure of the compound of interest. The purpose of DFT is to investigate the theoretical ground state electronic structure of a chemical structure. The information obtained from DFT are theoretical values for the HOMO and LUMO energy levels, the electronic distribution of orbitals across the entire or part of the compound, and the atomic geometry. The theoretical HOMO and LUMO energy levels can be compared to that of experimentally obtained values. Typically, the theoretical and experimental values are within a reasonable margin of error which provides supporting evidence that the synthesized compound is the desired structure. The electronic distribution of orbitals can provide a better understanding of the extent of electron delocalization. The electronic distribution can show which regions of the chemical structure are more electron accepting/donating and what effect substituents may have on the electronic structure of the compound. Finally, the atomic geometry can be important as well because twisting in the structure can cause interruptions in the delocalization of electrons. DFT calculations in this work used the 6-311G+(d,p) basis set and orbital pictures were obtained using GaussView 5.0 software<sup>35</sup>. Alkyl chains were replaced by methyl groups in the model compounds to reduce the computation time for the simulations.

### 1.4.3 Solid State Properties

There are two characterization techniques that can be used to assess the solid state properties of the semiconductor films. The most essential technique is X-ray diffraction (XRD) and the other technique is atomic force microscopy (AFM). XRD is a process of exposing a solid film to a x-ray beam of known wavelength (Cu K<sub>α</sub> radiation,  $\lambda = 1.54 \text{ \AA}$ ) at varying incident angles. The x-rays are scattered by the molecules in the film producing many secondary electromagnetic waves originating from each scattering point (each atom of the molecules). The majority of the secondary waves are canceled out by destructive interference with other secondary waves. However, if there is a regular array of scattering points, there will be some secondary waves that constructively interfere with each other at specific angles to create reflected x-rays. Figure 1.6 demonstrates the condition in which constructive interference will occur. The path length of the two reflected light beams differ only by an amount equal to twice the distance of  $d\sin\theta$ . When  $d\sin\theta$  is equal to an integer multiple of the wavelength of the x-ray, the two reflected beams are in phase with each other and constructive interference occurs. A detector measures the relative intensity of these reflected x-rays as the angle of incident is changed, producing an output spectrum of intensity vs.  $2\theta$  (in degrees). There will only be intensity peaks when the film has crystalline domains to satisfy Bragg's law. Therefore, XRD is used

to determine the crystallinity of a solid film. The molecular packing distance of a crystalline film can be calculated by using Bragg's law, equation 5:

$$2d \sin \theta = n\lambda \quad (5)$$

where  $d$  is the molecular packing distance,  $\theta$  is the incident angle,  $n$  is any integer, and  $\lambda$  is the wavelength of the x-ray beam<sup>36</sup>. The molecular packing distance is an important parameter for OFETs since the intermolecular distance directly influences the charge transport mobility. XRD in this work were obtained using a Bruker D8 Advance powder Diffractometer with standard Bragg-Brentano geometry. XRD samples are prepared in the same manner as device films (discussed later) except there are no source/drain contacts.

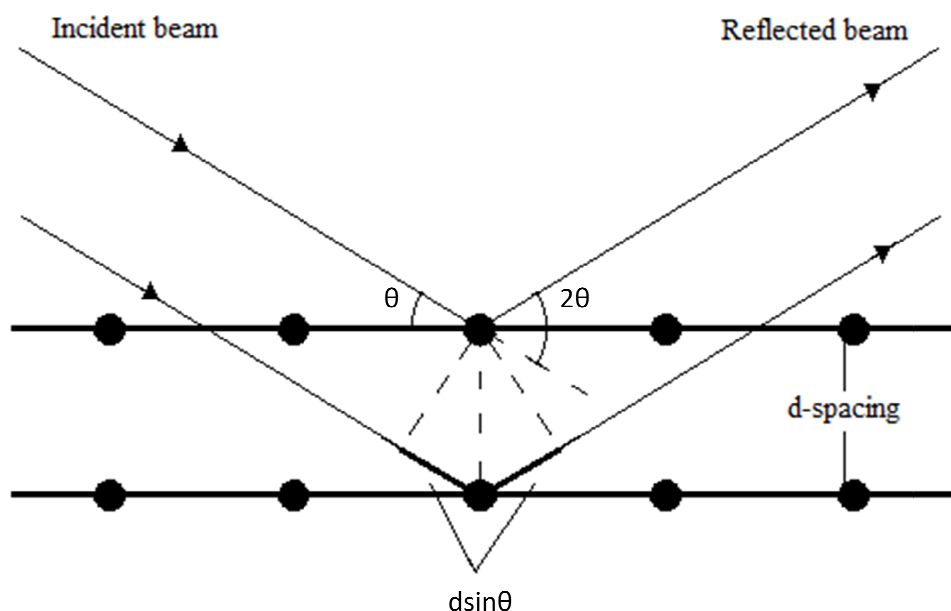


**Figure 1.6: X-ray diffraction diagram.**

AFM is a technique to evaluate the surface morphology of a solid film. In AFM, a small cantilever with a sharp tip at the free end is positioned close to the sample surface. The tip can either be touching or oscillating just above the surface depending on the operating mode. Preferably, the tip is close enough to the surface to be affected by van der Waals forces between tip and sample but not touching the surface to avoid damaging the surface and/or tip. A laser is reflected off the free end of the cantilever into a photodiode. As the sample is moved in a direction, the tip of the cantilever will bend based on the surface morphology and the deflections in the laser on the photodiode is used to

map the surface for computational visualization. The surface map generated by the computer can be used to determine surface roughness and size of crystalline domains<sup>37</sup>. AFM images in this work were collected using a Dimension 3100 scanning probe microscope. AFM samples are the same samples used for XRD.

## **1.5 Fabrication and Evaluation**

### **1.5.1 Fabrication**

After an organic semiconductor is designed, synthesized and characterized, the semiconductor needs to be tested in use. This requires the fabrication of OFET devices which can then be evaluated based on the three main OFET parameters; charge carrier mobility, threshold voltage and current on/off ratio. As mentioned before, there are four configurations of OFET devices. For laboratory convenience and cost effectiveness, the work presented uses only bottom gate bottom contact devices. Bottom gate bottom contact devices are much more convenient because they do not require patterning of gold after the deposition of the semiconductor. Patterning of the gold contacts utilizes photolithography techniques which require time and use of expensive equipment from an external laboratory. With bottom contact devices, the gold contacts can be patterned onto a large substrate (e.g. a wafer) at one time and then cut into many smaller substrates for later use. This reduces the amount of gold used and the frequency of visits to the external laboratory.

The bottom gate bottom contact devices fabricated in this work consist of a heavily n-doped silicon (Si) wafer which acts as the substrate and gate. The Si wafer has a thermally grown oxide layer (silicon dioxide, SiO<sub>2</sub>) of approximately 300 nm. The SiO<sub>2</sub> acts as the dielectric for the OFET. Gold contacts (source and drain) are patterned on top of the oxide layer by photolithography techniques. The photolithography techniques involve: deposition of a negative photoresist, pre-bake of photoresist, exposure to UV through a photo mask of designed pattern, hard bake of photoresist, removal of unexposed photoresist using a developer solution, thermal evaporation of contact material (typically gold), and finally the lift off of excess material by sonication in acetone followed by sonication in isopropyl alcohol (IPA). The contacts form the channel area of the device which is designed to have a width of 1 mm and a length of 30 μm. A single Si wafer will contain many substrates and each substrate has 40 devices patterned on. After the contacts have been patterned onto the substrates, the substrates can be stored away for later use if needed. Before an organic semiconductor is to be deposited onto the substrates to complete the bottom gate bottom contact

devices, the substrate must be cleaned once more and the oxide layer may be modified. To clean the substrates, plasma treatment followed by sonication is used to ensure the surface is void of contaminants. Oxide modification by short alkyl chains reduces the surface charge trapping and can affect adhesion of the semiconductor to the substrate. Modification is typically done by submerging the substrate in a solution of dodecyltrichlorosilane (DDTS) for a few minutes. DDTS modification renders the substrate surface hydrophobic which greatly improves the adhesion of non-polar organic semiconductors. For more polar organic semiconductors, the hydrophobicity of DDTS may decrease the adhesion. Therefore, modification by a shorter alkyl chain can be used such as hexamethyldisilazane (HMDS) to maintain good adhesion. After oxide modification, an organic semiconductor can be deposited onto the substrate. In this work, solution deposition, referred to as spin coating, is used to coat a thin layer of semiconductor over the entirety of the substrate. The thickness of the semiconductor layer is targeted to be approximately 40 nm but may differ depending on the spin coating conditions. Controllable parameters for spin coating include the concentration of solution, amount of solution applied, spin rate and spin time. Higher concentration and application of more solution results in thicker films while higher spin rates results in thinner films. Spin time should be long enough to provide adequate drying of the film. Spin time depends on the boiling point and vapour pressure of the solvent used in the solution. Solvents with higher boiling points and lower vapour pressures require longer spin times. A short drying step at 25 - 50 °C for 20 minutes may follow spin coating to ensure a dry film before testing. Optional annealing is the final step in the fabrication process. The annealing temperatures will depend on the thermal stability of the semiconductor as well as the glass transition and melting temperatures. Typically, annealing is done in 50 °C increments for 20 minutes each i.e. 100 °C, 150 °C, 200 °C, etc.

### **1.5.2 Evaluation**

A completed device is tested using an Agilent B2912A Precision Source/Measure Unit with three probes. Each contact (source, drain and gate) is connected to their respective probe by visual guidance using an optical microscope. Once all of the probes are in good contact with the substrate, a series of programs are run which sweeps drain and gates voltages while measuring the current through source and drain. Four graphs can be produced from the input and output data collected which are used to obtain the three main OFET parameters. The four graphs are: electron output, electron transfer, hole output and hole transfer. Figure 1.7 shows an example of each graph.

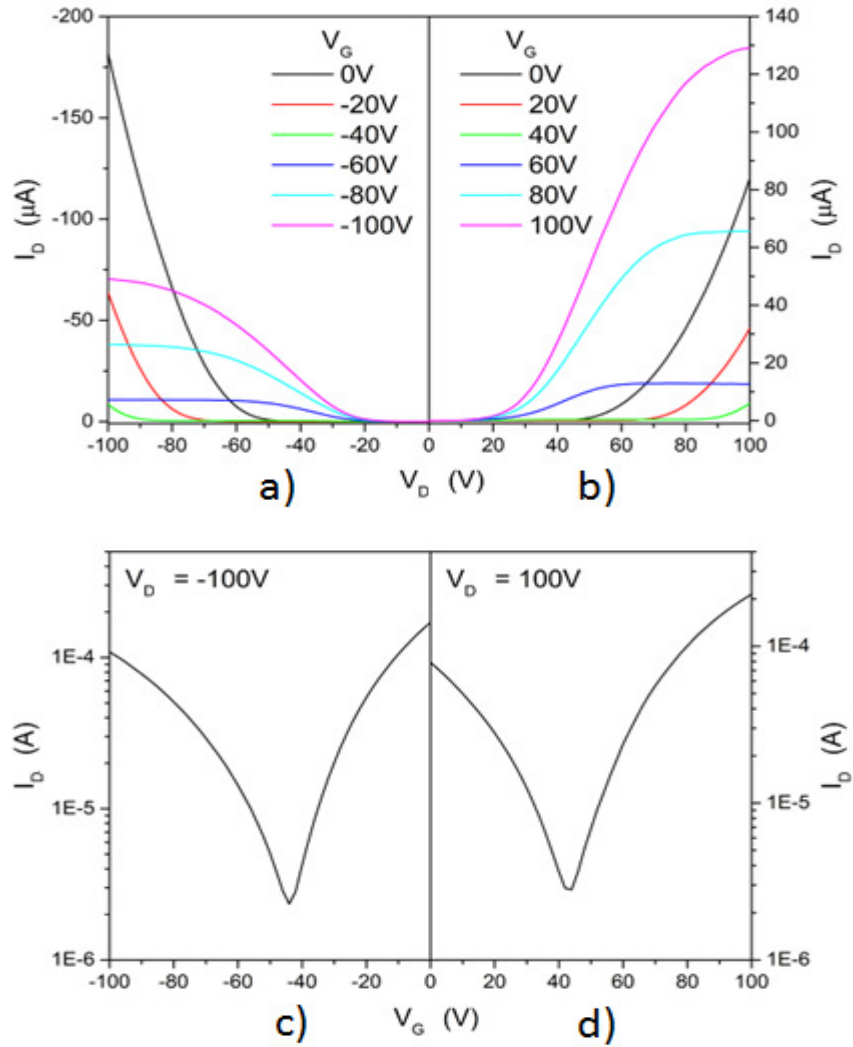


**Figure 1.7: Output graphs of a) hole and b) electron as well as transfer graphs for c) hole and d) electron.**

The output graphs plot drain current vs. drain voltage at varying gate voltages. A linear region can be seen at low drain voltages and a drain current saturation region occurs beyond the pinch-off point at higher drain voltages. In the ideal case the output graph can be fitted using equation 6 for the linear region and equation 7 for the saturation region<sup>38</sup>:

$$I_D = \mu C_i \frac{W}{L} \left( (V_G - V_T) - \frac{V_D}{2} \right) V_D \quad (6)$$

$$I_D = \mu C_i \frac{W}{2L} (V_G - V_T)^2 \quad (7)$$

where  $I_D$  is the drain current,  $W$  and  $L$  are the channel width and length,  $C_i$  is the capacitance per area of the dielectric ( $\sim 11.6 \text{ nF cm}^{-2}$  for  $\text{SiO}_2$ ),  $V_G$  is the gate voltage and  $V_T$  is the threshold voltage. The transfer graphs are a logarithmic plot of drain current vs. gate voltage. Another useful plot is of drain current<sup>1/2</sup> vs. gate voltage using a high  $V_D$ . The charge carrier mobility and threshold voltage can be obtained from the drain current<sup>1/2</sup> vs. gate voltage curve. The mobility is directly calculated from the linear slope in the positive/negative gate voltages for n-/p-type. The threshold voltage is extrapolated from the intersection between the x-axis and the linear slope used for the mobility. Figure 1.8 visually demonstrates how these values are obtained from the graph. Finally, the current on/off ratio is simply calculated by dividing the drain current at saturation for a given gate voltage by the drain current when no gate voltage is applied. Data is collected from a minimum of 5 devices per substrate per annealing temperature. The mobilities are typically tabulated using the averages and standard deviation except for the maximum mobilities which are from a single measurement.

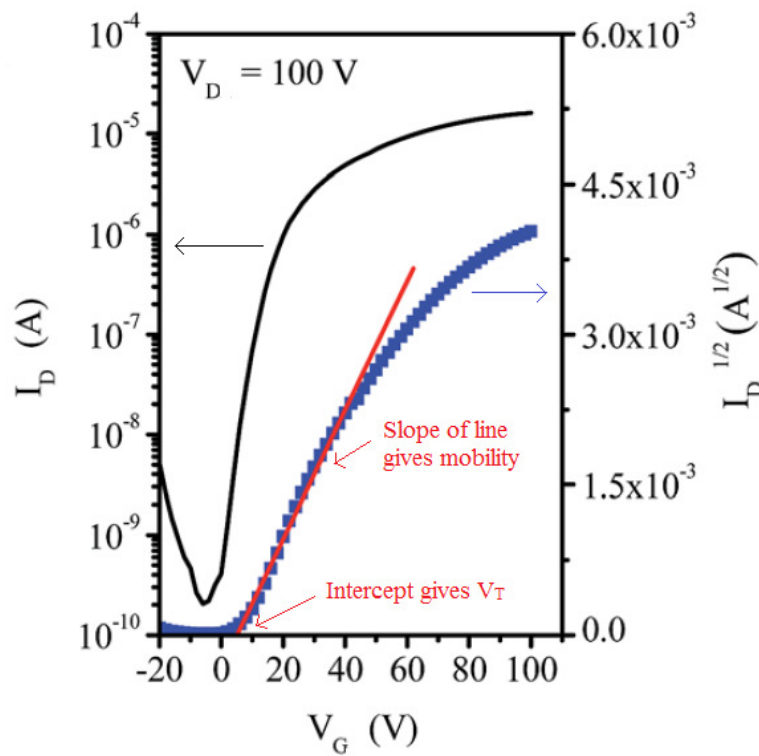


**Figure 1.8: Obtaining mobility and  $V_T$  from the graph.**

## 1.6 Objective and Scope of Work

The advantages that organic electronics have over traditional silicon electronics are the solubility and mechanical robustness of the materials. Soluble material opens up the possibility of low temperature, high volume production which lowers manufacturing cost immensely. Mechanically robust materials enable flexible devices that resist physical failure as well as opening up a wide range of new applications. Both of these advantages raise the importance of organic electronics in today's technologically dependent society, especially when consumer products are becoming more and more individualized and portable. There are however some challenges that are inhibiting the potential of organic electronics. The comparatively lower performance of organic electronics results in slower and less responsive devices. As well, the poor stability of some of the organic compounds used leads to less product lifetime. The following subsection gives an overview of some of the recent research that attempts to address these issues.

### 1.6.1 Research Problem

Many electronic circuits utilize transistors for switching or amplifying an electrical signal. One of the most used technologies in today's circuits are complementary metal-oxide-semiconductors (CMOS) which makes use of complementary pairs of n-type and p-type transistors. Since the pairs alternate on and off states, it is important that the individual transistors be similar in performance so that there is no noticeable performance change of the CMOS when switching states. Therefore, to make effective CMOS devices from organic semiconductors, it is important to have both n-type and p-type semiconductors that demonstrate similar performance parameters. In the past, high performance p-type organic semiconductors with mobilities over  $10 \text{ cm}^2\text{V}^{-1}\text{s}^{-1}$  have been developed<sup>39-41</sup>. However, development of high performance n-type organic semiconductors has been relatively slower<sup>42-48</sup>. Hence, there is a need to develop better n-type organic semiconductors.

The main difficulty with n-type organic semiconductors which has caused their slower development is that electrons travelling through an organic semiconductor are susceptible to oxidation by ambient species such as oxygen and water which results in instability<sup>49,50</sup>. This instability leads to a loss of mobile electrons and/or a chemical change in the structure of the organic semiconductor. Ultimately, instability results in reduced or complete loss of semiconductor performance. Another problem, which has made high electron mobility challenging, is that the work function of common electrode metals are quite often significantly mismatched with the LUMO energy level of the organic semiconductor creating a large injection barrier<sup>51</sup>. In both cases, the best

strategy to overcome them seems to be lowering the LUMO energy level. Studies have suggested that in order to realize a stable n-type organic semiconductor, the material must possess a low LUMO energy level about or below -3.7 eV to facilitate injection and transport of electrons<sup>49,52-55</sup>. To reach low LUMO energy levels, a few molecular strategies have been explored including the incorporation of highly electron deficient polycyclic rings<sup>56-62</sup>, electron rich moieties substituted with strong electron withdrawing groups<sup>63-67</sup>, and quinoidal structures (fully conjugated cyclic dione structures)<sup>68-70</sup>. With these strategies, there is a growing number of viable n-type organic semiconductors but there is still a significant gap between n-type and p-type organic semiconductors. Research is still needed to discover more n-type organic semiconductors that can continue to close the gap. Therefore, the objective of the work presented in this thesis is to develop a novel high performance n-type organic semiconductor that is stable for use in organic field-effect transistors. The work presented in this thesis follows the development of an n-type organic semiconductor based on the quinoidal molecule known as indophenine. The novel compound is called thiophene-*S,S*-dioxidized indophenine (IDTO).

### **1.6.2 Scope of Work**

The scope of work is limited to the development of thiophene-*S,S*-dioxidized indophenine and its use in organic field-effect transistors. The work is divided into the following sections:

1. Systematic improvement of synthesis
2. Use as a small molecule organic semiconductor
3. Use as a building block for polymeric organic semiconductors
4. Use in polymer blends as an additive

## Chapter 2

### Thiophene-*S,S*-dioxidized Indophenine

#### 2.1 Introduction

Indophenine is a blue dyestuff that was discovered in 1879<sup>71</sup>. The chemical structure of indophenine, shown in Figure 2.1, is a planar quinoidal bithiophene structure with six inseparable isomers. The planar structure should promote efficient charge transport while the quinoidal moieties should result in a low LUMO energy level. The simplistic synthetic route and inexpensive starting materials also benefit indophenine as an organic semiconductor. As such, indophenine has already been investigated by Hwang et al. The OFET based on dodecyl-substituted indophenine displayed mediocre ambipolar charge transport with electron and hole mobilities of  $5.0 \times 10^{-3} \text{ cm}^2 \text{V}^{-1} \text{s}^{-1}$  and  $3.1 \times 10^{-2} \text{ cm}^2 \text{V}^{-1} \text{s}^{-1}$ , respectively. The HOMO and LUMO energy levels measured for indophenine were -5.25 eV and -3.76 eV, respectively<sup>72</sup>. To obtain a high performance unipolar n-type semiconductor based on indophenine, the objectives were to increase the hole injection barrier by lowering the HOMO energy level and establish a method to obtain a pure isometric form to improve the mobility. Conveniently, both objectives could be achieved through a simple oxidation and subsequent thermally treatment of indophenine. The oxidation of indophenine bonds the sulfur atoms of the thiophene moieties with oxygen atoms which significantly lowers the energy levels. Thermal treatment of the oxidized product causes isomerization to a single isomer (E,E,E) due to steric hinderance of the newly added oxygen atoms in the unfavourably isomers. The new compound is named thiophene-*S,S*-dioxidized indophenine. The following sections detail the work that has been done using IDTO.

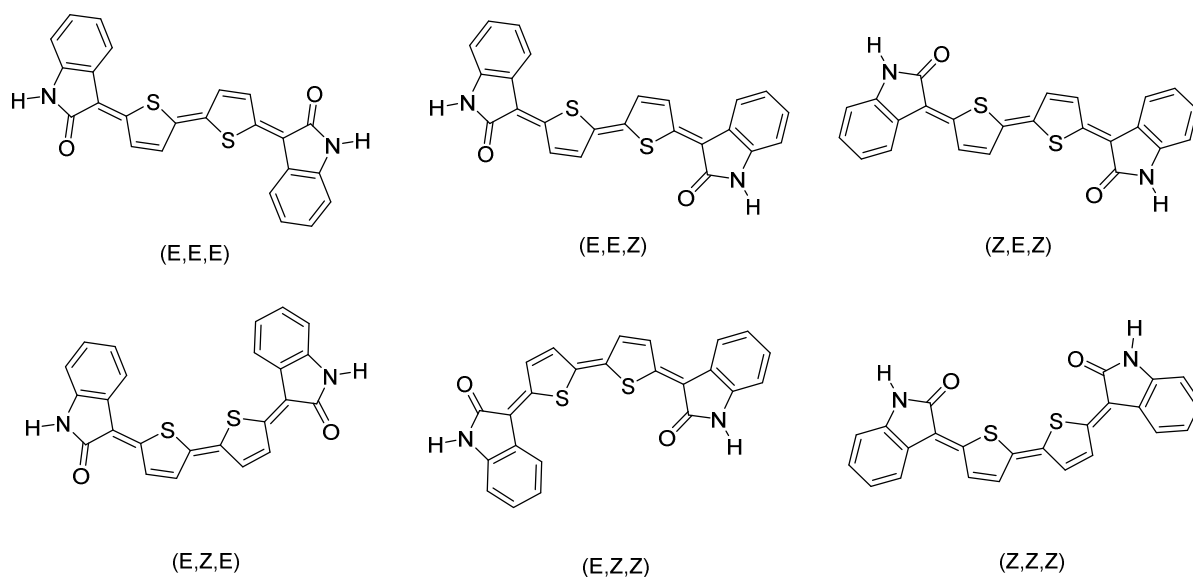


**Figure 2.1: Chemical structures for the six isomers of indophenine.**

## 2.2 IDTO Synthesis Improvement

The synthetic procedure for indophenine is well studied with yields ranging from ~40% to as high as 65%<sup>73,74</sup>. Using the procedure used by Hwang et al. for indophenine OFET synthesis as a model, IDTO was synthesized by adding an oxidation step immediately following the 3 hours required to form indophenine. The oxidant used is 3-chloroperoxybenzoic acid (m-CPBA) with a 2 molar equivalent to thiophene. An additional step for thermal treatment was also included during the purification to obtain the isometrically pure product. Unfortunately, the yield of IDTO following this procedure was very low (less than 10%). For practical application of IDTO, the yield would have to be improved. Therefore, systematic improvement of the synthetic procedure was carried out in a series of experiment with the primary goal of improving the yield of IDTO. Each factor that improves the yield will be carried over into subsequent experiments.

### 2.2.1 Experimental Details

The original synthetic route for IDTO is outlined in Figure 2.2. In detail, isatin (3.44 g, 23.4 mmol), 1-bromododecane (6.74mL, 28.1 mmol, 1.2 mole equivalent over isatin) and potassium carbonate ( $K_2CO_3$ ) (6.46g, 46.7 mmol, 2 mole equivalent over isatin) were added to a two-necked flask. The flask was then vacuumed and backfilled with nitrogen three times. 50 mL of anhydrous N,N'-dimethylformamide (DMF) was injected and the mixture was stirred at 70°C for 24 hours.



used as the solvent for the rest of the reactions to avoid further use of benzene. Chlorobenzene, chloroform and acetic acid were not investigated further due to either reduced or no product formation. The next series of experiments dealt with varying reagents. To start, the oxidant amount was increased. Since the oxidant gives one oxygen atom per oxidant molecule and each thiophene requires two oxygen additions, there is no sense in decreasing the oxidant amount. Therefore, oxidant amounts were increased to 3 or 4 molar equivalents to thiophene. The next reagent to be altered was the sulfuric acid. Different strong acids were attempted such as trifluoroacetic acid (TFA) and p-toluenesulfonic acid (p-TsOH). Sulfuric acid concentration was decreased to 75% and 50% by adding DI water before addition. Finally, sulfuric acid amount was varied. The amount of sulfuric acid had a large influence on the yield of IDTO; hence many acid amounts were attempted. Molar equivalents to isatin were tested as low as 0.25 and as high as 20. Following reactions use the optimal amount of acid of 2.5 molar equivalents. Finally, other parameters which could affect the reaction were investigated. The order of procedure was first considered. Three alterations could be tested, 1) thiophene could be added after sulfuric acid, 2) oxidant could be added prior to indophenine formation and 3) the thermal treatment for isomerization could be performed before purification. The results for the series of experiments are presented in Table 2.1.

**Table 2.1: IDTO Synthesis Improvement Results**

Experiment No.	Description	Solvent	Molar ratio Acid : Isatin	Molar ratio Oxidant : Thiophene	Yield (%)
1	Original synthetic route	Benzene	1 : 1	2 : 1	8.8
2	Toluene as solvent	Toluene	1 : 1	2 : 1	13.2
3	Chlorobenzene as solvent	Chlorobenzene	1 : 1	2 : 1	7.6
4	Chloroform as solvent	Chloroform	1 : 1	2 : 1	-
5	Acetic acid as solvent	Acetic acid	1 : 1	2 : 1	-
6	Oxidant 3 molar equivalent	Toluene	1 : 1	3 : 1	11.7
7	Oxidant 4 molar equivalent	Toluene	1 : 1	4 : 1	4.7
8	TFA as acid	Toluene	1 : 1	3 : 1	-
9	p-TsOH as acid	Toluene	1 : 1	3 : 1	-
10	75% sulfuric acid conc.	Toluene	1 : 1	3 : 1	-
11	50% sulfuric acid conc.	Toluene	1 : 1	3 : 1	-
12	Acid 0.7 molar equivalent	Toluene	0.7 : 1	3 : 1	17.6
13	Acid 0.25 molar equivalent	Toluene	0.25 : 1	3 : 1	0.5
14	Acid 2 molar equivalent	Toluene	2 : 1	3 : 1	30.2
15	Acid 2.5 molar equivalent	Toluene	2.5 : 1	3 : 1	36.2
16	Acid 3 molar equivalent	Toluene	3 : 1	3 : 1	28.7
17	Acid 4 molar equivalent	Toluene	4 : 1	3 : 1	24.0
18	Acid 10 molar equivalent	Toluene	10 : 1	3 : 1	-
19	Acid 20 molar equivalent	Toluene	20 : 1	3 : 1	-
20	Thiophene after acid	Toluene	2.5 : 1	3 : 1	22.3
21	Oxidant at start	Toluene	2.5 : 1	3 : 1	-
22	Thermal treatment before purification	Toluene	2.5 : 1	3 : 1	21.2

## 2.2.2 Results and Discussion

Experiment 1 is the original synthesis procedure using benzene as the solvent, 1:1 ratio of acid to isatin and 2:1 ratio of oxidant to thiophene. Experiments 2 - 5 investigate the choice of solvent. Although changing the solvent would more than likely not improve the yield, the goal was to eliminate the use of benzene because benzene is a known carcinogen. It was found that only benzene and its derivatives could facilitate the reaction. After investigation of the literature, it is still unclear as to why the reaction proceeds with ease at room temperature with the aromatic solvents. Acetic acid could be used as the solvent according to some references<sup>73,74,76</sup>. However, elevated temperatures were used in those cases. No reaction was observed using acetic acid at room temperature though.

Experiments 6 and 7 increase the oxidant amount. The best result was obtained using 3 molar equivalents of oxidant. It is believed that the yield was slightly increased for 3 molar equivalents of oxidant due to the purity of the m-CPBA. The m-CPBA used has a purity of  $\leq 77\%$  from purchase. The m-CPBA can decompose over time through heat and exposure to moisture. If the purity is decreased, then excess would need to be added. Increasing the oxidant amount further saw a significant decrease in yield which can be expected since m-CPBA is a strong oxidizing agent. Too much excess m-CPBA could result in over oxidation and loss of desired product.

In an attempt to simplify material handling, the sulfuric acid was substituted with other strong acids in experiments 8 and 9. In both cases no reaction was observed. This result was unexpected because the reaction mechanism suggested by Tormos et al. needs only protonation by an acid for the indophenine to form<sup>74</sup>. If the reaction truly could not proceed with the use of any strong acid, then another reaction mechanism is needed. It was postulated that the concentrated sulfuric acid may be acting as more than just an acid. Sulfuric acid is known to have some oxidizing properties as well when the concentration is high enough. A study showed that oxidation of thiophene by concentrated sulfuric acid could occur to create thiophene sulfonate<sup>77</sup>. It may be possible then that the indophenine reaction requires oxidation of thiophene in addition to isatin protonation. To test this theory, experiments 10 and 11 were performed utilizing less concentrated sulfuric acid. When the sulfuric acid concentration is lowered, it loses any oxidizing properties and no reactions were observed. Therefore, it appears as though concentrated sulfuric acid plays an important role in this reaction to both protonate isatin and oxidize thiophene. To further investigate the use of sulfuric acid in the reaction, experiments 12 - 19 change the amount of concentrated sulfuric acid that was added to the reaction. 2.5 molar equivalents of acid produced the largest yield of 36.2%. The yield decreased

significantly as the acid amount was decreased below 2 molar equivalents. Again, this supports the idea that the sulfuric acid has two roles requiring one sulfuric acid per isatin and one per thiophene. Slight excess of sulfuric acid is useful for drawing away the water molecules that form during the reaction which aid the reaction overall. Increasing the excess too much saw a decrease in yield and eventually loss of the desired product all together. It is thought that side reactions become more prevalent when too much concentrated sulfuric acid is present. Experiment 20 adds the thiophene after the acid to separate the protonation of isatin from the oxidation of thiophene. The result was a decrease in yield. By protonating the isatin first, a portion of the sulfuric acid is converted to hydrogen sulfate ions which effectively lowers the concentration of sulfuric acid. However, this dilution does not appear to inhibit the oxidation of thiophene but rather just slow it down resulting in a lower overall yield.

The last two experiments, 21 and 22, change the procedure in minor ways which could increase the simplicity of the reaction procedure. Adding the oxidant at the start of the reaction instead of three hours into the reaction would create the convenience of a onetime addition synthesis. Unfortunately, the oxidant presumably reacts unfavorably before the indophenine is formed because no product is observed. Thermal treatment before purification simplifies the column chromatography step due to the separation of just one product instead of a set of isomers but a lower yield was obtained. This could be due to remaining reactive species during the thermal treatment which react with the IDTO compounds at high temperatures. In both experiments, the procedure could not be simplified without adversely affecting the yield of the reaction.

There were a few other parameters which were considered but not tested. The reagents, isatin and thiophene, were not altered because of the possibility of other products forming. As revealed in the previous studies of indophenine<sup>73,74</sup>, the product structure can incorporate more or less thiophene units depending on the molar ratio of isatin to thiophene. Therefore, the 2:1 ratio of thiophene to isatin from the reference was kept to ensure the desired product is formed. Reaction time was also considered but it was determined that increasing the reaction time had no effect. Decreasing time was not tested because yield will not increase by less reaction time.

### 2.2.3 Conclusions

Based on the yields obtained from the experiments performed, yields approaching 40% can be achieved for the synthesis of IDTO. As an additional bonus, benzene was replaceable with toluene which removed the harmful carcinogen from the reaction. The improved conditions were 2.5 molar equivalents of concentrated sulfuric acid to isatin and 3 molar equivalents of m-CPBA to thiophene. It was proposed that the sulfuric acid acts to protonate isatin and oxidize thiophene in order for the reaction to proceed. This is supported by the need for highly concentrated sulfuric acid and the benefit of using at least 2 molar equivalents of sulfuric acid. The improved procedure involved addition of the acid to a mixture of isatin and thiophene in toluene, followed by addition of the oxidant three hours later. Work up and purification are best performed before thermal treatment. This improved synthetic procedure is used for the synthesis of IDTO and its derivatives for the remainder of the work presented.

## Chapter 3

### IDTO as a Small Molecule N-type Organic Semiconductor

This chapter is based on the results published in RSC Advances<sup>78</sup> in which I supported the main author, Dr. Deng, with the synthesis and characterization of the IDTO compounds. More specifically, I performed synthetic experiments, work-up and purification of the compounds. As well, I performed the UV-Vis and CV characterization measurements. The figures and data presented in this section are the same as what is presented in the publication. Three IDTO compounds, IDTO, 5-bromo-IDTO and 6-bromo-IDTO, were synthesized for use as n-type organic semiconductors. Each compound was characterized by <sup>1</sup>H NMR, <sup>13</sup>C NMR, MS, TGA, DSC, DFT, UV-Vis and CV. Thin films of each compound were characterized by XRD and AFM. The OFET performance parameters were determined using bottom gate bottom contact devices.

#### 3.1 Experimental Details

##### 3.1.1 Synthesis of IDTO

All starting materials were purchased from commercial sources and used without further purification. The IDTO compounds were synthesized based on the improved synthetic route discussed in the previous section. Briefly, 1-bromododecane (1.12 g, 4.5 mmol) and K<sub>2</sub>CO<sub>3</sub> (1.05 g, 7.6 mmol) were added to a solution of isatin/5-bromo-isatin/6-bromo-isatin (0.56/0.94/0.94 g, 3.8 mmol) in anhydrous DMF. The mixture was stirred at 70 °C overnight under nitrogen. The solvent was removed *in vacuo* and the residue was dissolved in chloroform. The solution was washed with water and the organic layer was separated and dried over anhydrous MgSO<sub>4</sub>. The solution was filtered and the solvent was removed. The crude product was purified by column chromatography on silica gel using hexane/DCM v/v = 1/1 to give the N-dodecyl-isatin/5-bromo-isatin/6-bromo-isatin as an orange solid. Then, concentrated sulfuric acid (0.25 g, 2.5 mmol) was added dropwise to a stirring solution of N-dodecyl-isatin/5-bromo-isatin/6-bromo-isatin (0.32/0.39/0.39 g, 1 mmol) and thiophene (0.17 g, 2 mmol) in toluene at room temperature. After three hours, m-CPBA (77%, 0.67 g, 3 mmol) was added and the mixture was stirred overnight under nitrogen. The mixture was then quenched with saturated aqueous K<sub>2</sub>CO<sub>3</sub> solution and the products were extracted with DCM. The DCM portion was dried over anhydrous MgSO<sub>4</sub>, filtered and the solvent was removed *in vacuo*. The crude product was purified by column chromatography on silica gel using hexane/DCM v/v = 1/3 to give the product as

an isomer mixture. The mixture was heated in refluxing toluene overnight under nitrogen to afford the final product as a dark brown solid. The reaction schemes are shown in Figure 3.1. NMR and MS measurements for the small molecule IDTO compounds can be found in Appendix B. Specific details about the chemical used can be found in Appendix A.

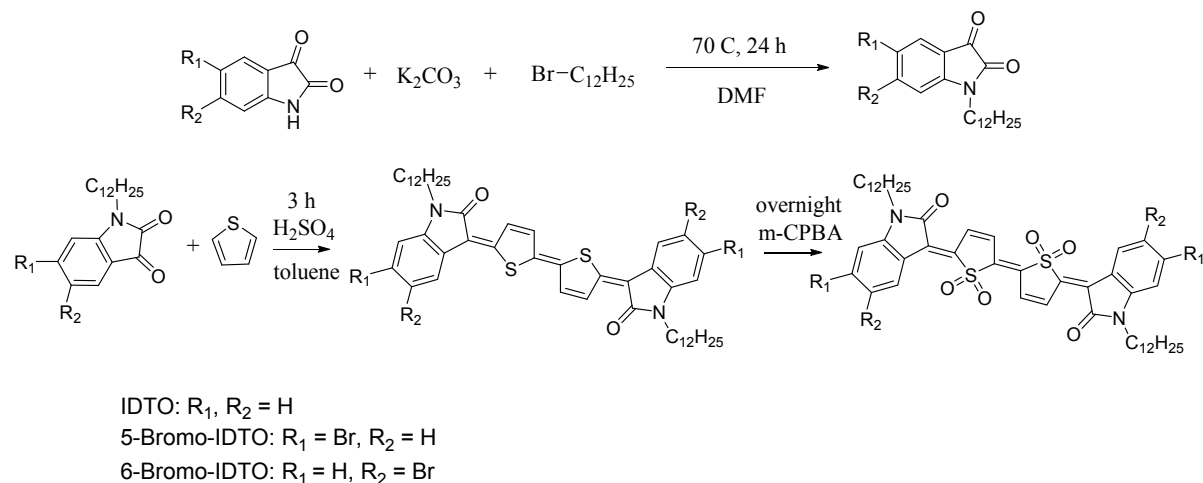


**Figure 3.1: General reaction scheme for IDTO compounds.**

### 3.1.2 Characterization

NMR data were recorded using a Bruker DPX 300 MHz spectrometer. The chemical shifts of  $^1H$  NMR were referenced to tetramethylsilane (TMS, 0 ppm). The chemical shifts of  $^{13}C$  NMR were referenced to residual  $CHCl_3$  in  $CDCl_3$ . High resolution mass spectroscopy (HR-MS) data were obtained using a Thermo Scientific Q-Exactive Orbitrap. DFT calculations were performed with the 6-311G+(d,p) basis set and the orbital diagrams were obtained using GaussView 5.0 software. TGA and DSC were carried out on a TA Instruments SDT 2960 and a Perkin-Elmer DSC 7, respectively, at a scan rate of  $10\text{ }^\circ\text{C min}^{-1}$  under nitrogen. UV-Vis spectra were recorded on a Thermo Scientific Genesys 10 UV instrument using chloroform solutions ( $10^{-5}$  M) and films spin-coated onto quartz substrates ( $5\text{ mg mL}^{-1}$  chloroform solutions). CV data were obtained on a CHI600E electrochemical analyzer in dry acetonitrile. 0.1 M  $n\text{-Bu}_4\text{NPF}_6$  was used as the electrolyte and the experiment was done under nitrogen at a scan rate of  $50\text{ mV s}^{-1}$ . A three-electrode cell was used. The working and counter electrodes were platinum, and the reference electrode was Ag/AgCl. Ferrocene was used as a reference, which has a HOMO energy level of -4.8 eV. XRD plots of the thin films spin-coated on DDTs-modified Si/SiO<sub>2</sub> substrates were obtained using a Bruker D8 Advance powder Diffractometer

with standard Bragg–Brentano geometry. Cu  $K_{\alpha 1}$  radiation ( $\lambda = 1.5406 \text{ \AA}$ ) was used. The same samples were used to record AFM images with a Dimension 3100 scanning probe microscope.

## 3.2 Results and Discussion

### 3.2.1 DFT: Theoretical Calculations

Computer simulations using DFT are graphically represented in Figure 3.2. The optimized molecular geometries show that the compounds maintain high planarity even with the addition of oxygen atoms onto the thiophene units. The calculated HOMO energy level for IDTO is significantly lowered by the oxidation of the thiophene units and the LUMO energy level is slightly raised. Expectedly, the energy levels are lowered by the introduction of bromine atoms because of their inductive (electron withdrawing) and resonance (lone pair electrons) effects. Interestingly, the LUMO energy level of 6-bromo-IDTO is lower than that of 5-bromo-IDTO by 0.4 eV but their HOMO energy levels are very similar. This slight difference can be explained by looking at the electron density distributions of the two bromine substituted compounds. As shown, the 6,6' position bromine atoms participate in both the HOMO and LUMO conjugation paths. However, the 5,5' position bromine atoms only participate in the HOMO conjugation path and not the LUMO conjugation path. Since the 5,5' position bromine atoms are not part of the LUMO conjugation, those bromine atoms cannot exert resonance effects to the LUMO wavefunction which results in a smaller delocalization of electrons and a slightly raised LUMO energy level. This differing influence of positional substitutions on isatin units were previously investigated in indigo-based polymers for switching carrier polarity<sup>79</sup>. The effect that the position of the bromine substituents have will be seen throughout the characterization and evaluation of the three IDTO compounds.

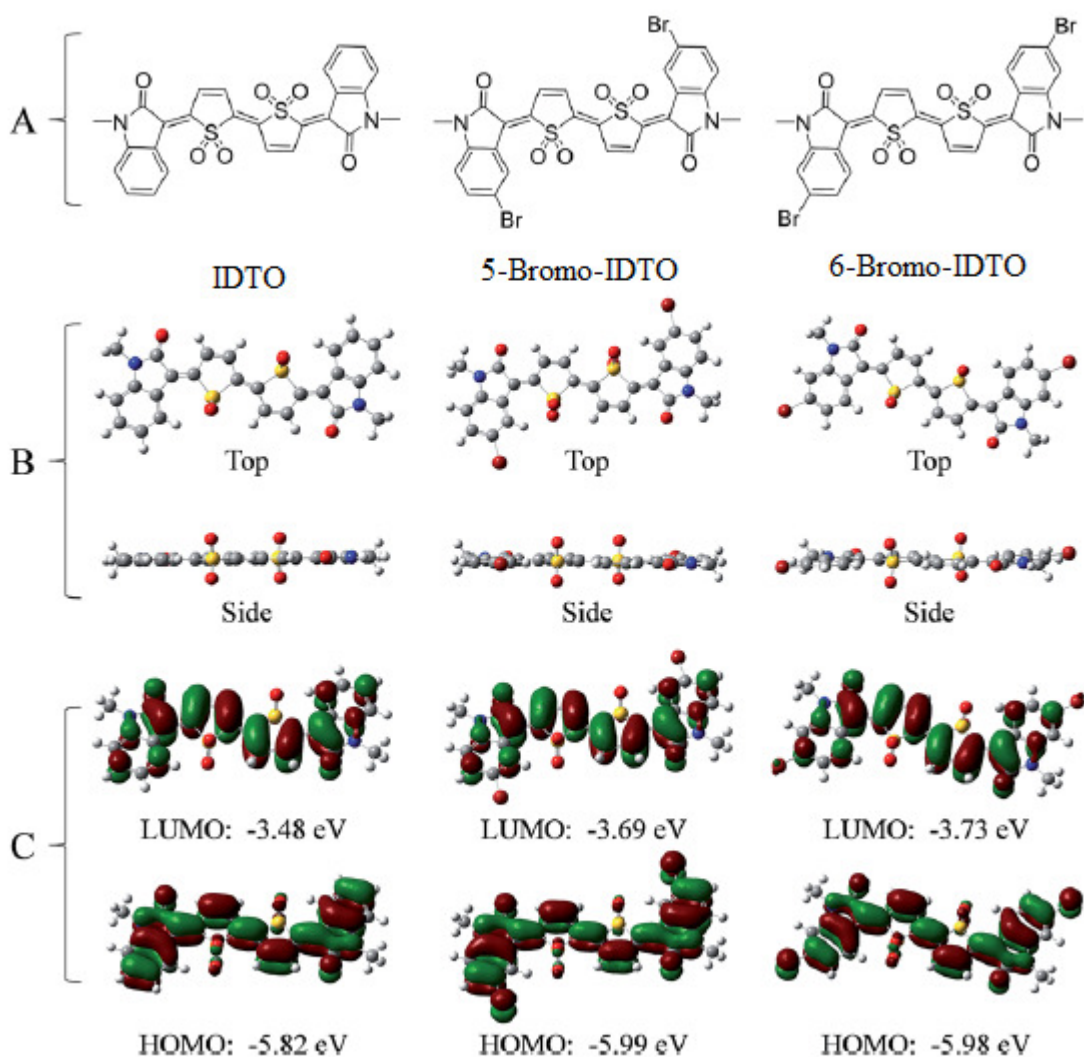


**Figure 3.2: A) Chemical structures, B) optimized geometries and C) electron density distributions obtained from DFT calculations for the IDTO compounds.**

### 3.2.2 TGA and DSC: Thermal Properties

The thermal properties of the IDTO compounds were measured with TGA and DSC, shown in Figure 3.3. TGA was able to discern the same two step degradation process for all three compounds. The first degradation step of approximately 13% mass loss can be associated with the elimination of the  $\text{SO}_2$  because the C-S bonds are the weakest bonds present in the molecules<sup>80,81</sup>. The second degradation step which represents the rest of the mass loss is caused by the continuing degradation of the entire molecule. The onset decomposition temperatures for IDTO, 5-bromo-IDTO

and 6-bromo-IDTO are 244 °C, 248 °C and 278 °C, respectively. The higher onset decomposition temperature of 6-bromo-IDTO is thought to be due to increased C-S bond stability caused by the larger delocalization of electrons over the 6,6' position bromine substituents. DSC did not show any melting points for the compounds, meaning the compounds decompose before melting.

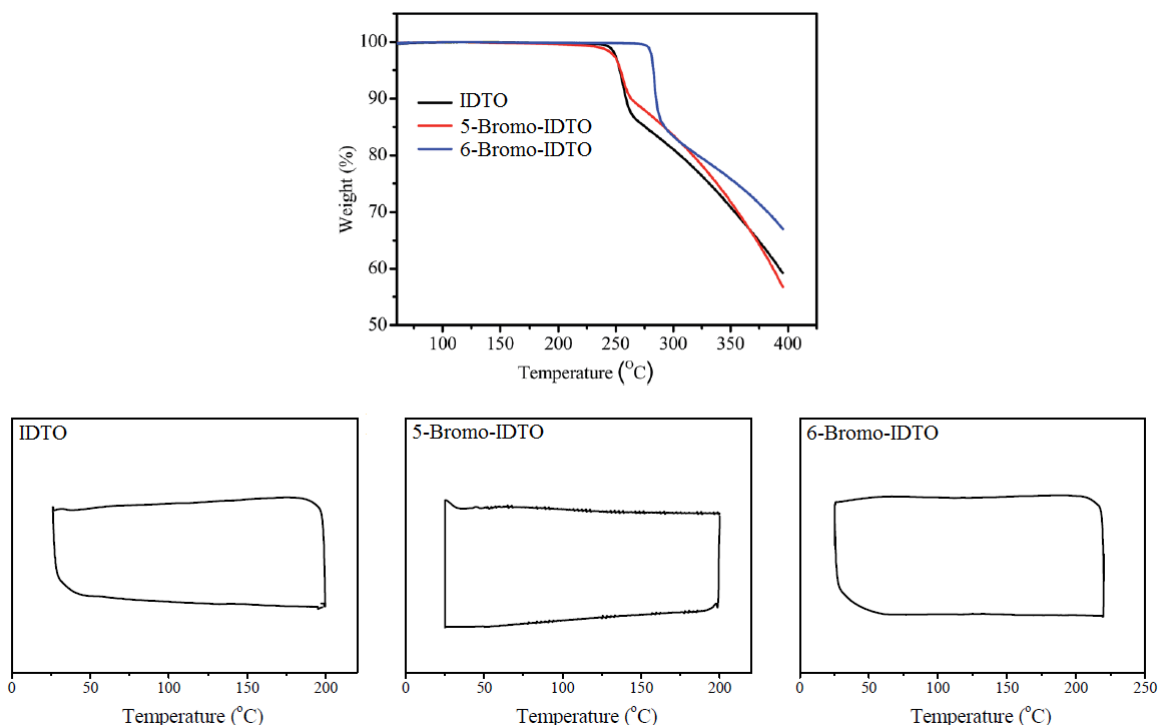


**Figure 3.3: TGA (top) and DSC (bottom) for the IDTO compounds.**

### 3.2.3 UV-Vis and CV: Optical and Electrochemical Properties

The optical and electrochemical properties of the IDTO compounds were obtained through UV-Vis and CV measurements. UV-Vis spectra and data for dilute solutions and thin films are given in Figure 3.4 and Table 3.1. The dilute solutions show one major peak and two minor vibronic peaks/shoulders for all of the compounds.  $\lambda_{\text{max}}$  is seen to red shift in all compounds when going from solution to thin film. The longer wavelength shoulders are red shifted as well as more intense in the thin films. This red shifting is indicative of enhanced van der Waals interactions<sup>32,33</sup>. 6-bromo-IDTO possesses a much more intense shoulder at ~535 nm than the other two compounds. A more intense vibronic shoulder implies stronger intermolecular interactions which could enhance intermolecular

charge transport<sup>82</sup>. The optical band gaps ( $E_g^{opt}$ ) are calculated from the onset wavelengths of the film absorptions to be 1.74 eV for IDTO, 1.67 eV for 5-bromo-IDTO and 1.72 eV for 6-bromo-IDTO.

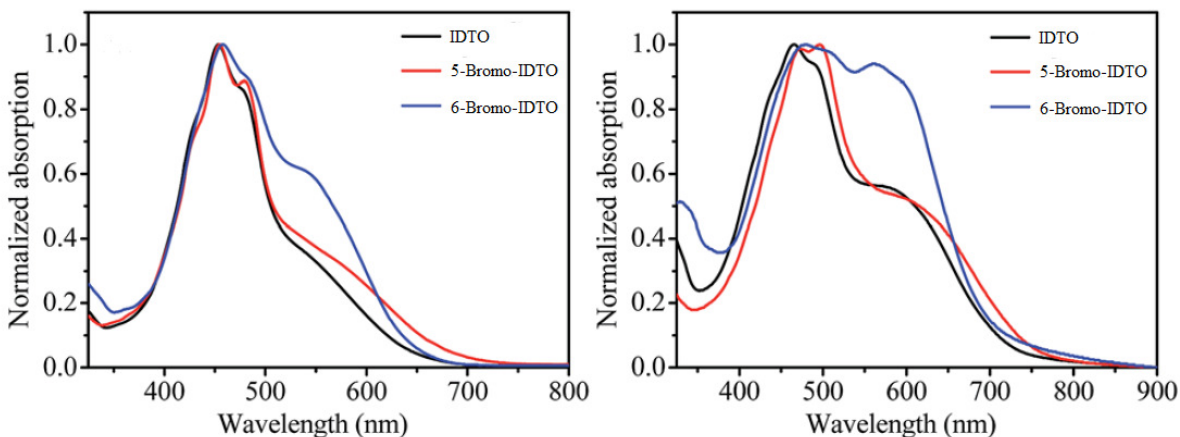


**Figure 3.4: UV-Vis spectra for the IDTO compounds in solution (left) and thin film (right).**

**Table 3.1: UV-Vis absorption properties of IDTO compounds.**

Compound	$\lambda_{max}$ (nm)		$E_g^{opt}$ (eV)
	Solution	Thin Film	
IDTO	453, 476 (s) <sup>a</sup> , 532 (s)	466, 491 (s), 577 (s)	1.74
5-bromo-IDTO	456, 479 (s), 535 (s)	472, 497 (s), 583 (s)	1.67
6-bromo-IDTO	460, 482 (s), 540 (s)	480, 507 (s), 566 (s)	1.72

<sup>a</sup> Shoulder

Thin film CV of the three compounds reveals a similar trend in energy levels found by the DFT calculations. Figure 3.5 is the cyclic voltammograms and energy level diagrams of the three IDTO compounds. The CV confirms that the oxidation of indophenine to IDTO significantly decreases the HOMO energy level to -5.85 eV and the LUMO energy level to -3.99 eV. It is also observed that bromine substitution further decreases both energy levels. 5-bromo-IDTO has HOMO and LUMO energy levels of -4.12 eV and -6.33 eV, respectively. 6-bromo-IDTO still shows the lowest LUMO energy level at -4.18 eV but has a slightly higher HOMO energy level at 6.30 eV. The electrochemical band gaps are calculated to be 1.86 eV for IDTO, 2.21 eV for 5-bromo-IDTO and 2.12 eV for 6-bromo-IDTO. The much deeper HOMO energy levels of the IDTO compounds should prevent hole injection and enable unipolar n-type performance.

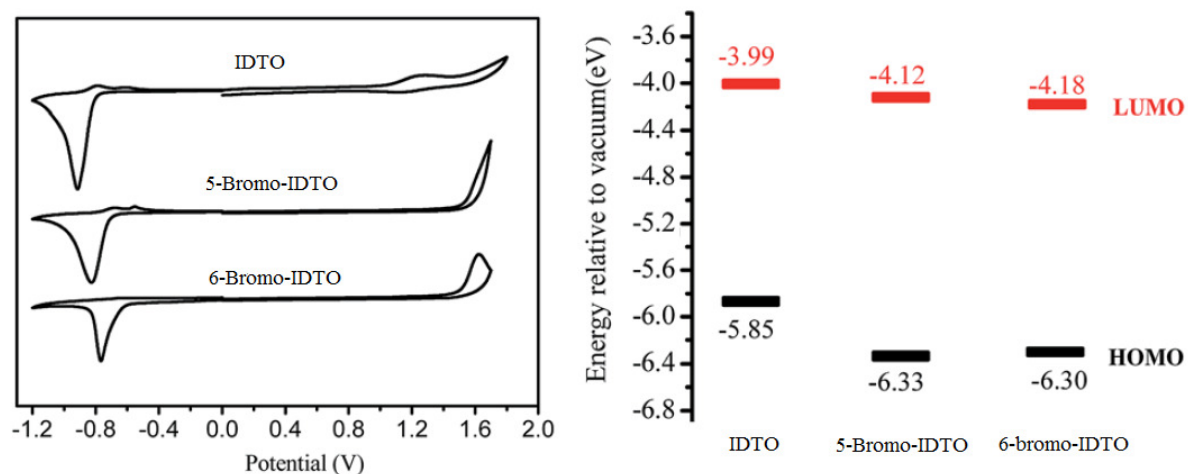


**Figure 3.5: CV measurements and energy level diagrams for the IDTO compounds.**

### 3.2.4 XRD and AFM: Solid State Properties

XRD and AFM were used to determine the crystallinity and morphology of thin films made of the three IDTO compounds. For each film, measurements were taken for non-annealed, 100 °C annealed and 150 °C annealed. Figure 3.6 shows the XRD plots and AFM images. XRD confirms that the films possess some molecular ordering and that annealing enhanced the crystallinity of the films in all cases. 5-bromo-IDTO showed the most intense primary peak out of the three compounds, suggesting a much more crystalline film. 6-bromo-IDTO on the other hand, surprisingly showed the weakest primary peak. IDTO had a primary peak at 7.3° which corresponds to an interlayer lamellar d-spacing of 12.1 Å. 5-bromo-IDTO had its primary peak at 5.6° for a d-spacing of 15.78 Å. Unlike the other compounds, 6-bromo-IDTO saw a shift in primary peak from 6.5° (d-spacing = 13.6 Å) for no annealing to 3.5° (d-spacing = 25.2 Å) after annealing. Larger d-spacing should decrease the observed mobility of 6-bromo-IDTO. Without further information, such as single crystal x-ray diffraction which would give more precise details about atomic arrangement, no conclusion can be drawn as to why 6-bromo-IDTO shows an increase in d-spacing after annealing. Although the AFM images are difficult to discern, a change in morphology is observed with increasing annealing temperature. Non-annealed films have worm-like domains that are well connected, whereas the annealed films show more circular domains. The circular domains could potentially impede charge transport due to gaps between grains. 6-bromo-IDTO shows smaller crystalline domains (most

noticeable at 150 °C annealing) as compared to the other compounds. Smaller domains would increase the resistance of the film and decrease overall mobility through the film.

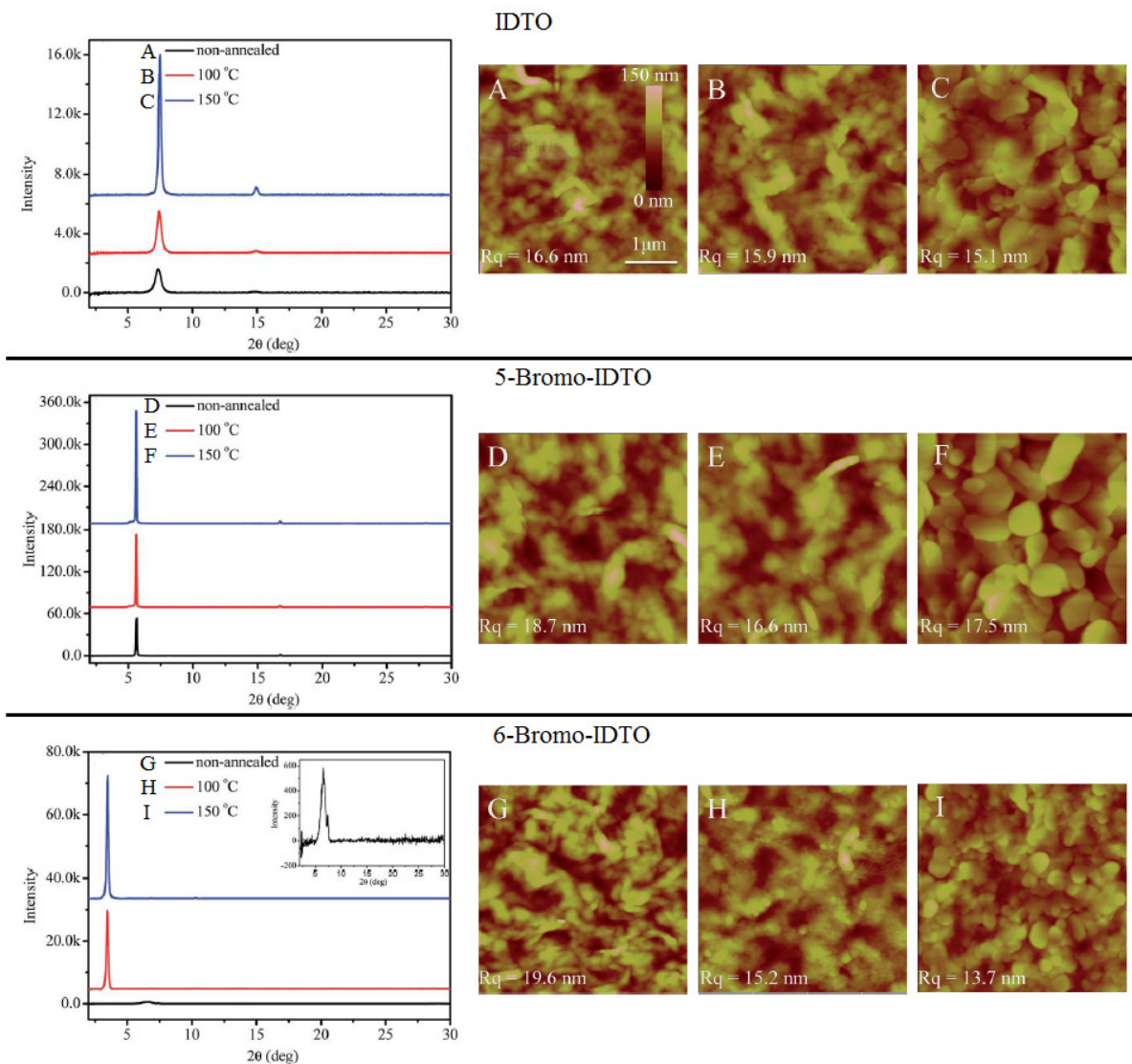


**Figure 3.6: XRD (right) and AFM (left) results for the IDTO compounds. Inset of 6-bromo-IDTO XRD is an enlarged view of non-annealed.**

### 3.2.5 OFET Evaluation

Bottom gate bottom contact OFET devices were fabricated using DDTs modified Si/SiO<sub>2</sub> substrates with patterned gold contacts. The IDTO compounds were spin-coated onto the substrates using 20 mg mL<sup>-1</sup> chloroform solutions at 5000 rpm for 60 seconds. All of the compounds were tested

with no annealing, 100 °C annealing and 150 °C annealing. All devices were fabricated and tested in a nitrogen environment.

All three IDTO compounds displayed unipolar n-type performance. The n-type output and transfer graphs can be found in Figure 3.7. P-type graphs are omitted since there is no p-type performance to be seen. All of the calculated OFET parameters are summarized in Table 3.2. The mobilities are found to be in the range of  $10^{-2}$  to  $10^{-1}$   $\text{cm}^2\text{V}^{-1}\text{s}^{-1}$ , with the largest mobility measured to be  $0.11 \text{ cm}^2\text{V}^{-1}\text{s}^{-1}$  for one of the non-annealed 6-bromo-IDTO devices. Threshold voltages,  $V_T$ , are fairly low (less than 20) and current on/off ratios,  $I_{\text{on}}/I_{\text{off}}$ , are high ( $\sim 10^4$ ). The trend that was observed in mobility is that mobility decreases with increasing annealing temperature. Degradation of the compounds is very unlikely at the temperatures tested according to the TGA measurements. Therefore, the decrease in mobility must be connected to how the film changes with annealing. XRD showed that crystallinity increased with annealing temperature which should have also increased mobility. However, as discussed before, AFM revealed a morphological change in the films as the films were annealed. The decrease in mobility with increasing annealing is then ascribed to the change from well connected worm-like domains to circular domains. Another trend observed is that mobility increases from IDTO to 5-bromo-IDTO to 6-bromo-IDTO. The bromine substitutions definitely benefit the overall charge transport. This can be attributed to the lower LUMO energy levels caused by the addition of bromine atoms. The lower LUMO energy levels facilitate better electron injection and transport.

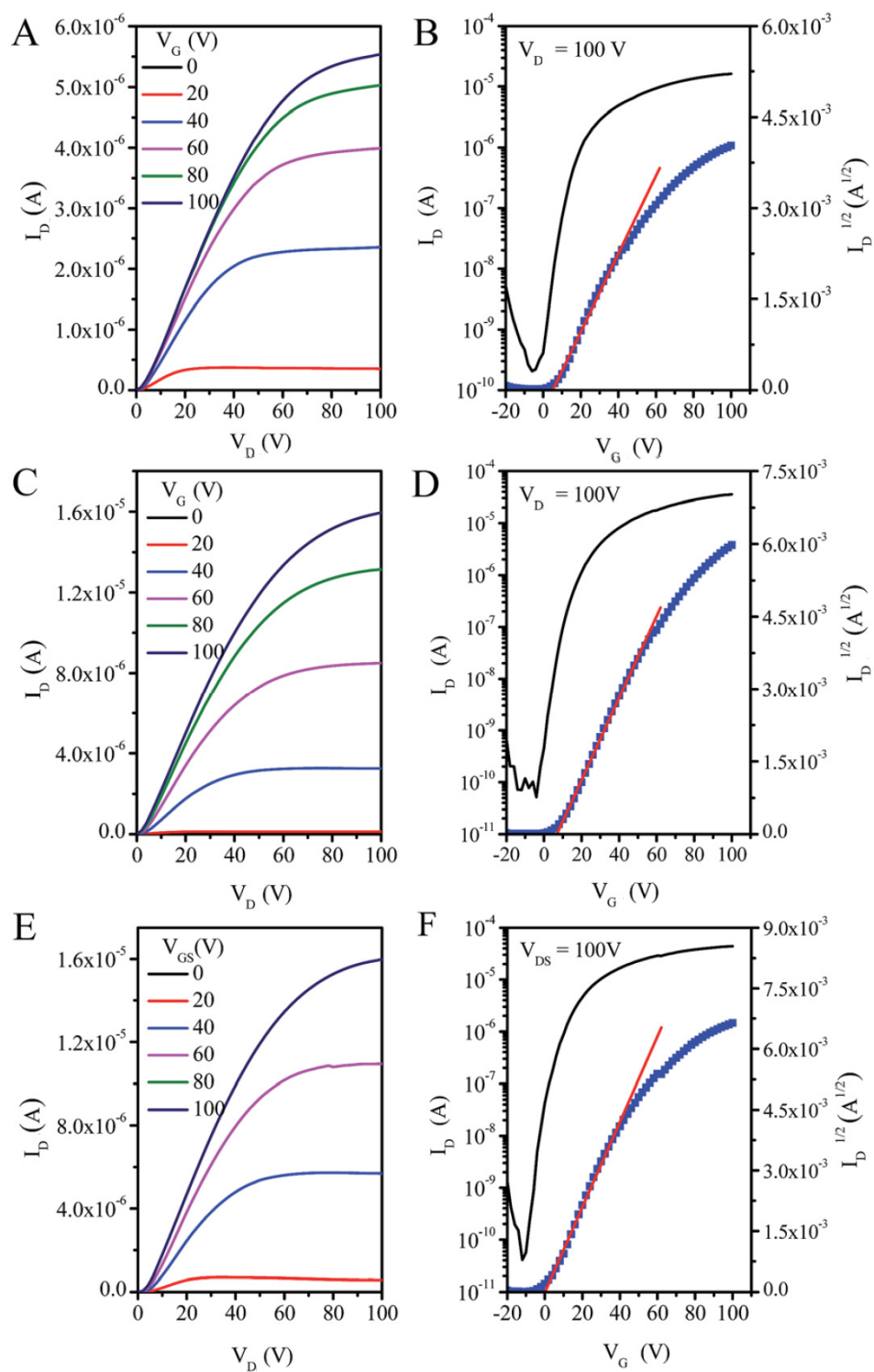


**Figure 3.7: Output (A, C and E) and transfer (B, D and F) graphs of IDTO (A and B), 5-bromo-IDTO (C and D) and 5-bromo-IDTO (E and F).**

**Table 3.2: OFET performance parameters for IDTO compounds.**

Compound	Annealing Temperature (°C)	$\mu_{\max}$ ( $\text{cm}^2\text{V}^{-1}\text{s}^{-1}$ )	$\mu_{\text{ave}} \pm \text{std}$ ( $\text{cm}^2\text{V}^{-1}\text{s}^{-1}$ )	$V_T$ (V) <sup>a</sup>	$I_{\text{on}}/I_{\text{off}}$
IDTO	Non-annealed	0.046	$0.041 \pm 0.0051$	6.6	$\sim 10^5$
	100	0.030	$0.022 \pm 0.0059$	7.2	$\sim 10^4$
	150	0.011	$0.008 \pm 0.0024$	6.9	$\sim 10^4$
5-bromo-IDTO	Non-annealed	0.071	$0.055 \pm 0.0095$	13.5	$\sim 10^5$
	100	0.053	$0.041 \pm 0.0900$	12.0	$\sim 10^4$
	150	0.029	$0.014 \pm 0.0055$	15.5	$\sim 10^4$
6-bromo-IDTO	Non-annealed	0.110	$0.093 \pm 0.0027$	3.5	$\sim 10^5$
	100	0.088	$0.069 \pm 0.0023$	5.0	$\sim 10^4$
	150	0.040	$0.027 \pm 0.0019$	3.9	$\sim 10^4$

<sup>a</sup> Average threshold voltage

The challenge faced when all of the information is put together is why does 6-bromo-IDTO have higher mobility than 5-bromo-IDTO? Obviously, the lower LUMO energy level plays a role but XRD and AFM both showed that 6-bromo-IDTO had lower crystallinity and worse morphology. The difference in LUMO energy levels between the two bromine substituted IDTO compounds is not large enough to be expected to outweigh the difference in film quality. Therefore, given the available information, the larger mobility of 6-bromo-IDTO is thought to be related to the extended delocalization of the LUMO wavefunction. The additional orbital overlap caused by the larger conjugation path could provide a better and more efficient intermolecular electron hopping pathway.

### 3.3 Conclusions

To develop new high performance unipolar n-type organic semiconductors, three thiophene-*S,S*-dioxidized indophenine compounds were synthesized and their OFET performance was tested. All three compounds, IDTO, 5-bromo-IDTO and 6-bromo-IDTO, demonstrated unipolar n-type characteristics with mobilities on the order of  $10^{-2}$  to  $10^{-1} \text{ cm}^2\text{V}^{-1}\text{s}^{-1}$ . As compared to the non oxidized parent molecule, indophenine showed ambipolar characteristics with mobilities one order of magnitude lower. The unipolarization of IDTO is due to the suppression of hole injection by a deep HOMO energy level. The increased mobility of IDTO is correlated to deeper LUMO energy levels and the absence of isomers. Bromine substitution onto the isatin units further lowered the energy levels and resulted in higher electron mobilities. 6-bromo-IDTO showed the highest mobility of up to

0.11  $\text{cm}^2\text{V}^{-1}\text{s}^{-1}$  due to the participation of the 6,6' position bromine atoms to the HOMO and LUMO wavefunctions, which resulted in a more extended conjugation. The three IDTO compounds exhibited good performance and provide a promising foundation for a new group of n-type, solution processable, small molecule organic semiconductors. Side chain engineering, different substituents and device optimization are just some of the strategies that could be explored to improve the performance of IDTO in OFETs.

## Chapter 4

### IDTO as a Polymeric N-type Organic Semiconductor

Again, this chapter is based on the results published in RSC Advances<sup>83</sup> in which I supported the main author, Dr. Deng, with the synthesis and characterization of the IDTO polymers. More specifically, I performed synthesis, work-up, purification, UV-Vis and CV for the polymers. The figures and data presented in this section are the same as what is presented in the publication. Two IDTO D-A polymers, PIDTOBT and PIDTOBTz, were synthesized for use as n-type organic semiconductors *via* Stille-coupling between IDTO-40 (accepting moiety) and organotin monomers (donating moiety) of bithiophene (BT) or bithiazole (BTz). Each polymer was characterized by <sup>1</sup>H NMR, TGA, DSC, DFT, UV-Vis and CV. Thin films of each compound were characterized by XRD and AFM. The OFET performance parameters were determined using bottom gate bottom contact devices.

#### 4.1 Experimental Details

##### 4.1.1 Synthesis

All starting materials were purchased from commercial sources and used without further purification. Synthesis of IDTO-40<sup>84</sup> and 5,5'-bis(trimethylstannyl)-2,2'-bithiazole<sup>85</sup> can be found according to reported methods. The polymers were synthesized using the following procedure. IDTO-40 (100 mg, 0.056 mmol), 5,5'-bis(trimethylstannyl)-2,2'-bithiophene/5,5'-bis(trimethylstannyl)-2,2'-bithiazole (28.34/28.46 mg, 0.056 mmol) and tri(*o*-tolyl)phosphine (1.36 mg, 8 mol%) were added to a dry Schlenk flask. The flask was degassed and refilled with argon three times before a solution of tris(dibenzylideneacetone)-dipalladium (1.03 mg, 2 mol%) in dry chlorobenzene (4 mL) was added under argon. The flask was sealed and the mixture was stirred at 130 °C for 48 hours. Then, four drops of bromobenzene were added followed by an additional 12 hours of stirring at 130 °C. After the mixture was cooled to room temperature, the mixture was added dropwise into methanol (100 mL) and stirred for one hour. The precipitated product was collected by filtration. Purification to remove oligomers was performed by consecutive Soxhlet extractions using acetone, hexane and then chloroform. Finally, the product was dissolved and precipitated from methanol one more time affording PIDTOBT/PIDTOBTz as a dark solid. High temperature GPC at 140 °C yielded  $M_n$  of 25.9 kDa with a PDI of 2.7 for PIDTOBT and  $M_n$  of 14.3 kDa with a PDI of 2.5 for PIDTOBTz. The

lower molecular weight of PIDTOBTz is thought to be due to some decomposition of the more unstable BTz monomer during polymerization. The polymerization reaction schemes are shown in Figure 4.1. NMR measurements for the IDTO polymers can be found in Appendix C. Specific details about the chemical used can be found in Appendix A.

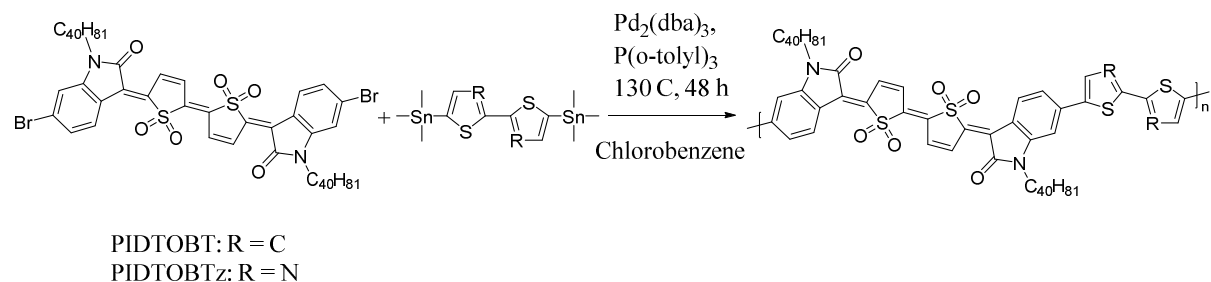


**Figure 4.1: General reaction scheme for IDTO polymers *via* Stille-coupling polymerization.**

#### 4.1.2 Characterization

NMR data were recorded using a Bruker DPX 300 MHz spectrometer. The chemical shifts of  $^1\text{H}$  NMR were referenced to tetramethylsilane (TMS, 0 ppm). Elemental analysis was performed on a VarioEL elemental analysis system. GPC measurements were performed on Malvern HT-GPC at 140 °C using 1,2,4-trichlorobenzene as the eluent and polystyrene as standards. The polymer solutions were pre-dissolved at 170 °C for at least 2 h. DFT calculations were performed with the 6-311G+(d,p) basis set and the orbital diagrams were obtained using GaussView 5.0 software. TGA and DSC were carried out on a TA Instruments SDT 2960 and a Perkin-Elmer DSC 7, respectively, at a scan rate of 10 °C  $\text{min}^{-1}$  under nitrogen. UV-Vis spectra were recorded on a Thermo Scientific Genesys 10 UV instrument using 1,1,2,2-tetrachloroethane (TCE) solutions ( $10^{-5}$  M) and films spin-coated onto quartz substrates (5 mg  $\text{mL}^{-1}$  TCE solutions). CV data were obtained on a CHI600E electrochemical analyzer in dry acetonitrile. 0.1 M  $n\text{-Bu}_4\text{NPF}_6$  was used as the electrolyte and the experiment was done under nitrogen at a scan rate of 100  $\text{mV s}^{-1}$ . A three-electrode cell was used. The working and counter electrodes were platinum, and the reference electrode was Ag/AgCl. Ferrocene was used as a reference, which has a HOMO energy level of -4.8 eV. XRD plots of the thin films spin-coated on DDTS-modified Si/SiO<sub>2</sub> substrates were obtained using a Bruker D8 Advance powder Diffractometer with standard Bragg-Brentano geometry. Cu  $K_{\alpha 1}$  radiation ( $\lambda = 1.5406 \text{ \AA}$ ) was used. The same samples were used to record AFM images with a Dimension 3100 scanning probe microscope.

## 4.2 Results and Discussion

### 4.2.1 DFT: Theoretical Calculation

DFT computer simulations were performed for both polymers using model dimers. The results are graphically presented in Figure 4.2. Overall, the model shows a fairly planar geometry. The IDTO segments are completely planar while there is slight twisting of  $\sim 20^\circ$  between IDTO and thiophene/thiazole segments. The BT segment has a  $0.8^\circ$  dihedral angle while the BTz segment is nearly planar. The calculated HOMO and LUMO energy levels for the IDTOBT dimer are  $-5.32$  eV and  $-3.55$  eV, respectively. The energy levels are lowered for the IDTOBTz dimer to  $-5.64$  eV and  $-3.67$  eV due to the BTz segments being more electron withdrawing than BT. Lastly, the electron density distributions of both dimers are relatively the same. The HOMO wavefunctions are extended across the majority of the backbone while the LUMO wavefunctions are centralized more to the IDTO segments.

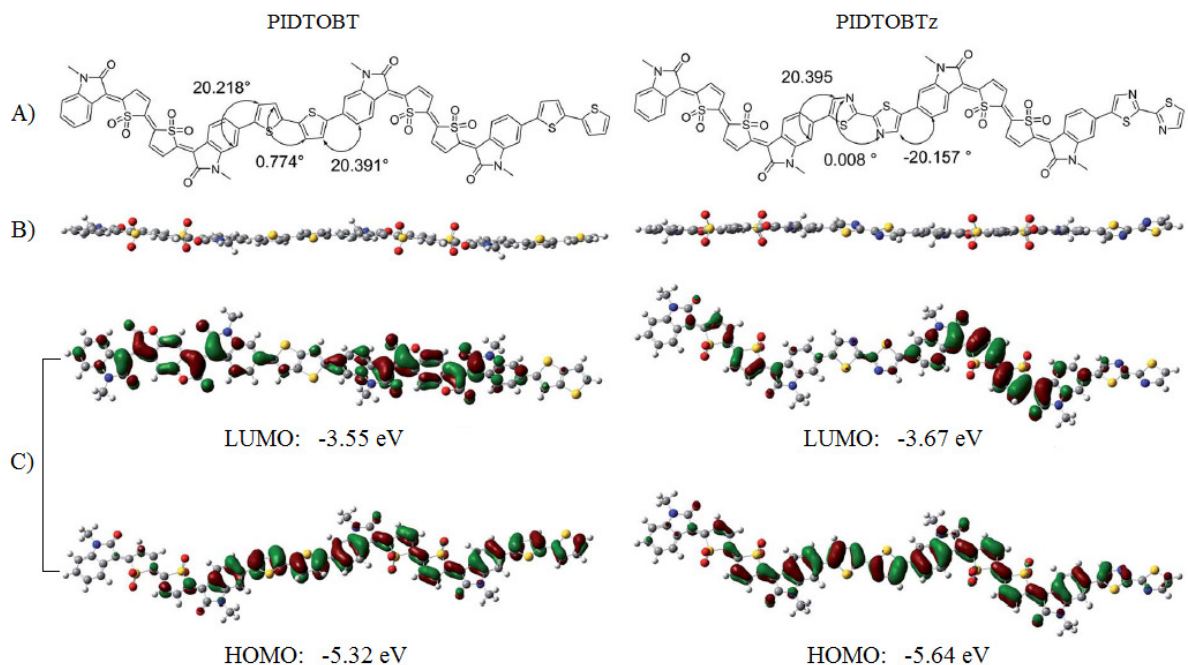


**Figure 4.2:** A) Chemical structures, B) optimized geometries and C) electron density distributions obtained from DFT calculations for the IDTO polymers.

#### 4.2.2 TGA and DSC: Thermal Properties

TGA and DSC measurements are displayed in Figure 4.3. TGA concluded that both polymers are thermally stable up to ~260 °C where PIDTOBTz starts to lose some mass. PIDTOBT shows a similar decrease in mass starting at ~310 °C. A two step degradation is observed for the IDTO polymers similar to that of IDTO small molecules. The first degradation step is attributed to loss of SO<sub>2</sub> from the IDTO segments and the second degradation step is decomposition of the remainder of the polymer. DSC showed no transition temperatures.

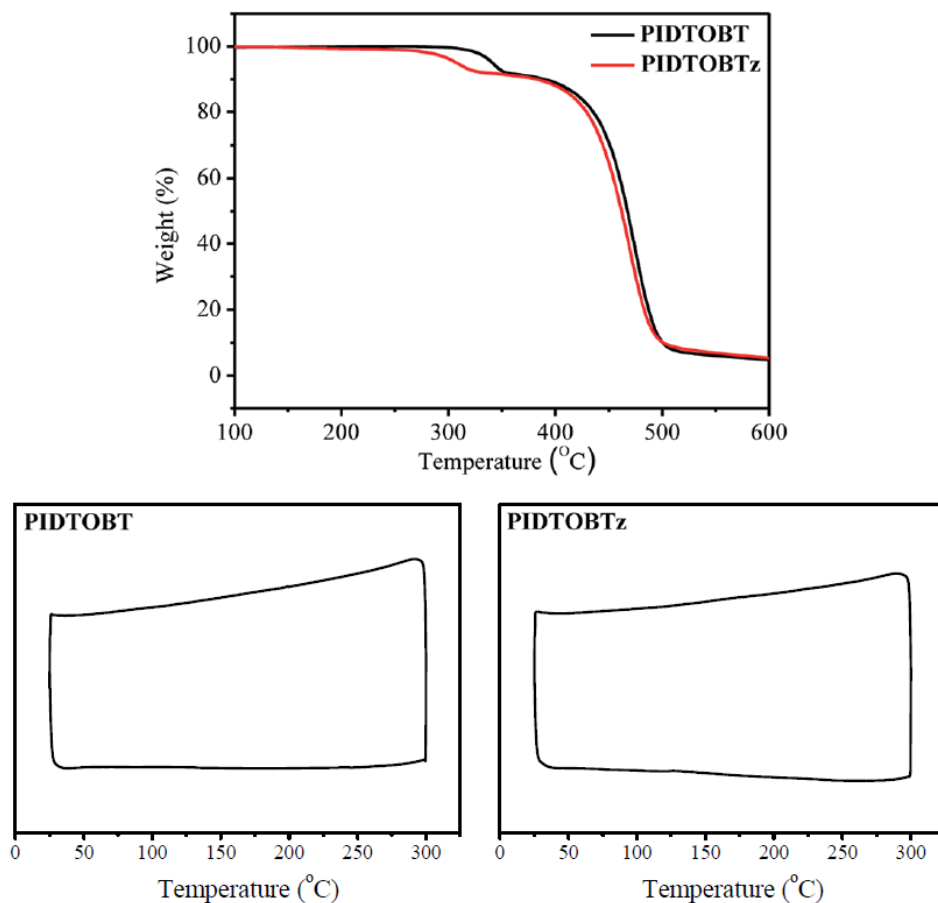


**Figure 4.3: TGA (top) and DSC (bottom) for the IDTO polymers.**

#### 4.2.3 UV-Vis and CV: Optical and Electrochemical Properties

UV-Vis spectra (Figure 4.4) were collected for the polymers using both dilute 1,1,2,2-tetrachloroethane (TCE) solutions and thin films on quartz. The absorption profiles do not change significantly from solution to film, indicating that there is some pre-aggregation of the polymers in

solution. This phenomena has been seen in other D-A polymers as well<sup>86-88</sup>. The  $\lambda_{\text{max}}$  of PIDTOBT and PIDTOBTz are 780 nm and 636 nm, respectively. The more electron withdrawing BTz segments are the likely reason for PIDTOBTz having a shorter  $\lambda_{\text{max}}$ . The optical band gaps are calculated to be 1.43 eV for PIDTOBT and 1.62 eV for PIDTOBTz. The data for UV-Vis is presented in Table 4.1.

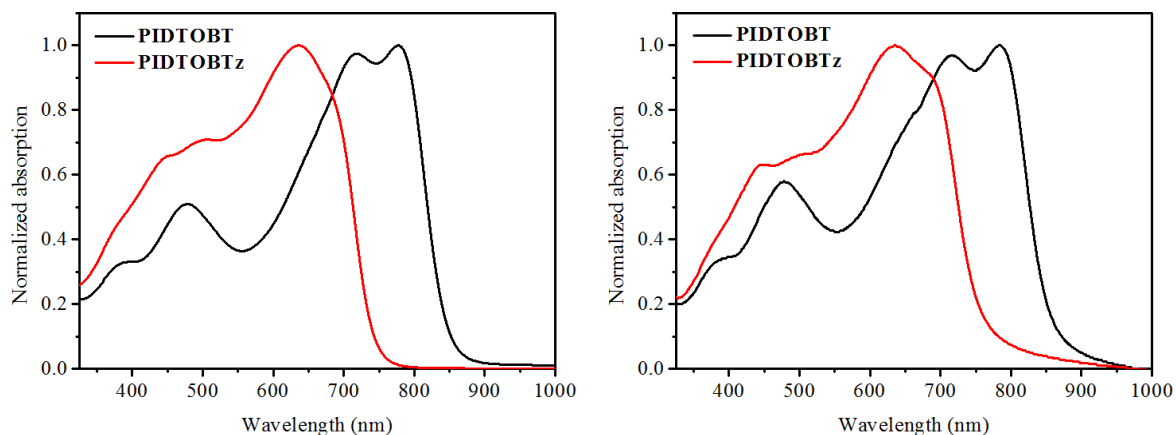


**Figure 4.4:** UV-Vis spectra for the IDTO polymers in solution (left) and thin film (right).

**Table 4.1:** UV-Vis absorption properties of IDTO polymers.

Compound	$\lambda_{\text{max}}$ (nm)		$E_{\text{g}}^{\text{opt}}$ (eV)
	Solution	Thin film	
PIDTOBT	381 (s) <sup>a</sup> , 476 (s), 719 (s), 780	387 (s), 475 (s), 717 (s), 782	1.43
PIDTOBTz	448 (s), 504 (s), 636, 688 (s)	446 (s), 503 (s), 636, 687 (s)	1.62

<sup>a</sup> Shoulder

CV measurements, shown in Figure 4.5, exhibit clear oxidation and reduction peaks for both polymers. The HOMO and LUMO energy levels of PIDTOBT are calculated to be -5.78 eV and -4.09 eV, respectively. PIDTOBTz possesses slightly lower energy levels at -5.99 eV for HOMO and -4.18 eV for LUMO. The measured trend in energy levels is in good agreement with that of the DFT calculations. The electrochemical band gaps are calculated to be 1.69 eV for PIDTOBT and 1.81 eV for PIDTOBTz.

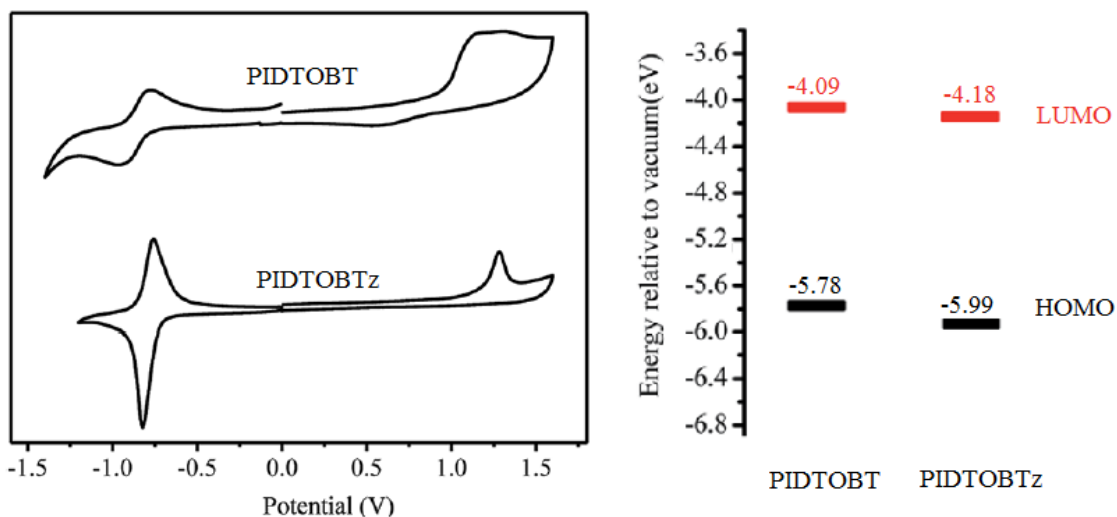


**Figure 4.5: CV measurements and energy level diagrams for the IDTO polymers.**

#### 4.2.4 XRD and AFM: Solid State Properties

The polymers were spin coated onto substrates and characterized by XRD and AFM at the three annealing temperature of 100 °C, 150 °C and 200 °C, shown in Figure 4.6. The polymer films show no noticeable peaks except for PIDTOBT at 200 °C annealing. The one weak primary peak is measured at  $2\theta = 3.4^\circ$  which corresponds to a d-spacing of 26.0 Å. This suggests that PIDTOBT is gaining some crystallinity at higher annealing temperatures, whereas PIDTOBTz is not changing very much with annealing. The AFM images are in agreement with the XRD findings. PIDTOBT has small interconnected grains which increase in size with annealing, indicating gradual development of crystallinity. PIDTOBTz has very small grains that are not well connected. The grains only slightly increase in size with annealing.

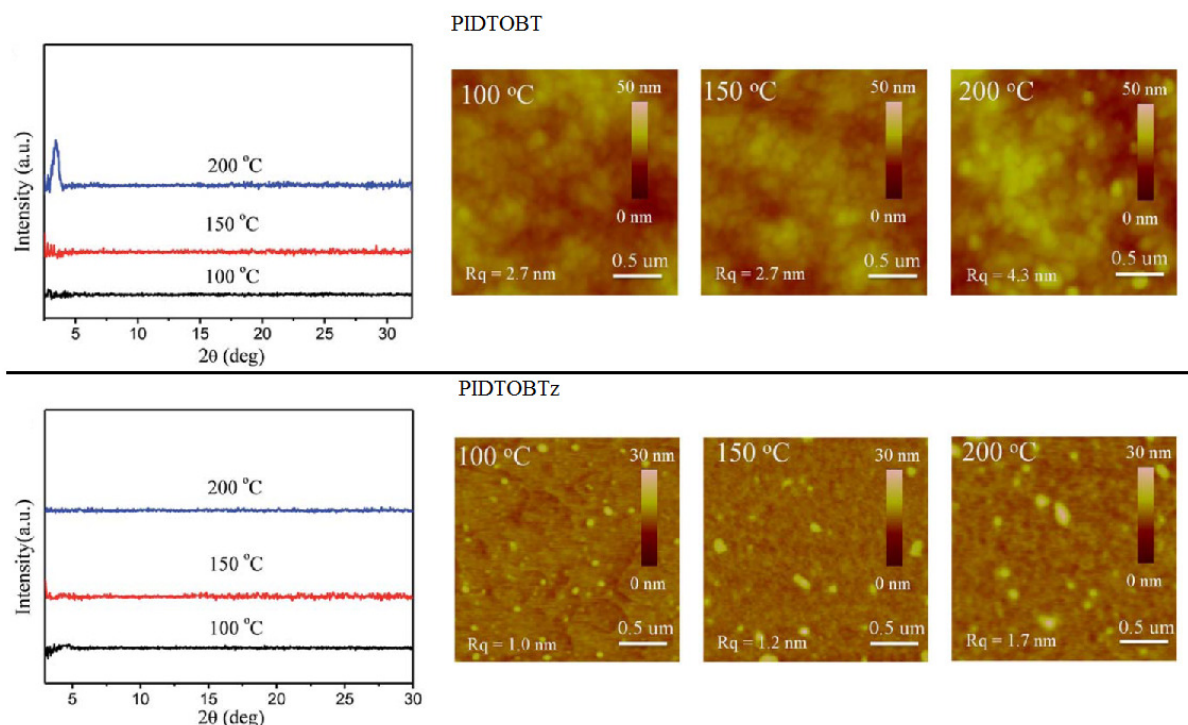


**Figure 4.6: XRD (right) and AFM (left) results for the IDTO polymers.**

#### 4.2.5 OFET Evaluation

Bottom gate bottom contact OFET devices were fabricated using DDTs modified Si/SiO<sub>2</sub> substrates with patterned gold contacts. The IDTO polymers were spin-coated onto the substrates using a 5 mg mL<sup>-1</sup> TCE (PIDTOBT) or chloroform (PIDTOBTz) solution at 3000 rpm for 60 seconds. The polymers were tested with 100 °C annealing, 150 °C annealing and 200 °C annealing. All devices were fabricated and tested in a nitrogen environment. The 200 °C annealed devices were also tested in ambient atmosphere.

The results, shown in Figure 4.7 and Table 4.2, confirm that the two polymers have n-type characteristics. The electron mobilities are in the range of 10<sup>-2</sup> to 10<sup>-1</sup> cm<sup>2</sup>V<sup>-1</sup>s<sup>-1</sup> with the highest mobility measured to be 0.18 cm<sup>2</sup>V<sup>-1</sup>s<sup>-1</sup>. As expected based on the XRD and AFM data, it was found that the mobility of PIDTOBT increased with annealing while the mobility of PIDTOBTz did not change with annealing. The threshold voltages are close to 0 V for PIDTOBT and less than 20 V for PIDTOBTz. Current on/off ratios are large (~10<sup>4</sup>) for both polymers. PIDTOBT shows significantly better performance than PIDTOBTz which is attributed to the poor crystallinity and low molecular weight of PIDTOBTz. To evaluate the air stability of both polymers, the 200 °C annealed devices

were tested in ambient atmosphere. PIDTOBT saw a ~40% drop in mobility whereas PIDTOBTz only had a ~24% drop. The slightly better air stability of PIDTOBTz can be credited to its lower LUMO energy level.

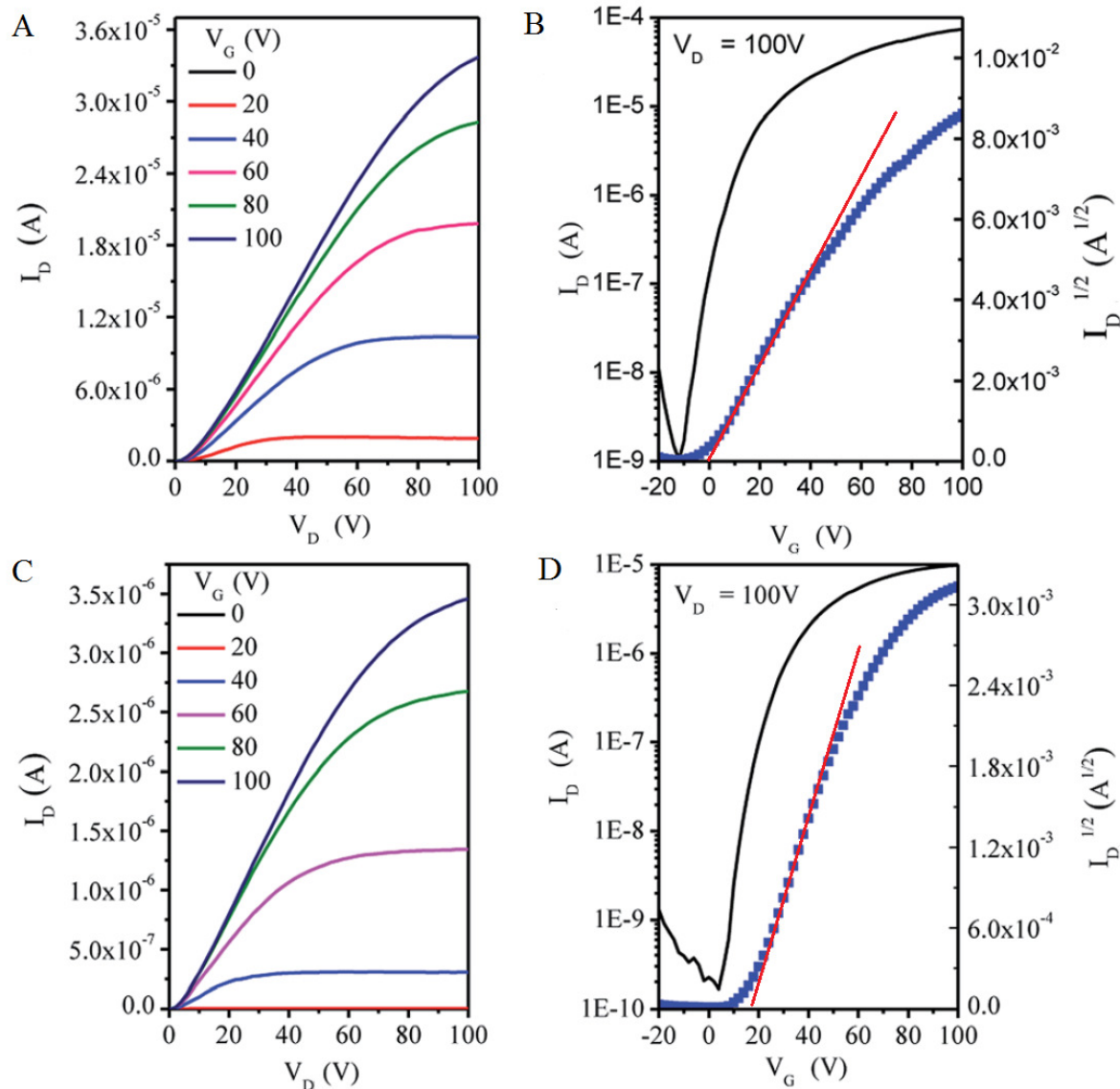


**Figure 4.7: Output (A and C) and transfer (B and D) graphs of PIDTOBT (A and B) and PIDTOBTz (C and D).**

**Table 4.2: OFET performance parameters for IDTO polymers.**

Compound	Annealing Temperature (°C)	$\mu_{\max}$ ( $\text{cm}^2\text{V}^{-1}\text{s}^{-1}$ )	$\mu_{\text{ave}} \pm \text{std}$ ( $\text{cm}^2\text{V}^{-1}\text{s}^{-1}$ )	$V_T$ (V) <sup>a</sup>	$I_{\text{on}}/I_{\text{off}}$
PIDTOBT	100	0.072	$0.060 \pm 0.0091$	3.4	$\sim 10^5$
	150	0.125	$0.110 \pm 0.0120$	2.5	$\sim 10^5$
	200	0.180	$0.140 \pm 0.0153$	2.3	$\sim 10^5$
PIDTOBTz	100	0.016	$0.015 \pm 0.0001$	19.2	$\sim 10^5$
	150	0.017	$0.016 \pm 0.0015$	15.6	$\sim 10^5$
	200	0.016	$0.014 \pm 0.0019$	18.0	$\sim 10^5$

<sup>a</sup> Average threshold voltage

### 4.3 Conclusions

Two IDTO-based polymers, PIDTOBT and PIDTOBTz, were synthesized for use as unipolar n-type organic semiconductors. Both polymers exhibited mediocre electron mobilities on the order of  $10^{-2}$  to  $10^{-1} \text{ cm}^2\text{V}^{-1}\text{s}^{-1}$ . PIDTOBTz had lower performance out of the two polymers because it had poor crystallinity and nearly half the molecular weight. However, PIDTOBTz showed better air stability than PIDTOBT because of a deeper LUMO energy level. Overall, both polymers demonstrated decent performance as unipolar n-type organic semiconductors. It is expected that higher mobilities could be achieved if the crystallinity of the polymers is improved. Methods to improve crystallinity could include incorporation of different comonomers, side chain engineering and/or device optimization.

## Chapter 5

### IDTO Additive Blended with Ambipolar Polymer

#### 5.1 Introduction

IDTO has proven to be a good n-type organic semiconductor whether as a small molecule or in a polymer. The question now becomes, is there more ways to use IDTO? A possible answer is to blend IDTO with other material to produce a positive effect. In the past, small molecule organic semiconductors have been blended with polymers to improve the performance of the OFET<sup>89-93</sup>. Small molecules typically have high crystallinity resulting in high mobilities but they can encounter difficulties with solution processing such as non-uniform films and dewetting which makes them impractical. Polymers on the other hand, suffer from the opposite. Polymers usually have great film forming characteristics but low crystallinity which reduces mobility. By blending small molecules with polymers it is possible to find a middle ground of good film quality and high mobility. However, IDTO small molecules do not suffer from poor film quality and thus blends using IDTO must serve a different purpose.

More recently, it was observed that the OFET charge transport behavior of a polymer could be tuned by addition of small molecules as a dopant. Ambipolar polymers could be converted into n-type or p-type depending on what small molecule was added<sup>94,95</sup>. A similar effect was observed with a polymer/polymer blend where ambipolar and even p-type polymers could be change to n-type devices<sup>96</sup>. This tunability of charge transport behavior was attributed to hole or electron trapping effects. Charge carrier trapping had a greater effect when the trapping energy exceeded 0.25 eV. The trapping energy is defined as the difference in HOMO/LUMO energy of the polymer to that of the dopant. That is, for electron trapping, the LUMO energy level of the polymer should be higher than that of the dopant. In a similar manner, hole trapping occurs when the HOMO energy level of the polymer is lower than the dopant. The trapping phenomena take places when a charge carrier hops into a more favorable energy level but is unable to hop back. For example, a polymer with a LUMO of -4 eV is doped with a molecule with a LUMO of -4.5 eV. Electrons are injected into the polymers and travel through the polymers at the -4 eV energy level. When the electrons encounter the dopants, the electrons are driven to hop into the -4.5 eV energy level because electrons prefer lower energy levels. The electrons become trapped on the dopants because there is not sufficient external energy (typically thermal energy and the applied bias) to push the electrons off the dopants. The value of

0.25 eV mentioned earlier was experimentally observed to be approximately the barrier size where ambient thermal energy and the applied bias could assist in freeing charge carriers from the dopants. Since IDTO has very deep energy levels, it would be difficult for IDTO to trap holes but its low LUMO energy level could be suitable for electron trapping. This chapter investigates the electron trapping effect of IDTO small molecules for the purpose of converting ambipolar polymer devices to p-type.

To test the electron trapping of IDTO it is necessary to find an ambipolar polymer with a suitable LUMO energy level. However, to prove the trapping is caused by the difference in LUMO energy levels, it is important to show that IDTO and the chosen polymer have no negative interactions which could cause similar effects. To do this, it is desired to see both trapping and no trapping for the IDTO/polymer blend. The only way to observe both effects is to use multiple IDTO compounds of differing LUMO energy levels. Therefore, three IDTO compounds are used: IDTO, 5-bromo-IDTO and 6-bromo-IDTO. The LUMO energy levels are -3.99 eV, -4.12 eV and -4.18 eV, respectively. To observe both trapping and no trapping, an ambipolar polymer with a LUMO energy level that is between -3.74 eV and -3.93 eV must be chosen. This allows the trapping energy to be less than 0.25 eV for IDTO but greater than 0.25 eV for 6-bromo-IDTO. The observed effect for 5-bromo-IDTO will depend on whether the polymer LUMO energy level is above or below -3.87 eV. Figure 5.1 visually demonstrates the criteria for the LUMO energy of the suitable polymers. Assuming the three IDTO compounds behave the same in a blend with the chosen polymer, IDTO should not trap electrons while 6-bromo-IDTO should trap electrons.

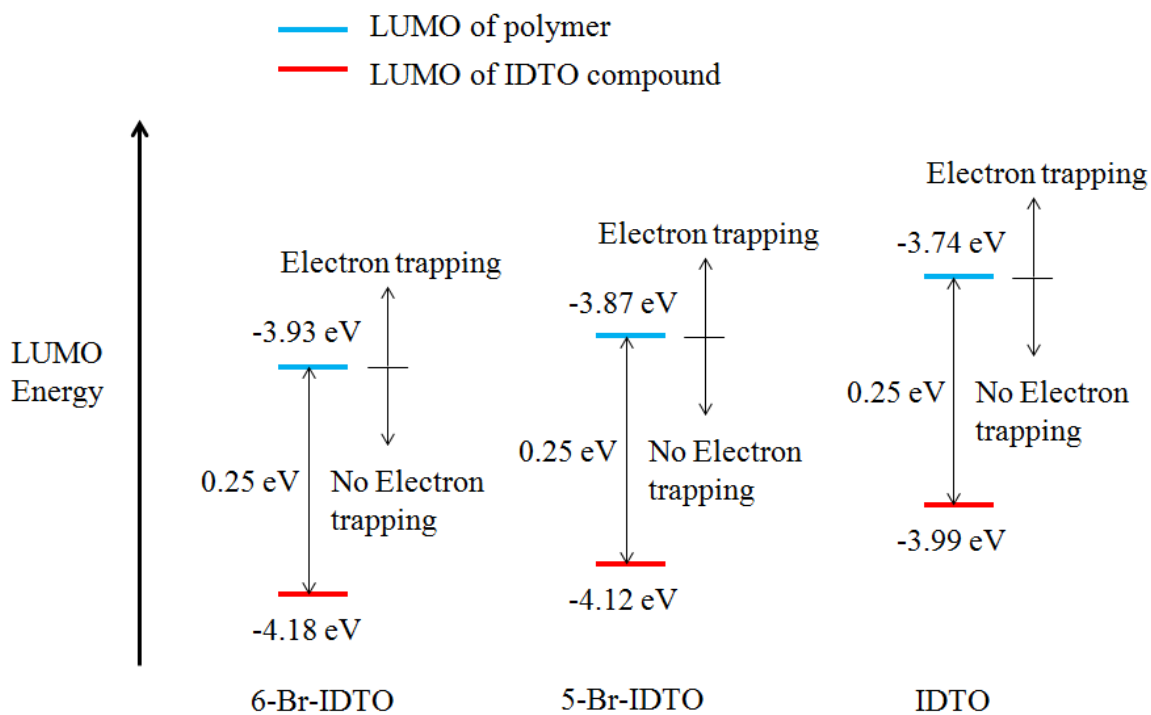


**Figure 5.1: LUMO energy level diagram for the selection of suitable polymers.**

As a starting point and for convenience, PINDFBT (TT) and PINDFBT (HH) were chosen as polymers to be blended with IDTO. These two polymers were previously synthesized by Dr Chang Guo, another member of Dr. Li's research group, following the published procedure for PINDFBT<sup>97</sup> except with the addition of dodecyl chains on the thiophene units in a tail-to-tail or head-to-head configuration. Figure 5.2 details the synthesis procedure for the two polymers. Both polymers exhibit ambipolar charge transport and LUMO energy levels of -3.78 eV and -3.77 eV for PINDFBT (TT) and PINDFBT (HH), respectively. These characteristics make these polymers suitable to assess electron trapping by IDTO.

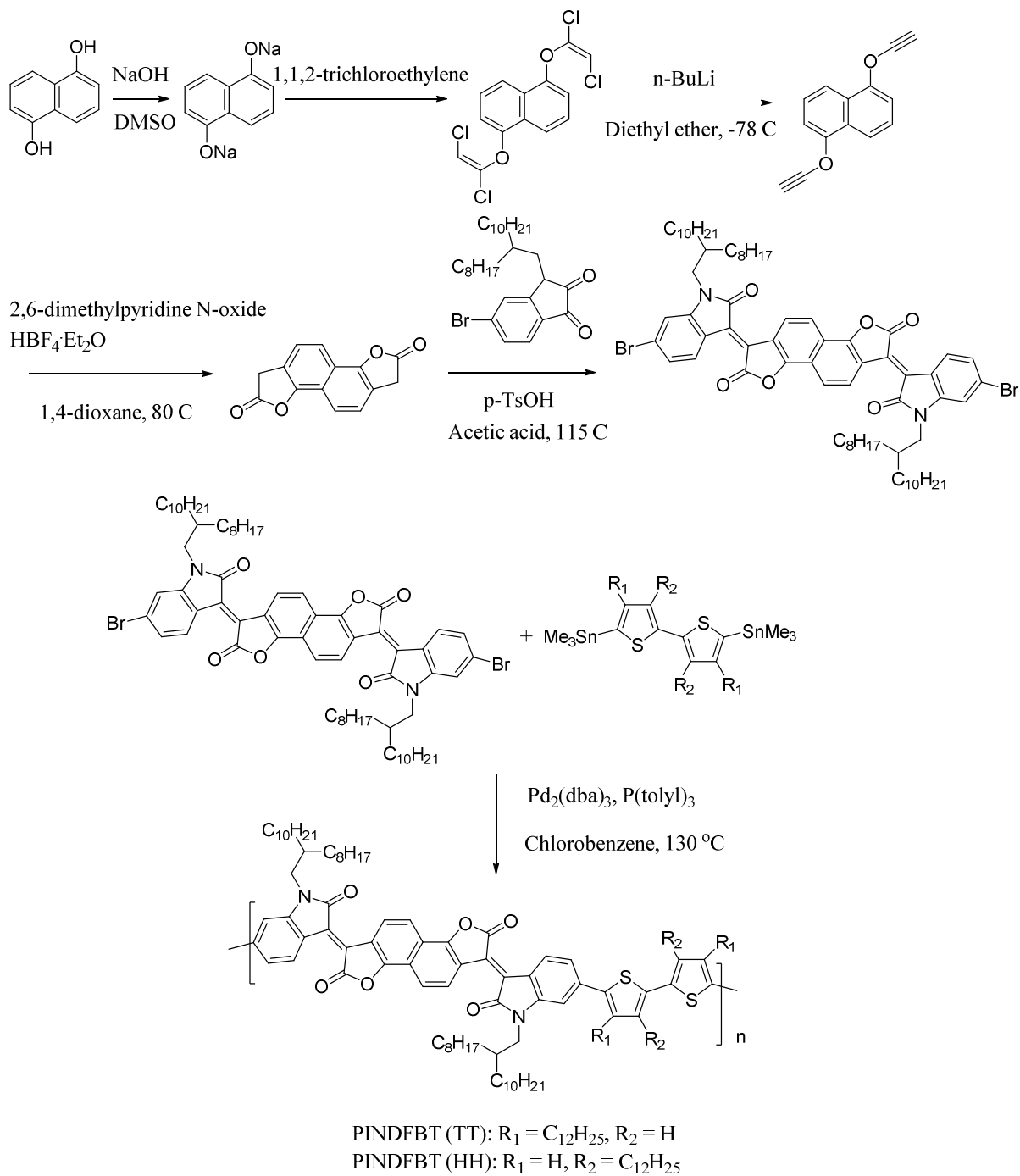


**Figure 5.2: Reaction scheme for PINDFBT (TT) and PINDFBT (HH).**

## 5.2 Experimental Details

Blends of 0%, 2%, 5% and 10% IDTO compound by weight with PINDFBT (TT) were first prepared to evaluate the effectiveness of the IDTO compounds to trap electrons. Each blend solution had a total weight concentration of 5 mg mL<sup>-1</sup> and the solvent was anhydrous chloroform. I.e. 0% blend = 5 mg of polymer in 1 mL of chloroform, 2% blends = 0.1 mg of IDTO plus 4.9 mg of polymer in 1 mL of chloroform, 5% blends = 0.25 mg of IDTO plus 4.75 mg of polymer in 1 mL of chloroform, and 10% blends = 0.5 mg of IDTO plus 4.5 mg of polymer in 1 mL of chloroform. Bottom gate bottom contact devices were fabricated using DDTs modified Si/SiO<sub>2</sub> substrates. Gold contacts were patterned to the substrate following conventional photolithography methods discussed in previous sections. The blend solutions were spin coated onto the cleaned substrates at 3000 rpm for 60 seconds followed by 20 minutes of drying at 80 °C. Annealing at higher temperatures were avoided due to potential phase separation which was observed in a previous study<sup>94</sup>. The 5% and 10% blends were also tested using 50 °C drying to investigate how lower temperatures might affect the mobilities. Next, similar blends were prepared with PINDFBT (HH) but drying was done only at 50 °C. All devices were fabricated and tested in a nitrogen environment.

## 5.3 Results and Discussion

Table 5.1 summarizes the results obtained for all of the PINDFBT (TT) blends. Since complete suppression of electron transport was not observed, a mobility ratio of electron mobility to hole mobility is used to quantify the relative strength of electron trapping. Essentially, as the electron mobility decreases due to hindrance by the IDTO compounds, the ratio will also decrease. Ideally, a ratio of zero is desired as that would mean complete suppression of electron transport

**Table 5.1: OFET performance parameters for PINDFBT (TT) / IDTO compound blends.**

Name	T (°C)	$\mu_e$ (cm <sup>2</sup> V <sup>-1</sup> s <sup>-1</sup> ) <sup>a</sup>	$\mu_h$ (cm <sup>2</sup> V <sup>-1</sup> s <sup>-1</sup> )	$V_{th,e}$ (V) <sup>b</sup>	$V_{th,h}$ (V)	$I_{on}/I_{off}$	$\mu_e/\mu_h$
PINDFBT (TT)	80	0.0148 (0.0098)	0.0063 (0.0048)	18	-32	10 <sup>2</sup>	2.36
2% IDTO	80	0.0197 (0.0043)	0.0137 (0.0034)	25	-25	10 <sup>2</sup> - 10 <sup>3</sup>	1.44
5% IDTO	80	0.0063 (0.0025)	0.0033 (0.0026)	22	-43	10 <sup>3</sup> - 10 <sup>5</sup>	1.90
	50	0.0067 (0.0022)	0.0031 (0.0025)	31	-29	10 <sup>3</sup> - 10 <sup>6</sup>	2.12
10% IDTO	80	0.0067 (0.0022)	0.0017 (0.0008)	19	-25	10 - 10 <sup>3</sup>	3.84
	50	0.0050 (0.0029)	0.0019 (0.0011)	29	-18	10 <sup>2</sup> - 10 <sup>3</sup>	2.69

Name	T (°C)	$\mu_e$ (cm <sup>2</sup> V <sup>-1</sup> s <sup>-1</sup> ) <sup>a</sup>	$\mu_h$ (cm <sup>2</sup> V <sup>-1</sup> s <sup>-1</sup> )	V <sub>th,e</sub> (V) <sup>b</sup>	V <sub>th,h</sub> (V)	I <sub>on</sub> /I <sub>off</sub>	$\mu_e/\mu_h$
2% 5-Br-IDTO	80	0.0117 (0.0036)	0.0100 (0.0034)	24	-20	10 <sup>2</sup> - 10 <sup>3</sup>	1.18
5% 5-Br-IDTO	80	0.0033 (0.0014)	0.0050 (0.0011)	18	-33	10 <sup>2</sup> - 10 <sup>3</sup>	0.66
	50	0.0012 (0.0004)	0.0050 (0.0005)	22	-24	10 <sup>2</sup> - 10 <sup>5</sup>	0.25
10% 5-Br-IDTO	80	0.0026 (0.0010)	0.0065 (0.0018)	21	-31	10 <sup>2</sup> - 10 <sup>5</sup>	0.40
	50	0.0007 (0.0004)	0.0062 (0.0018)	25	-21	10 <sup>3</sup> - 10 <sup>6</sup>	0.11
2% 6-Br-IDTO	80	0.0088 (0.0030)	0.0164 (0.0072)	41	-31	10 <sup>2</sup> - 10 <sup>5</sup>	0.53
5% 6-Br-IDTO	80	0.0004 (0.0020)	0.0053 (0.0027)	- <sup>c</sup>	-15	10 - 10 <sup>5</sup>	0.07
	50	10 <sup>-5</sup> (10 <sup>-5</sup> )	0.0052 (0.0038)	-	-9	10 - 10 <sup>5</sup>	0.02
10% 6-Br-IDTO	80	10 <sup>-5</sup> (10 <sup>-5</sup> )	0.0013 (0.0010)	-	-23	10 <sup>3</sup> - 10 <sup>5</sup>	0.01
	50	10 <sup>-5</sup> (10 <sup>-5</sup> )	0.0021 (0.0016)	-	-17	10 <sup>2</sup> - 10 <sup>6</sup>	0.01

<sup>a</sup> Average mobility (standard deviation), <sup>b</sup> average threshold voltage, <sup>c</sup> mobility too low to get an accurate threshold voltage

Firstly, the devices dried at 80 °C in general have a higher mobility ratio than the devices dried at 50 °C. This is due to the electron mobility increasing but little to no change in the hole mobility. Next, when the data for the 80 °C devices are presented in Figure 5.3 -Figure 5.8, several patterns can be observed. Regarding the relative strength of electron trapping, it is clear that IDTO is the weakest while 6-bromo-IDTO is the strongest. This pattern agrees with what was expected from the LUMO energy levels of the three IDTO compounds. In terms of the mobilities, 2% blends generally showed an increase while 5% blends had a slight decrease and 10% blends had an even greater decrease. The increase in mobility at 2% is possibly due to the IDTO compounds acting as an anti-plasticizer at low concentrations. By improving the crystallinity of the polymer as an anti-plasticizer, the film quality could be improved resulting in a higher observed mobility. However, in larger amounts the IDTO compounds become more like an impurity interrupting the packing of the polymer molecules resulting in lower mobilities. XRD and possibly AFM would be needed to verify if this is truly the case. An interesting observation was made when looking at the mobility ratios at different blend amounts for the same compound. The ratio is increased as the amount of IDTO is increased but the opposite effect is seen for the brominated IDTO compounds. This trend is likely to be the result of the trapping energies of the compounds. Since IDTO has a trapping energy less than the ~0.25 eV barrier, hole mobility and electron mobility change by approximately the same absolute value. As both mobilities decrease at larger amounts of IDTO, the ratio increases. On the other hand,

the brominated IDTO compounds with trapping energy greater than the  $\sim 0.25$  eV barrier see a larger decrease in electron mobility than the hole mobility. Therefore, the ratio decreases as the amount of brominated IDTO increases. Unipolar p-type is almost achieved when 6-Bromo-IDTO is blended at 5% or greater. Unfortunately, the hole mobility becomes quite low as well. For a test of concept, these results are promising as the data shows the expected trends. There is much more that can be done to add and improve to the results present here. As mentioned before, XRD and AFM would add useful information about the crystallinity and morphology of the blends. Blending with other polymers of higher mobilities and different LUMO energy levels could realize complete suppression of electron transport while maintaining a decent hole mobility. Finally, investigating different annealing temperatures could information about phase separation.

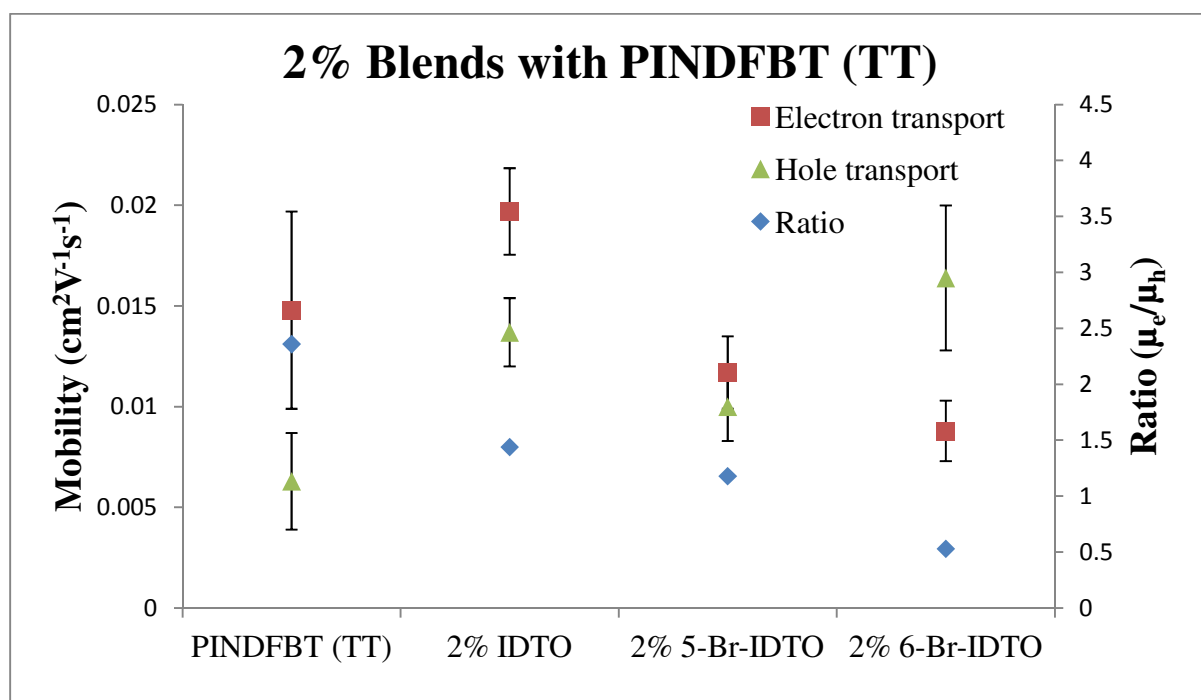


**Figure 5.3: Comparison of 2% blends with PINDFBT (TT).**

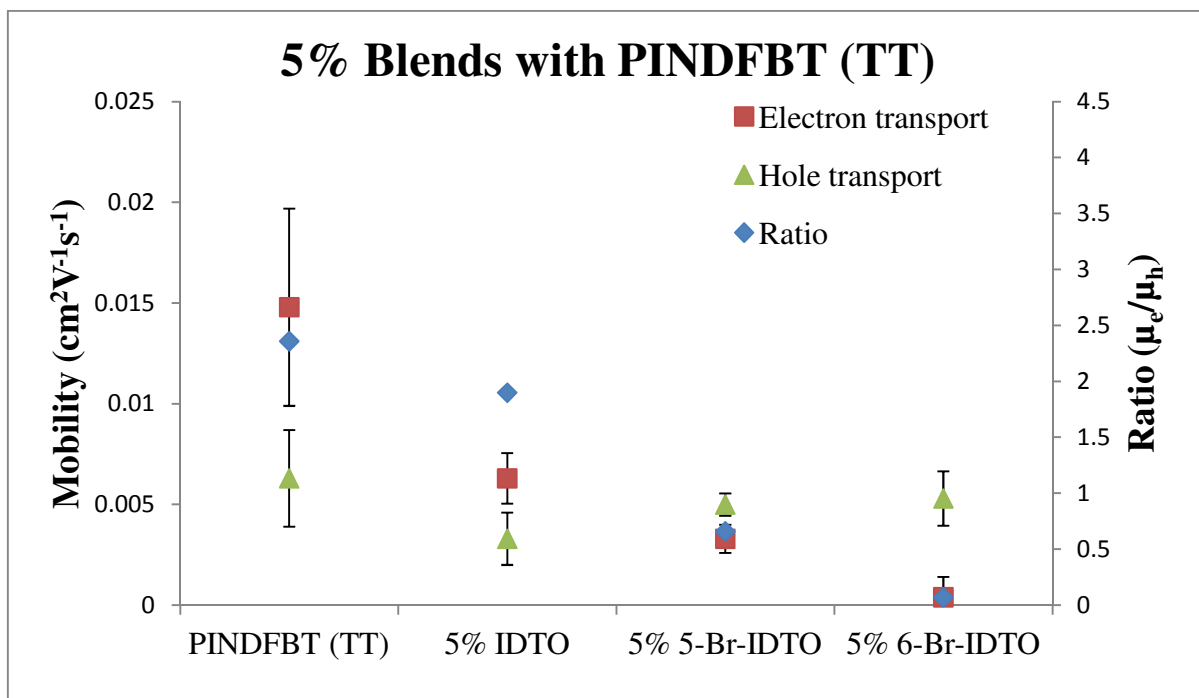


Figure 5.4: Comparison of 5% blends with PINDFBT (TT).

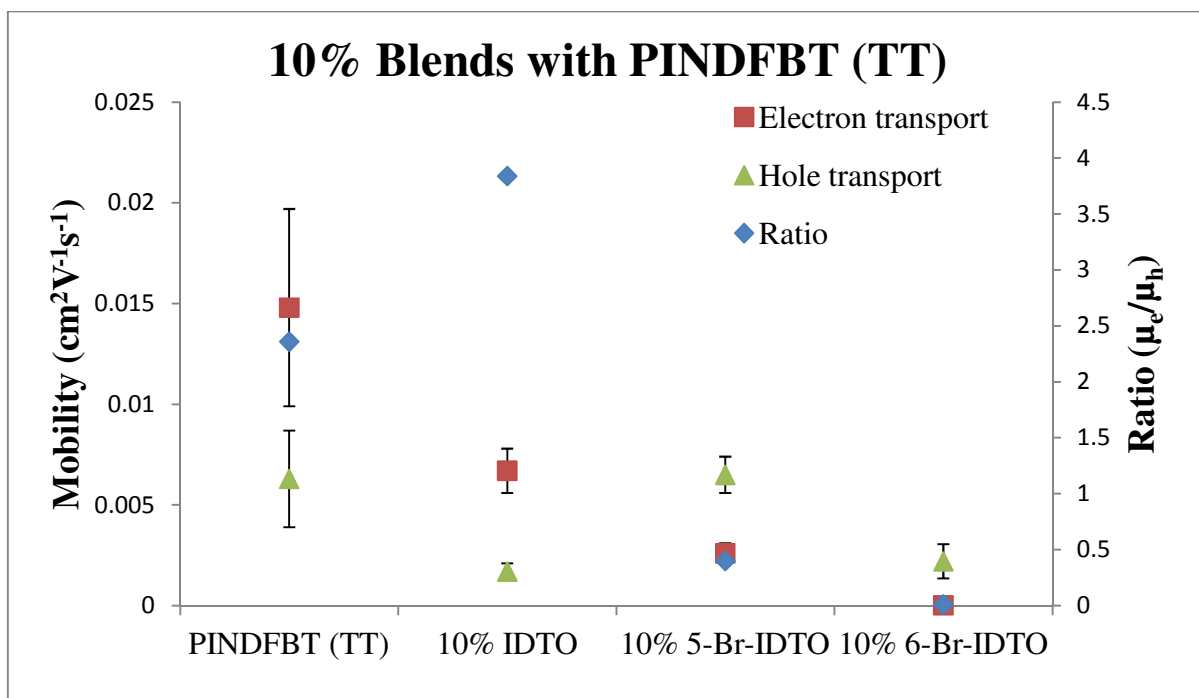


Figure 5.5: Comparison of 10% blends with PINDFBT (TT).

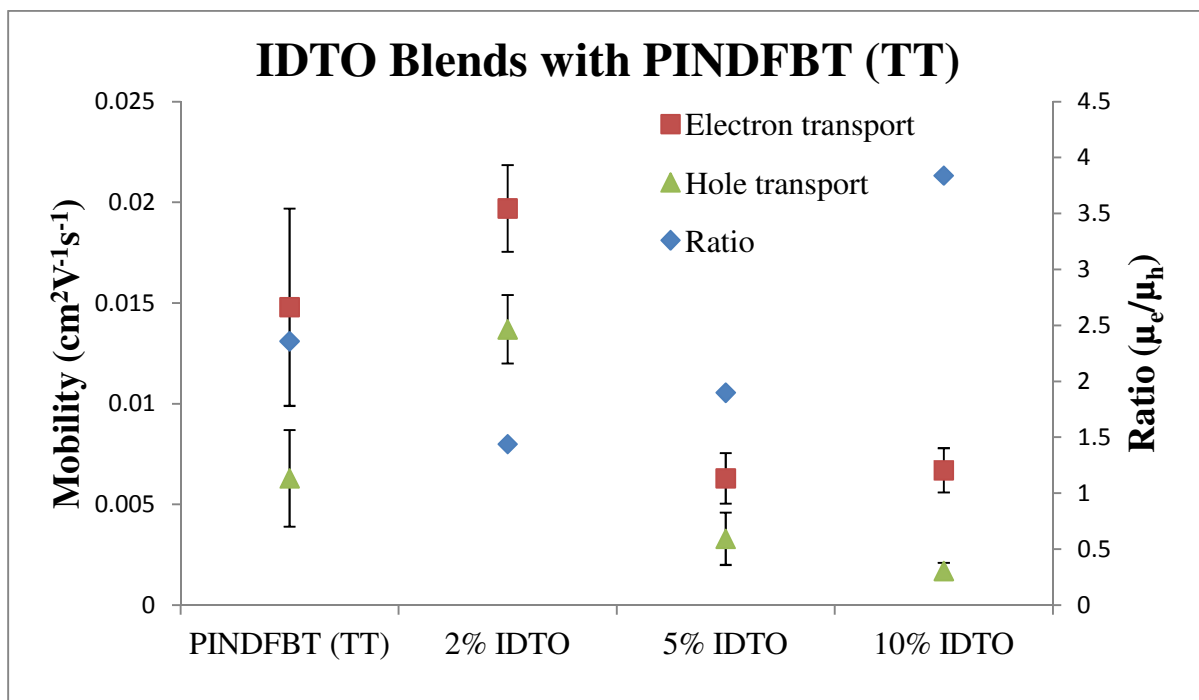


Figure 5.6: Comparison of IDTO blends with PINDFBT (TT).

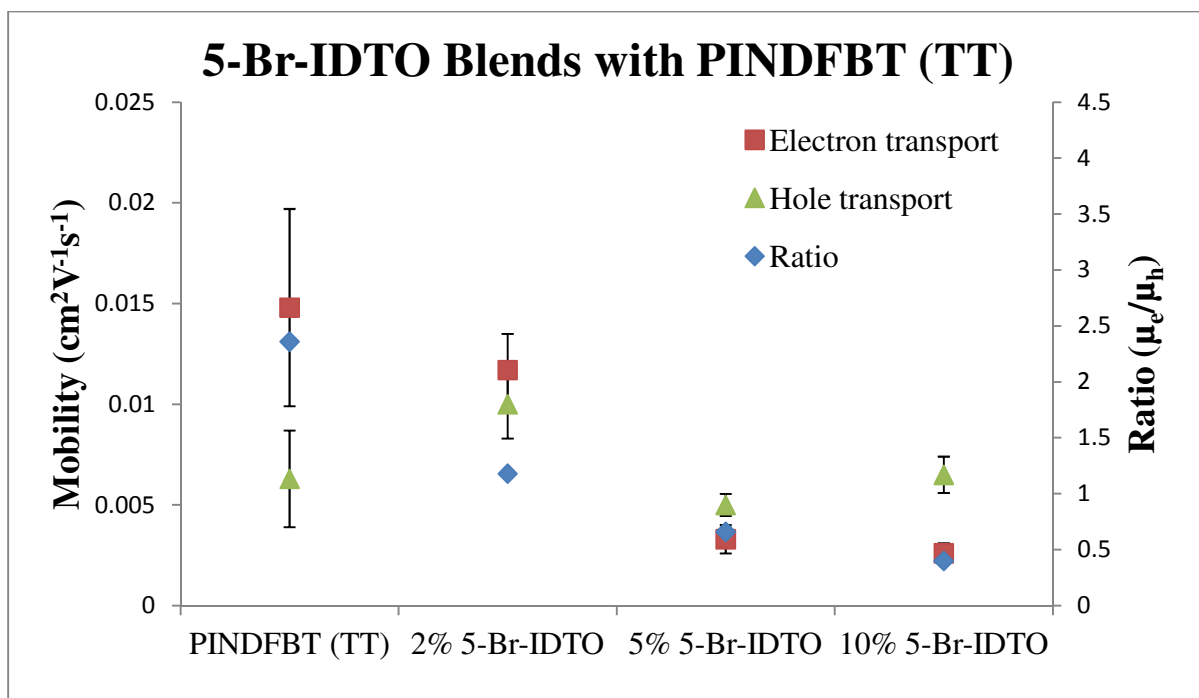
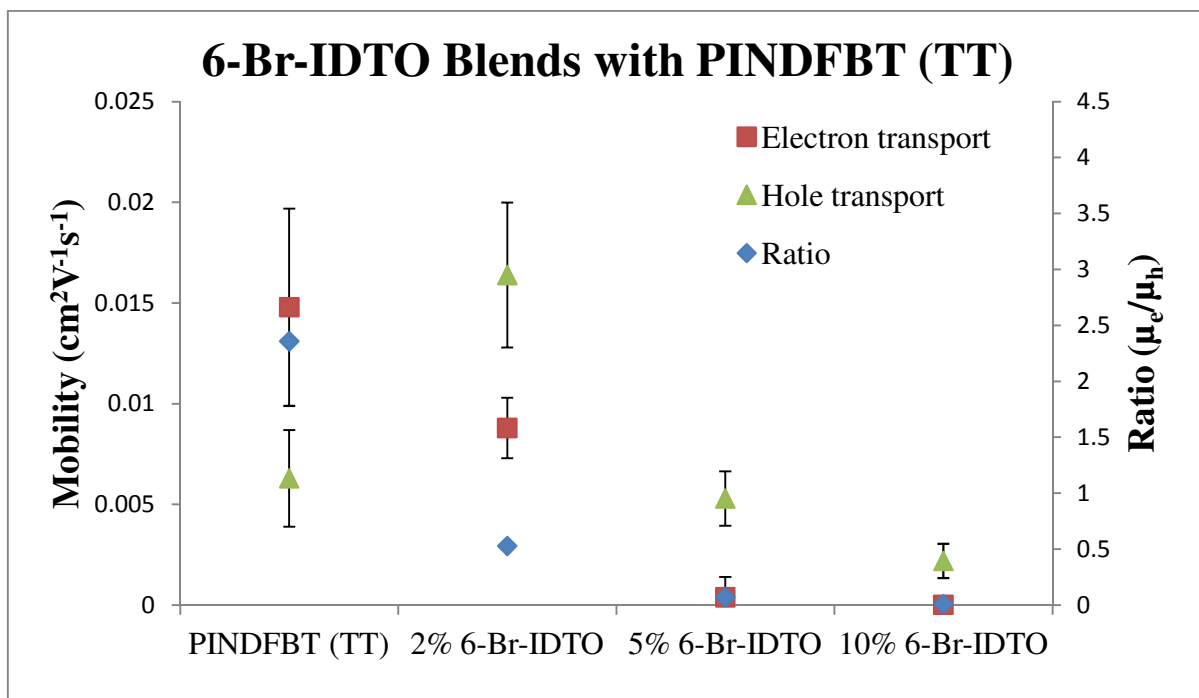


Figure 5.7: Comparison of 5-Br-IDTO blends with PINDFBT (TT).



**Figure 5.8: Comparison of 6-Br-IDTO blends with PINDFBT (TT).**

Table 5.2 summarizes the results of the blends with PINDFBT (HH). Similar trends to the previous polymer blends were observed with the exception of IDTO showing a decrease in mobility ratio as the amount of IDTO is increased. The decrease in mobility ratio with increasing amount was previously only seen for the brominated IDTO compounds but now IDTO is showing the same trend. This indicates that the IDTO is demonstrating some electron trapping effects when blended with PINDFBT (HH). In addition, the strength of electron trapping for the brominated IDTO compounds is overall stronger with PINDFBT (HH) than with PINDFBT (TT). A possible reason for this could be because PINDFBT (HH) has a slightly higher LUMO energy level which increases the size of the trapping energy. However, the difference in LUMO energy levels of PINDFBT (HH) and PINDFBT (TT) is only 0.01 eV which one would think is not large enough to cause a noticeable change. Therefore, another possible reason the electron trapping is stronger with PINDFBT (HH) could be that the IDTO compounds are more soluble with PINDFBT (HH). The head-to-head configuration of the alkyl chains on the thiophene units is more spatially compact which could allow more space for the IDTO compounds. The IDTO compounds would then be better distributed throughout the blend and more interaction between PINDFBT (HH) and the IDTO compounds could occur leading to stronger observable electron trapping effects. These results are more impressive than the previous

results using PINDFBT (TT) since hole mobility could be kept at a reasonable level while decreasing electron mobility significantly. The results for the PINDFBT (HH) blends are also plotted in a similar fashion to the PINDFBT (TT) blends, which can be found in Appendix D.

**Table 5.2: OFET performance parameters for PINDFBT (HH) / IDTO compound blends.**

Name	$\mu_e$ (cm <sup>2</sup> V <sup>-1</sup> s <sup>-1</sup> )	$\mu_h$ (cm <sup>2</sup> V <sup>-1</sup> s <sup>-1</sup> )	V <sub>th,e</sub> (V)	V <sub>th,h</sub> (V)	I <sub>on</sub> /I <sub>off</sub>	$\mu_e/\mu_h$
PINDFBT (HH)	0.0470 (0.0017)	0.0571 (0.0297)	39	-36	10 - 10 <sup>2</sup>	0.82
2% IDTO	0.0876 (0.0207)	0.1108 (0.0179)	55	-4	10 - 10 <sup>3</sup>	0.79
5% IDTO	0.0419 (0.0123)	0.0779 (0.0045)	35	2	10 - 10 <sup>3</sup>	0.54
10% IDTO	0.0124 (0.0019)	0.0419 (0.0055)	49	-5	10 <sup>2</sup> - 10 <sup>3</sup>	0.30
2% 5-Br-IDTO	0.0189 (0.0042)	0.0777 (0.0076)	41	-4	10 - 10 <sup>3</sup>	0.24
5% 5-Br-IDTO	0.0001 (10 <sup>-5</sup> )	0.0386 (0.0117)	32	-12	10 <sup>2</sup> - 10 <sup>5</sup>	0.01
10% 5-Br-IDTO	0.0004 (0.0004)	0.0428 (0.0214)	29	-14	10 <sup>2</sup> - 10 <sup>5</sup>	0.01
2% 6-Br-IDTO	0.0017 (0.0016)	0.1007 (0.0236)	48	-12	10 - 10 <sup>6</sup>	0.02
5% 6-Br-IDTO	0.0007 (0.0012)	0.0320 (0.0216)	60	-20	10 - 10 <sup>5</sup>	0.02
10% 6-Br-IDTO	0.0001 (0.0001)	0.0235 (0.0217)	38	-26	10 <sup>4</sup> - 10 <sup>6</sup>	0.01

## 5.4 Conclusions

To explore other uses for IDTO, blends were made which mixed small amounts of IDTO with an ambipolar polymer. The aim was convert the ambipolar characteristic to unipolar p-type by suppressing the electron transport of the device by having the IDTO additive act as an electron trap. To investigate the electron trapping effect of IDTO and its derivative, PINDFBT (TT) and PINDFBT (HH) were chosen as polymers to blend with IDTO because they have a LUMO energy level that is slightly higher than the IDTO compounds. By blending these polymers with IDTO, 5-bromo-IDTO and 6-bromo-IDTO the predicted outcome was that IDTO would impede electron transport but not suppress it. Whereas, the brominated IDTO compounds would have a greater effect of suppressing the electron transport due to their deeper LUMO energy levels. The IDTO compounds were blended at weight percents of 2%, 5% and 10%. OFETs tested using these blends showed that the electron trapping effect was greatest for 6-bromo-IDTO and weakest for IDTO. Although complete suppression of the electron transport was not observed, the lowest ratio of electron mobility over hole mobility of 0.01 was achieved for a few of the blends. Unfortunately for the PINDFBT (TT) blends,

the hole mobility decreases to  $\sim 10^{-3} \text{ cm}^2\text{V}^{-1}\text{s}^{-1}$ . On the other hand, the PINDFBT (HH) blends were able to maintain decent hole mobilities. Based on the results, there is a lot of potential for realizing complete conversion of ambipolar to unipolar p-type. More work is needed to fully investigate the electron trapping effect of IDTO and its derivatives. XRD and AFM of the blended films could grant information about the crystallinity and morphology of the blends. Polymers with different LUMO energy levels could be blended with IDTO to realize complete suppression of electron transport. Lastly, phase separation could be investigated to find the optimal annealing temperature for the blends.

## Chapter 6

### Summary and Future Directions

#### 6.1 Summary

The work presented in this thesis has covered the development of a novel n-type organic semiconductor referred to as thiophene-*S,S*-dioxidized Indophenine (IDTO). IDTO was developed to address the lack of high performance n-type organic semiconductors. IDTO is a planar quinoidal molecule with deep energy levels to support stable and efficient electron transport. The synthesis of IDTO is very straightforward and made from simple starting materials. These factors make IDTO a promising material in the design and fabrication of high performance n-type organic field-effect transistors. The development of IDTO started with a systematic improvement of the synthesis, followed by evaluation as a small molecule organic semiconductor and as an electron accepting building block for donor-acceptor polymers. Lastly, IDTO was used in blends as an electron trap to suppress the electron transport of an ambipolar polymer. Overall, IDTO has demonstrated usefulness in organic field-effect transistors. More work can be done to improve the results obtained which will be discussed in the next section.

Synthesis improvement of IDTO was necessary because the original route had yields less than 10% and used benzene, a known carcinogen, as the solvent. The benzene was found to be replaceable with toluene at no loss to the final yield. During the improvement process, it was proposed that the concentrated sulfuric acid does not only serve as an acid for the reaction as previously thought. Since other strong acids could not promote the reaction and sulfuric acid needed to be a very high concentration, the idea is that the sulfuric acid has to oxidize the thiophene as well for the reaction to proceed. Through multiple experiments, the yield was improved to ~40% by increasing the amount of concentrated sulfuric acid and oxidant added to the reaction. The improved synthesis is a great enhancement upon the original method in terms of both yield and safety.

Three small molecule IDTO compounds were synthesized and evaluated for new n-type organic semiconductors. All three compounds, IDTO, 5-bromo-IDTO and 6-bromo-IDTO, demonstrated unipolar n-type characteristics with mobilities on the order of  $10^{-2}$  to  $10^{-1}$   $\text{cm}^2\text{V}^{-1}\text{s}^{-1}$ . IDTO is well suited for unipolar electron transport due to its very low energy levels which stabilize electrons and prevents the injection of holes. 6-bromo-IDTO demonstrated the highest mobility of the three compounds with a maximum electron mobility of  $0.11 \text{ cm}^2\text{V}^{-1}\text{s}^{-1}$ . The 6,6' position bromine

atoms showed greater benefit to the electron transport due an extension of conjugation by the participation of the atoms to the LUMO energy wavefunction of the molecule. The three IDTO compounds show potential as a new group of n-type, solution processable, small molecule organic semiconductors.

Polymerization of IDTO as an electron accepting building block was performed to synthesis two different donor-acceptor polymers for use as n-type organic semiconductors. The polymers, PIDTOBT and PIDTOBTz, exhibited electron mobilities on the order of  $10^{-2}$  to  $10^{-1}$   $\text{cm}^2\text{V}^{-1}\text{s}^{-1}$ . The highest mobility measured was  $0.18 \text{ cm}^2\text{V}^{-1}\text{s}^{-1}$  for PIDTOBT annealed at  $200 \text{ }^\circ\text{C}$ . The superior performance of PIDTOBT over PIDTOBTz was due to increased crystallinity and a larger molecular weight. PIDTOBTz had the advantage of better air stability due to a deeper LUMO energy level. The two IDTO polymers demonstrate that IDTO is an effective electron accepting moiety for use in polymeric organic semiconductors.

IDTO, 5-bromo-IDTO and 6-bromo-IDTO were blended with PINDFBT (TT) and PINDFBT (HH) to investigate the electron trapping ability of the IDTO compounds. By using an ambipolar polymer with a LUMO energy level that is slightly above that of the IDTO compounds, the expected outcome was a conversion of ambipolar to p-type by the brominated IDTO compounds. IDTO was expected not to show the same result because it would serve as a much shallower electron trap due to its higher LUMO energy level. The results did not show complete suppression of the electron transport for any of the IDTO compounds. However, the trends observed support the hypothesis. 6-bromo-IDTO exhibited the strongest electron trapping effect and IDTO had a very weak effect.

## 6.2 Future Directions

Evaluation of IDTO thus far has shown mobilities on the order of  $10^{-2}$  to  $10^{-1}$   $\text{cm}^2\text{V}^{-1}\text{s}^{-1}$  for both small molecule and polymer. These values are well below the 1 to  $10 \text{ cm}^2\text{V}^{-1}\text{s}^{-1}$  of record high materials. There are several strategies which can be explored to improve the performance. Side chain engineering (lengthening, shortening, branching and/or functionalizing the side chain) can affect how the molecules pack and thus the crystallinity can be adjusted. Energy levels can be tuned by choice and position of substituents. Device optimization through material selection, film deposition method, substrate modification, OFET configuration, etc. can potentially improve performance as well by enhancing interfaces, better film quality, decrease injection barriers, influence molecular packing, etc.

So much can be done to improve the performance of IDTO and IDTO related material for use in organic field-effect transistors.

The IDTO blend experiments could also benefit from additional work to fully investigate the electron trapping ability of IDTO. In the immediate future, XRD and AFM can be measured for the blended films to provide information about how the addition of IDTO affects the crystallinity and morphology of the film. Phase separation is another issue that can be looked at to find the optimal conditions where no phase separation occurs. Later on, other polymers with different LUMO energy levels and preferably higher mobilities could be blended with IDTO. Complete suppression of electron transport should be achievable using an ambipolar polymer with a higher LUMO energy level.

## Bibliography

1. Shirakawa, H., Louis, E. J., MacDiarmid, A. G., Chiang, C. K. & Heeger, A. J. Synthesis of electrically conducting organic polymers: halogen derivatives of polyacetylene, (CH)<sub>x</sub>. *J. Chem. Soc. Chem. Commun.* 578–580 (1977). doi:10.1039/C39770000578
2. Ebisawa, F., Kurokawa, T. & Nara, S. Electrical properties of polyacetylene/polysiloxane interface. *J. Appl. Phys.* **54**, 3255–3259 (1983).
3. Tsumura, A., Koezuka, H. & Ando, T. Macromolecular electronic device: Field-effect transistor with a polythiophene thin film. *Appl. Phys. Lett.* **49**, 1210–1212 (1986).
4. Madru, R. *et al.* A well-behaved field effect transistor based on an intrinsic molecular semiconductor. *Chem. Phys. Lett.* **145**, 343–346 (1988).
5. Garnier, F., Horowitz, G., Peng, X. & Fichou, D. An all-organic ‘soft’ thin film transistor with very high carrier mobility. *Adv. Mater.* **2**, 592–594 (1990).
6. Takeya, J. *et al.* Very high-mobility organic single-crystal transistors with in-crystal conduction channels. *Appl. Phys. Lett.* **90**, 102120 (2007).
7. Naab, B. D. *et al.* High mobility N-type transistors based on solution-sheared doped 6,13-bis(triisopropylsilylethynyl)pentacene thin films. *Adv. Mater.* **25**, 4663–4667 (2013).
8. Shukla, D. *et al.* Thin-film morphology control in naphthalene-diimide-based semiconductors: high mobility n-type semiconductor for organic thin-film transistors. *Chem. Mater.* **20**, 7486–7491 (2008).
9. Kymissis, I. *Organic Field Effect Transistors Theory, Fabrication and Characterization.* (Springer Science+Business Media, LLC, 2009). doi:10.1007/978-0-387-92134-1
10. Horowitz, G., Hajlaoui, R., Bourguiga, R. & Hajlaoui, M. Theory of the organic field-effect transistor. *Synth. Met.* **101**, 401–404 (1999).
11. Macomber, R. S., Pinhas, A. & Wilson, R. M. *The Vocabulary and concepts of Organic Chemistry.* (John Wiley & Sons, Inc., 2005). doi:10.1002/0471713740.ch1
12. Pauling, L. The nature of the chemical bond. Application of results obtained from the quantum mechanics and from a theory of paramagnetic susceptibility to the structure of molecules. *J. Am. Chem. Soc.* **53**, 1367–1400 (1931).

13. Lennard-Jones, J. E. The electronic structure of some diatomic molecules. *Trans. Faraday Soc.* **25**, 668–686 (1929).
14. Jean, Y., Volatron, F. & Burdett, J. K. *An Introduction to Molecular Orbitals*. (Oxford University Press, 1993).
15. Fleming, I. *Frontier orbitals and organic chemical reactions*. (Wiley, 1976).
16. Singh, R. K. & Dixit, A. *Basic Electronics Engineering & Devices*. (Laxmi Publications Pvt Limited, 2007).
17. Bassler, H. & Kohler, A. Charge Transport in Organic Semiconductors. *Top. Curr. Chem.* **312**, 1–66 (2011).
18. Asadi, K. *et al.* Polaron hopping mediated by nuclear tunnelling in semiconducting polymers at high carrier density. *Nat. Commun.* **4**, 1710 (2013).
19. Kallmann, H. & Pope, M. Bulk Conductivity in Organic Crystals. *Nature* **186**, 31–33 (1960).
20. Kallmann, H. & Pope, M. Positive hole injection into organic crystals. *J. Chem. Phys.* **32**, 300–301 (1960).
21. March, J. *Advanced Organic Chemistry reactions, mechanisms and structure*. (John Wiley & Sons, Inc., 1985).
22. Li, Y. Molecular design of photovoltaic materials for polymer solar cells: Toward suitable electronic energy levels and broad absorption. *Acc. Chem. Res.* **45**, 723–733 (2012).
23. Heeger, A. J. Semiconducting polymers: the Third Generation. *Chem. Soc. Rev.* **39**, 2354–2371 (2010).
24. He, Y., Hong, W. & Li, Y. New building blocks for  $\pi$ -conjugated polymer semiconductors for organic thin film transistors and photovoltaics. *J. Mater. Chem. C* **2**, 8651–8661 (2014).
25. Hill, J. W. & Petrucci, R. H. *General Chemistry: An Integrated Approach*. (Prentice Hall College Div, 1999).
26. Roberts, J. D. *Nuclear magnetic resonance: applications to organic chemistry*. (McGraw-Hill, 1959).
27. Bernstein, H. J., Pople, J. A. & Schneider, W. G. The analysis of nuclear magnetic resonance spectra. *Can. J. Chem.* **35**, 65–81 (1957).

28. Hoffmann, E. de & Stroobant, V. *Mass Spectrometry: Principles and Applications*. (John Wiley & Sons, Inc., 2007).
29. Lathe, G. H. & Ruthven, C. R. The separation of substances and estimation of their relative molecular sizes by the use of columns of starch in water. *Biochem. J.* **62**, 665–674 (1956).
30. Coats, A. W. & Redfern, J. P. Thermogravimetric Analysis. *Analyst* **88**, 906–924 (1963).
31. O'Neill, M. J. The Analysis of a Temperature-Controlled Scanning Calorimeter. *Anal. Chem.* **36**, 1238–1245 (1964).
32. Wakita, J. & Ando, S. Characterization of Electronic Transitions in Polyimide Films Based on the Spectral Variations Induced by Hydrostatic Pressure up to 400 MPa. *J. Phys. Chem. B* 8835–8846 (2009).
33. Wakita, J., Sekino, H., Sakai, K., Urano, Y. & Ando, S. Molecular design, synthesis, and properties of highly fluorescent polyimides. *J. Phys. Chem. B* **113**, 15212–15224 (2009).
34. D'Andrade, B. W. *et al.* Relationship between the ionization and oxidation potentials of molecular organic semiconductors. *Org. Electron.* **6**, 11–20 (2005).
35. Davidson, E. R. & Feller, D. Basis Set Selection for Molecular Calculations. *Chem. Rev.* **86**, 681–696 (1986).
36. Birkholz, M. *Thin Film Analysis by X-Ray Scattering*. *Thin Film Analysis by X-Ray Scattering* (WILEY-VCH Verlag GmbH & Co. KGaA, 2006). doi:10.1002/3527607595.ch1
37. Binnig, G. & Quate, C. F. Atomic Force Microscope. *Phys. Rev. Lett.* **56**, 930–933 (1986).
38. Braga, D. & Horowitz, G. High-Performance organic field-effect transistors. *Adv. Mater.* **21**, 1473–1486 (2009).
39. Li, J. *et al.* A stable solution-processed polymer semiconductor with record high-mobility for printed transistors. *Sci. Rep.* **2**, 754 (2012).
40. Kang, I., Yun, H., Chung, D. S., Kwon, S. & Kim, Y. Record High Hole Mobility in Polymer Semiconductors via Side-Chain Engineering. *J. Am. Chem. Soc.* **135**, 14896–14899 (2013).
41. Kim, G. *et al.* A thienoisindigo-naphthalene polymer with ultrahigh mobility of 14.4 cm<sup>2</sup>/V.s that substantially exceeds benchmark values for amorphous silicon semiconductors. *J. Am. Chem. Soc.* **136**, 9477–9483 (2014).

42. Yan, H. *et al.* A high-mobility electron-transporting polymer for printed transistors. *Nature* **457**, 679–686 (2009).
43. Hahm, S. G. *et al.* High-performance n-channel thin-film field-effect transistors based on a nanowire-forming polymer. *Adv. Funct. Mater.* **23**, 2060–2071 (2013).
44. Lei, T., Dou, J. H., Cao, X. Y., Wang, J. Y. & Pei, J. A BDOPV-based donor-acceptor polymer for high-performance n-type and oxygen-doped ambipolar field-effect transistors. *Adv. Mater.* **25**, 6589–6593 (2013).
45. Zhao, Y., Guo, Y. & Liu, Y. 25th Anniversary Article: Recent advances in n-type and ambipolar organic field-effect transistors. *Adv. Mater.* **25**, 5372–5391 (2013).
46. Lei, T., Xia, X., Wang, J. Y., Liu, C. J. & Pei, J. ‘Conformation Locked’ Strong Electron-Deficient Poly(p-Phenylene Vinylene) Derivatives for Ambient-Stable n-Type Field-Effect Transistors: Synthesis, Properties, and Effects of Fluorine Substitution Position. *J. Am. Chem. Soc.* **136**, 2135–2141 (2014).
47. Sun, B., Hong, W., Yan, Z., Aziz, H. & Li, Y. Record high electron mobility of  $6.3 \text{ cm}^2\text{V}^{-1}\text{s}^{-1}$  achieved for polymer semiconductors using a new building block. *Adv. Mater.* **26**, 2636–2642 (2014).
48. Zhao, Z. *et al.* Naphthalenediimides Fused with 2-(1,3-Dithiol-2-ylidene)acetonitrile: Strong Electron-Deficient Building Blocks for High-Performance n-Type Polymeric Semiconductors. *ACS Macroletters* **3**, 1174–1177 (2014).
49. de Leeuw, D. M., Simenon, M. M. J., Brown, a. R. & Einerhand, R. E. F. Stability of n-type doped conducting polymers and consequences for polymeric microelectronic devices. *Synth. Met.* **87**, 53–59 (1997).
50. Gao, X. & Hu, Y. Development of n-type organic semiconductors for thin film transistors: a viewpoint of molecular design. *J. Mater. Chem. C* **2**, 3099 (2014).
51. Meng, Q. & Hu, W. Recent progress of n-type organic semiconducting small molecules for organic field-effect transistors. *Phys. Chem. Chem. Phys.* **14**, 14152 (2012).
52. Anthopoulos, T. D., Anyfantis, G. C., Papavassiliou, G. C. & De Leeuw, D. M. Air-stable ambipolar organic transistors. *Appl. Phys. Lett.* **90**, 122105 (2007).
53. Wang, Z., Kim, C., Facchetti, A. & Marks, T. J. Anthracenedicarboximides as air-stable N-

- channel semiconductors for thin-film transistors with remarkable current on-off ratios. *J. Am. Chem. Soc.* **129**, 13362–13363 (2007).
54. Zaumseil, J. & Sirringhaus, H. Electron and Ambipolar Transport in Organic Field-Effect Transistors. *Chem. Rev.* **107**, 1296–1323 (2007).
  55. Suzuki, Y., Miyazaki, E. & Takimiya, K. ((Alkyloxy)carbonyl)cyanomethylene-substituted thienoquinoidal compounds: A New class of soluble n-channel organic semiconductors for air-stable organic field-effect transistors. *J. Am. Chem. Soc.* **132**, 10453–10466 (2010).
  56. Katz, H. E. *et al.* A soluble and air-stable organic semiconductor with high electron mobility. *Nature* **404**, 478–481 (2000).
  57. Jones, B. A. *et al.* High-mobility air-stable n-type semiconductors with processing versatility: Dicyanoperylene-3,4:9,10-bis(dicarboximides). *Angew. Chemie - Int. Ed.* **43**, 6363–6366 (2004).
  58. Jones, B. A., Facchetti, A., Wasielewski, M. R. & Marks, T. J. Tuning orbital energetics in arylene diimide semiconductors. Materials design for ambient stability of n-type charge transport. *J. Am. Chem. Soc.* **129**, 15259–15278 (2007).
  59. Wen, Y. *et al.* Improvements in stability and performance of N,N'-dialkyl perylene diimide-based n-type thin-film transistors. *Adv. Mater.* **21**, 1631–1635 (2009).
  60. Zhan, X. *et al.* Rylene and related diimides for organic electronics. *Adv. Mater.* **23**, 268–284 (2011).
  61. Li, H. *et al.* Tetraazabenzodifluoranthene diimides: Building blocks for solution-processable n-type organic semiconductors. *Angew. Chemie - Int. Ed.* **52**, 5513–5517 (2013).
  62. Tilley, A. J. *et al.* Thionation enhances the electron mobility of perylene diimide for high performance n-channel organic field effect transistors. *Adv. Funct. Mater.* **25**, 3321–3329 (2015).
  63. Facchetti, A. *et al.* Tuning the Semiconducting Properties of Sexithiophene by  $\alpha,\omega$ -Substitution-- $\alpha,\omega$ -Diperfluorohexylsexithiophene: the first n-type sexithiophene for thin-film transistors. *Angew. Chemie Int. Ed.* **39**, 4547–4551 (2000).
  64. Yoon, M., Dibenedetto, S. a, Facchetti, A. & Marks, T. J. Organic Thin-Film Transistors Based on Carbonyl-Functionalized Quaterthiophenes: High Mobility N-Channel

- Semiconductors and Ambipolar Transport. *J. Am. Chem. Soc.* **127**, 1348–1349 (2005).
65. Babudri, F., Farinola, G. M., Naso, F. & Ragni, R. Fluorinated organic materials for electronic and optoelectronic applications: the role of the fluorine atom. *Chem. Commun.* 1003–1022 (2007). doi:10.1039/B611336B
  66. Tian, H. *et al.* A feasibly synthesized ladder-type conjugated molecule as the novel high mobility n-type organic semiconductor. *J. Mater. Chem.* **20**, 7998–8004 (2010).
  67. Wang, L. *et al.* A cyano-terminated dithienyldiketopyrrolopyrrole dimer as a solution processable ambipolar semiconductor under ambient conditions. *Chem. Commun.* **49**, 11272–4 (2013).
  68. Pappenfus, T. M. *et al.* A  $\pi$ -stacking terthiophene-based quinodimethane is an n-channel conductor in a thin film transistor. *J. Am. Chem. Soc.* **124**, 4184–4185 (2002).
  69. Handa, S., Miyazaki, E., Takimiya, K. & Kunugi, Y. Solution-Processible n-Channel Organic Field-Effect Transistors Based on Dicyanomethylene-Substituted Terthienoquinoid Derivative. *J. Am. Chem. Soc.* **129**, 11684–11685 (2007).
  70. Qiao, Y. *et al.* Diketopyrrolopyrrole-containing quinoidal small molecules for high-performance, air-stable, and solution-processable n-channel organic field-effect transistors. *J. Am. Chem. Soc.* **134**, 4084–4087 (2012).
  71. Baeyer, A. No Title. *Chem. Ber.* **12**, 1309–1319 (1879).
  72. Hwang, H. *et al.* Quinoidal molecules as a new class of ambipolar semiconductor originating from amphoteric redox behavior. *Adv. Funct. Mater.* **25**, 1146–1156 (2015).
  73. Marinez, F. & Naarmann, H. New Oligomers with Isatin Condensation Reactions of Thiophene and 2,2'-Bithiophene with Isatin. *Die Angew. Makromol. Chemie* **178**, 1–16 (1990).
  74. Tormos, G. V., Belmore, K. a. & Cava, M. P. The indophenine reaction revisited. Properties of a soluble dialkyl derivative. *J. Am. Chem. Soc.* **115**, 11512–11515 (1993).
  75. Wegmann, J. & Dahn, H. Uber den Einfluss des Katalysators bei der Addition von aromatischen Kohlenwasserstoffen an  $\alpha$ -Ketosuren und an cyclische Dicarbonylverbindungen. *Helv. Chim. Acta.* **29**, 415–432 (1946).

76. Schopov, I. Synthesis of a 'vat' polymer poly-5,5'-biisatyl-[thiophene]-indophenine. *Polym. Lett.* **4**, 1023–1028 (1966).
77. Nehlsen, J., Benziger, J. & Kevrekidis, I. Oxidation of aliphatic and aromatic sulfides using sulfuric acid. *Ind. Eng. Chem. Res.* **45**, 518–524 (2006).
78. Deng, Y. *et al.* Thiophene-S,S-dioxidized indophenines as high performance n-type organic semiconductors for thin film transistors. *RSC Adv.* **6**, 45410–45418 (2016).
79. Guo, C. *et al.* Regioisomeric control of charge transport polarity for indigo-based polymers. *Polym. Chem.* **6**, 6998–7004 (2015).
80. Molnár, G. *et al.* Thermal degradation of chemically modified polysulfones. *Polym. Degrad. Stab.* **89**, 410–417 (2005).
81. Samperi, F. *et al.* Thermal decomposition products of copoly(arylene ether sulfone)s characterized by direct pyrolysis mass spectrometry. *Polym. Degrad. Stab.* **92**, 1304–1315 (2007).
82. Hong, W. *et al.* A conjugated polyazine containing diketopyrrolopyrrole for ambipolar organic thin film transistors. *Chem. Commun.* **48**, 8413–8415 (2012).
83. Deng, Y. *et al.* Thiophene-S,S-dioxidized indophenine (IDTO) based donor-acceptor polymers for n-channel organic thin film transistors. *RSC Adv.* **6**, 34849–34854 (2016).
84. Deng, Y. *et al.* Thiophene-S,S-dioxidized Indophenine: A Quinoid-Type Building Block with High Electron Affinity for Constructing n-Type Polymer Semiconductors with Narrow Band Gaps. *Angew. Chemie - Int. Ed.* **55**, 3459–3462 (2016).
85. Fu, B. *et al.* Molecular engineering of nonhalogenated solution-processable bithiazole-based electron-transport polymeric semiconductors. *Chem. Mater.* **27**, 2928–2937 (2015).
86. Qian, D. *et al.* Design, application, and morphology study of a new photovoltaic polymer with strong aggregation in solution state. *Macromolecules* **45**, 9611–9617 (2012).
87. Chen, Z. *et al.* Low band-Gap conjugated polymers with strong interchain aggregation and very high hole mobility towards highly efficient thick-film polymer solar cells. *Adv. Mater.* **26**, 2586–2591 (2014).
88. Bencheikh, F., Duché, D., Ruiz, C. M., Simon, J. J. & Escoubas, L. Study of Optical

- Properties and Molecular Aggregation of Conjugated Low Band Gap Copolymers: PTB7 and PTB7-Th. *J. Phys. Chem. C* **119**, 24643–24648 (2015).
89. Kang, J., Shin, N., Jang, D. Y., Prabhu, V. M. & Yoon, D. Y. Structure and Properties of Small Molecule-Polymer Blend Semiconductors for Organic Thin Film Transistors. *J. Am. Chem. Soc.* **130**, 12273–12275 (2008).
90. Smith, J. *et al.* The influence of film morphology in high-mobility small-molecule: Polymer blend organic transistors. *Adv. Funct. Mater.* **20**, 2330–2337 (2010).
91. Arulkashmir, A., Mahale, R. Y., Dharmapurikar, S. S., Jangid, M. K. & Krishnamoorthy, K. Supramolecular interaction facilitated small molecule films for organic field effect transistors. *Polym. Chem.* **3**, 1641–1646 (2012).
92. Lee, S. G., Lee, H. S., Lee, S., Kim, C. W. & Lee, W. H. Thickness-dependent electrical properties of soluble acene–polymer blend semiconductors. *Org. Electron.* **24**, 113–119 (2015).
93. Zhao, K. *et al.* Vertical Phase Separation in Small Molecule:Polymer Blend Organic Thin Film Transistors Can Be Dynamically Controlled. *Adv. Funct. Mater.* **26**, 1737–1746 (2016).
94. Sun, B. *et al.* Utilization of hole trapping effect of aromatic amines to convert polymer semiconductor from ambipolar into n-type. *Org. Electron.* **37**, 190–196 (2016).
95. Ford, M. J., Wang, M., Phan, H., Nguyen, T. Q. & Bazan, G. C. Fullerene Additives Convert Ambipolar Transport to p-Type Transport while Improving the Operational Stability of Organic Thin Film Transistors. *Adv. Funct. Mater.* **26**, 4472–4480 (2016).
96. Sun, B. *et al.* Polyethylenimine (PEI) As an Effective Dopant to Conveniently Convert Ambipolar and p-Type Polymers into Unipolar n-Type Polymers. *ACS Appl. Mater. Interfaces* **7**, 18662–18671 (2015).
97. Deng, Y. *et al.* (3E,8E)-3,8-Bis(2-oxoindolin-3-ylidene)naphtho-[1,2-b:5,6-b']difuran-2,7(3H,8H)-dione (INDF) based polymers for organic thin-film transistors with highly balanced ambipolar charge transport characteristics. *Chem. Commun.* **51**, 13515–13518 (2015).

## Appendix A

### List of Chemicals

**Table A.1: List of Chemicals**

Chemical Name	Grade	Supplier
<b>Solvents</b>		
Dichloromethane (DCM), bulk	$\geq 99.5\%$	Sigma Aldrich
Chloroform, bulk	$\geq 99.8\%$	Sigma Aldrich
Hexane, bulk	$\geq 98.5\%$	Sigma Aldrich
Acetone, bulk	$\geq 99\%$	Sigma Aldrich
Toluene, anhydrous	99.8%	Sigma Aldrich
Benzene, anhydrous	99.8%	Sigma Aldrich
Chlorobenzene, anhydrous	99%	Oakwood Chemical
Acetic acid	$\geq 99.7\%$	Sigma Aldrich
Dimethylformamide (DMF), anhydrous	99.8%	Sigma Aldrich
1,1,2-Trichloroethane (TCE)	$\geq 98\%$	Sigma Aldrich
Trichlorobenzene (TCB)	$\geq 99\%$	Sigma Aldrich
<b>Reagents</b>		
Isatin	98%	Sigma Aldrich
5-Br-Isatin	90%	Sigma Aldrich
6-Br-Isatin	$\geq 95\%$	Matrix Scientific
1-Bromododecane	97%	Sigma Aldrich
Potassium Carbonate	99%	Sigma Aldrich
Magnesium Sulfate, anhydrous	$\geq 99.5\%$	Sigma Aldrich
Concentrated sulfuric acid	95.0-98.0%	Sigma Aldrich
Thiophene	99%	Alfa Aesar
m-CPBA	$\leq 77\%$	Sigma Aldrich
Sodium Carbonate	$\geq 99.5\%$	Sigma Aldrich
Tri(o-tolyl)phosphine	97%	Sigma Aldrich
Tris(dibenzylideneacetone)-dipalladium	98%	Oakwood Chemical
Bromobenzene	99%	Sigma Aldrich

## Appendix B

### NMR and MS Data for Small Molecule IDTO Compounds

#### IDTO:

$^1\text{H}$  NMR (300 MHz,  $\text{CDCl}_3$ ):  $\delta$  8.66 (d,  $J = 8.3$  Hz, 2H), 8.18 (d,  $J = 7.8$  Hz, 2H), 7.56 (d,  $J = 8.3$  Hz, 2H), 7.37 (m, 2H), 7.05 (m, 2H), 6.79 (d,  $J = 7.8$  Hz, 2H), 3.69 (t,  $J = 7.0$  Hz, 4H), 1.66 (m, 4H), 1.24–1.32 (m, 36H), 0.86 (t,  $J = 6.5$  Hz, 6H).  $^{13}\text{C}$  NMR ( $\text{CDCl}_3$ , 75 MHz, ppm):  $\delta$  165.9, 145.2, 139.4, 134.3, 134.4, 130.9, 127.7, 126.3, 124.9, 123.0, 118.3, 108.9, 40.1, 31.8, 29.5, 29.4, 29.3, 29.2, 29.1, 27.3, 26.8, 22.6, 13.9. HR-ESI-MS ( $\text{M}^+$ ) calc. for  $\text{C}_{48}\text{H}_{62}\text{N}_2\text{O}_6\text{S}_2^+$ , 827.40; found, 827.40981.

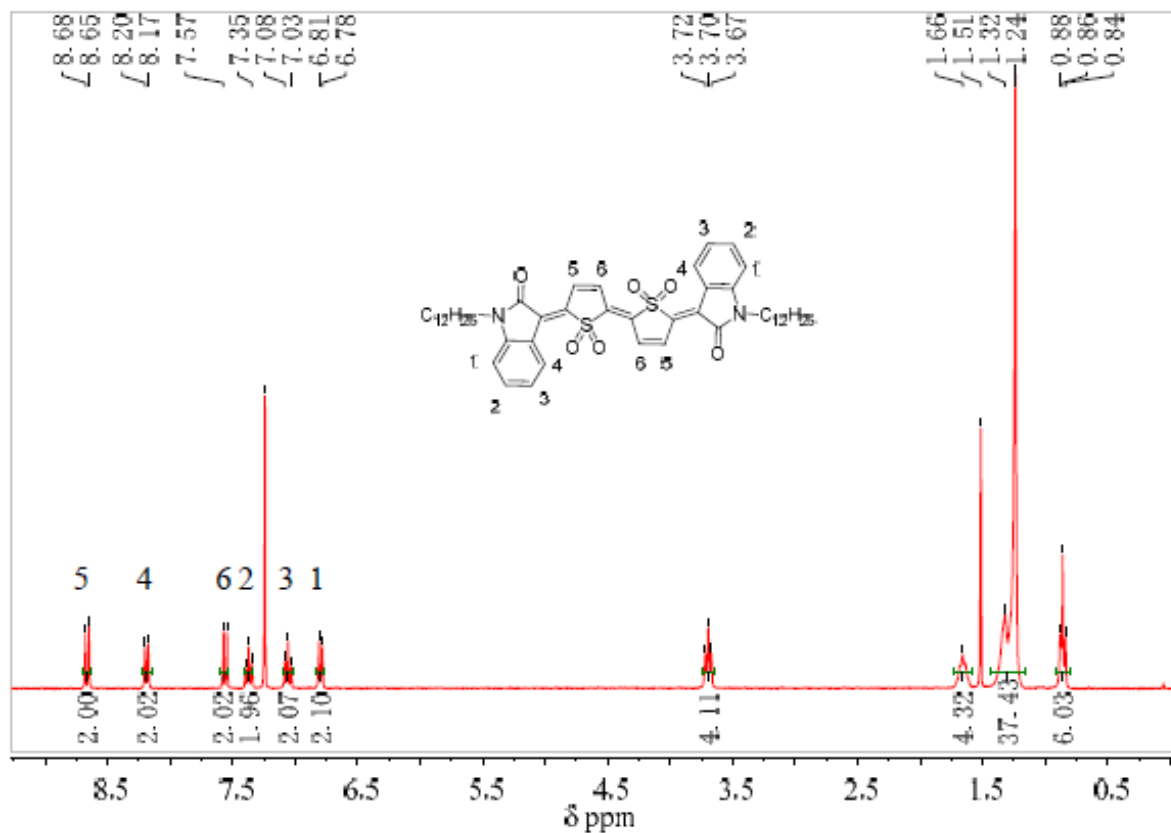


Figure B.1:  $^1\text{H}$  NMR spectrum for IDTO.

### 5-bromo-IDTO:

$^1\text{H}$  NMR (300 MHz,  $\text{CDCl}_3$ ):  $\delta$  8.65 (d,  $J = 8.3$  Hz, 2H), 8.28 (d,  $J = 1.7$  Hz, 2H), 7.62 (d,  $J = 8.3$  Hz, 2H), 7.49 (dd,  $J_1 = 1.7$  Hz,  $J_2 = 8.3$  Hz, 2H), 6.68 (d,  $J = 8.3$  Hz, 2H), 3.68 (t,  $J = 7.1$  Hz, 4H), 1.64 (m, 4H), 1.23–1.30 (m, 36H), 0.86 (t,  $J = 6.5$  Hz, 6H).  $^{13}\text{C}$  NMR ( $\text{CDCl}_3$ , 75 MHz, ppm):  $\delta$  165.5, 142.2, 140.4, 135.9, 134.1, 130.9, 127.5, 126.3, 123.5, 123.0, 119.8, 110.5, 40.3, 31.8, 29.6, 29.5, 29.4, 29.3, 29.2, 27.2, 26.8, 22.6, 14.0. HR-ESI-MS ( $\text{M}^+$ ) calc. for  $\text{C}_{48}\text{H}_{60}\text{Br}_2\text{N}_2\text{O}_6\text{S}_2^+$ , 983.23; found, 983.23317.

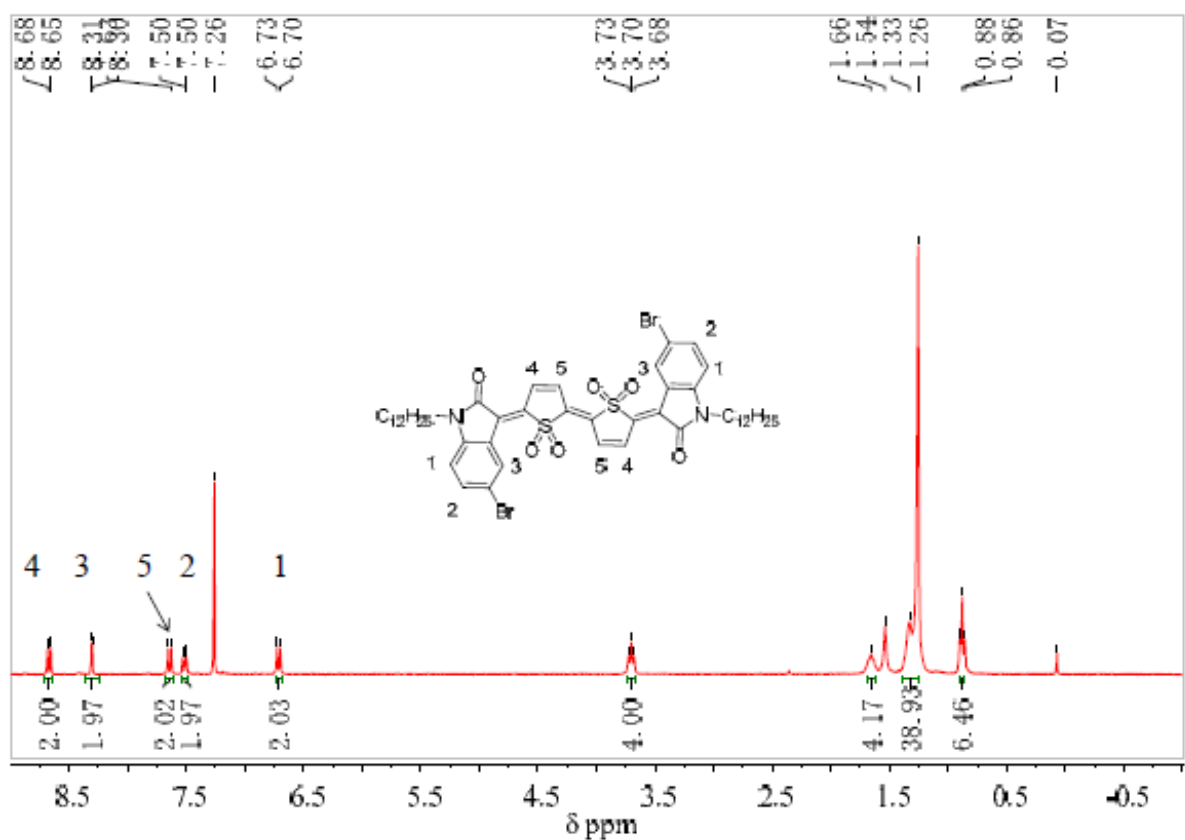


Figure B.2:  $^1\text{H}$  NMR spectrum for 5-bromo-IDTO.

**6-bromo-IDTO:**

$^1\text{H}$  NMR (300 MHz,  $\text{CDCl}_3$ ):  $\delta$  8.63 (d,  $J = 8.3$  Hz, 2H), 8.02 (d,  $J = 8.3$  Hz, 2H), 7.57 (d,  $J = 8.3$  Hz, 2H), 7.20 (dd,  $J_1 = 1.4$  Hz,  $J_2 = 8.3$  Hz, 2H), 6.96 (d,  $J = 1.4$  Hz, 2H), 3.68 (t,  $J = 7.1$  Hz, 4H), 1.65 (m, 4H), 1.24–1.34 (m, 36H), 0.86 (t,  $J = 6.5$  Hz, 6H).  $^{13}\text{C}$  NMR ( $\text{CDCl}_3$ , 75 MHz, ppm):  $\delta$  165.8, 145.9, 139.7, 134.4, 130.9, 128.4, 128.1, 126.9, 125.9, 123.8, 117.1, 112.4, 40.3, 31.8, 29.4, 29.3, 29.2, 29.1, 29.0, 27.2, 26.8, 22.6, 13.9. HR-ESI-MS ( $\text{M}^+$ ) calc. for  $\text{C}_{48}\text{H}_{60}\text{Br}_2\text{N}_2\text{O}_6\text{S}_2^+$ , 983.23; found, 983.23467.

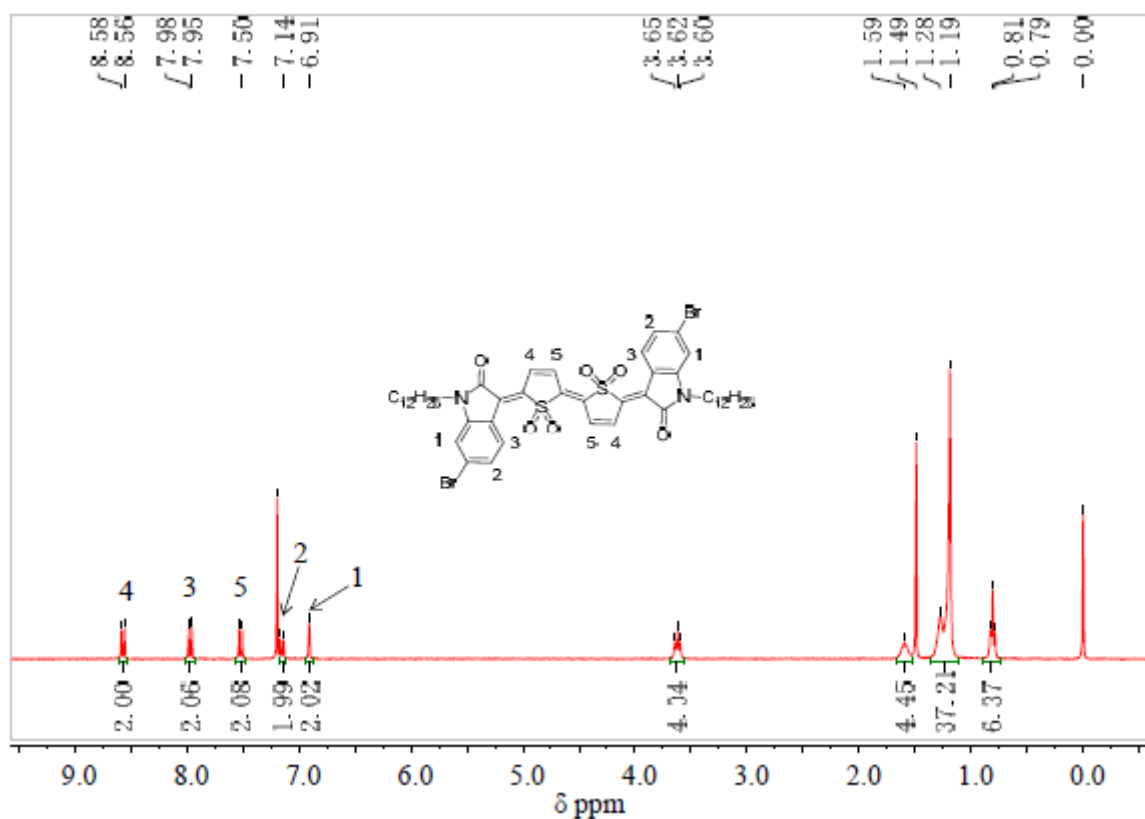
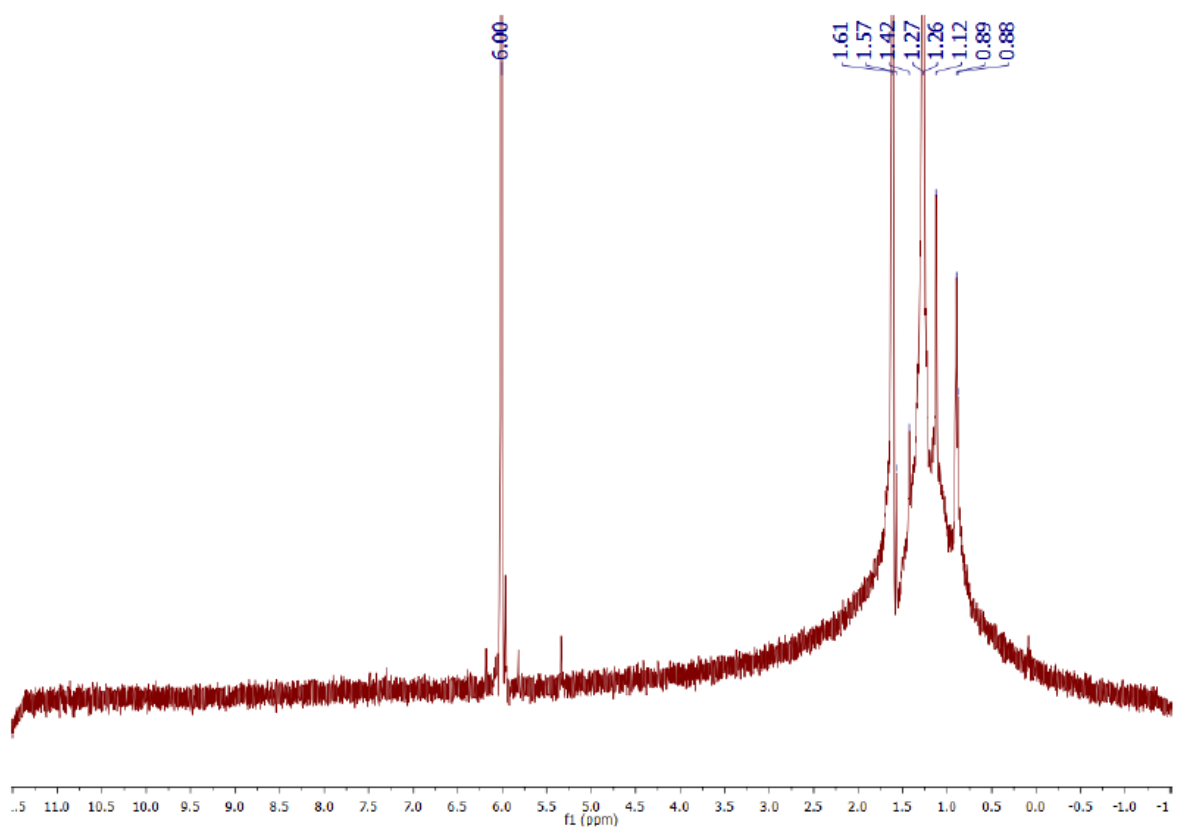


Figure B.3:  $^1\text{H}$  NMR spectrum for 6-bromo-IDTO.

## Appendix C

### NMR Data for IDTO Polymers

**PIDTOBT:**



**Figure C.1:**  $^1\text{H}$ -NMR spectrum of PIDTOBT measured in  $\text{TCE-D}_2$ .

**PIDTOBTz:**

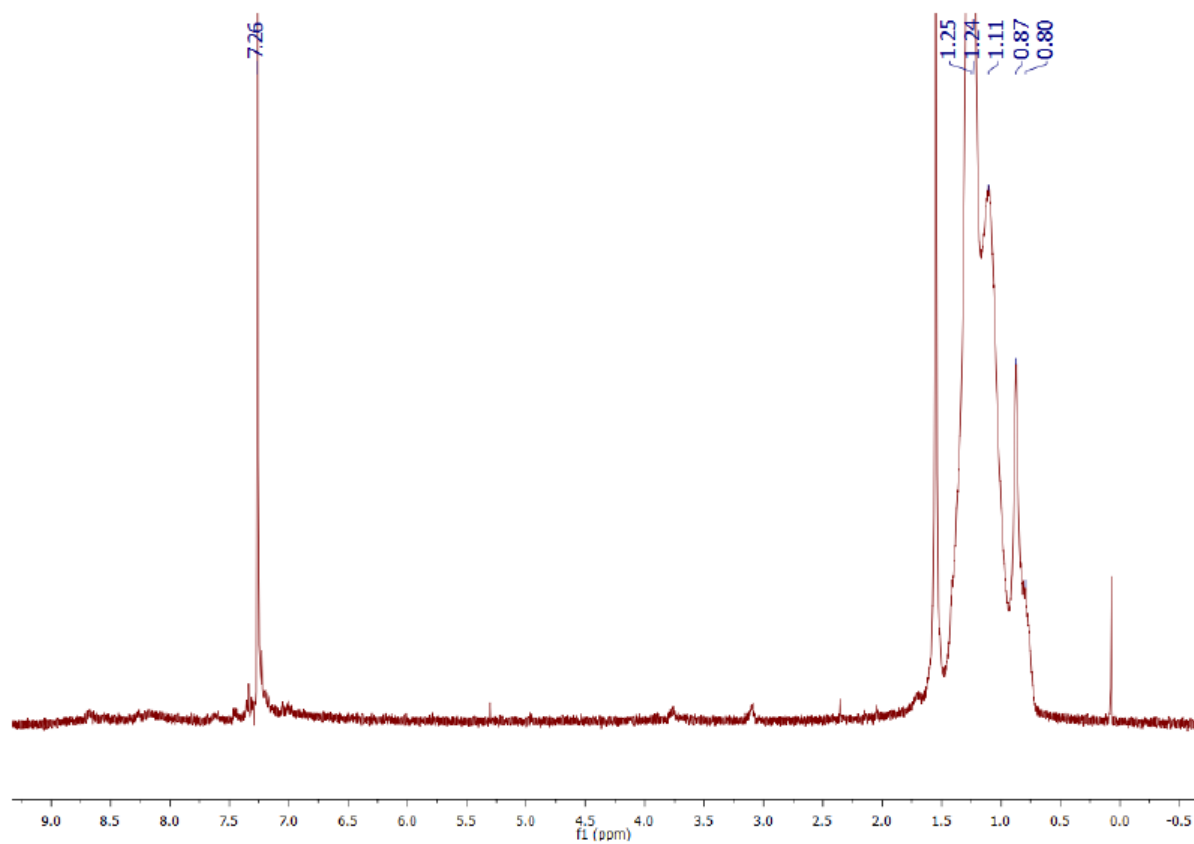


**Figure C.2:**  $^1\text{H-NMR}$  spectrum of PIDTOBTz measured in  $\text{CDCl}_3$ .

## Appendix D

### PINDFBT (HH) Blend Comparison Graphs

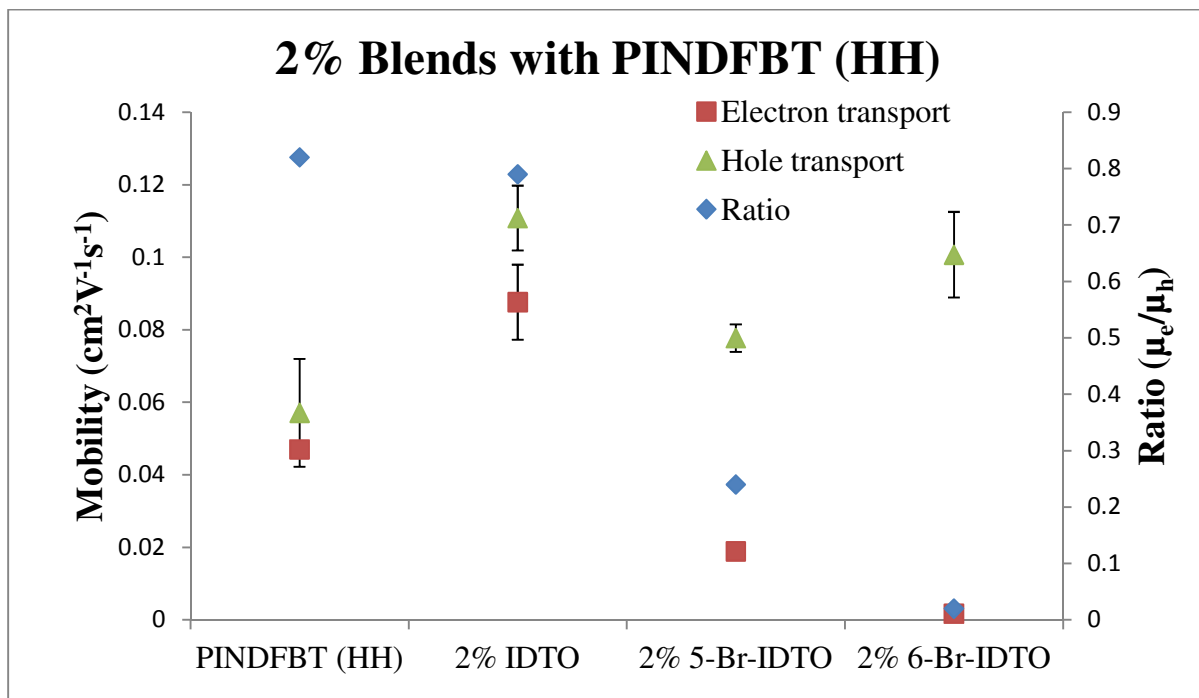


Figure D.1: Comparison of 2% blends with PINDFBT (HH).

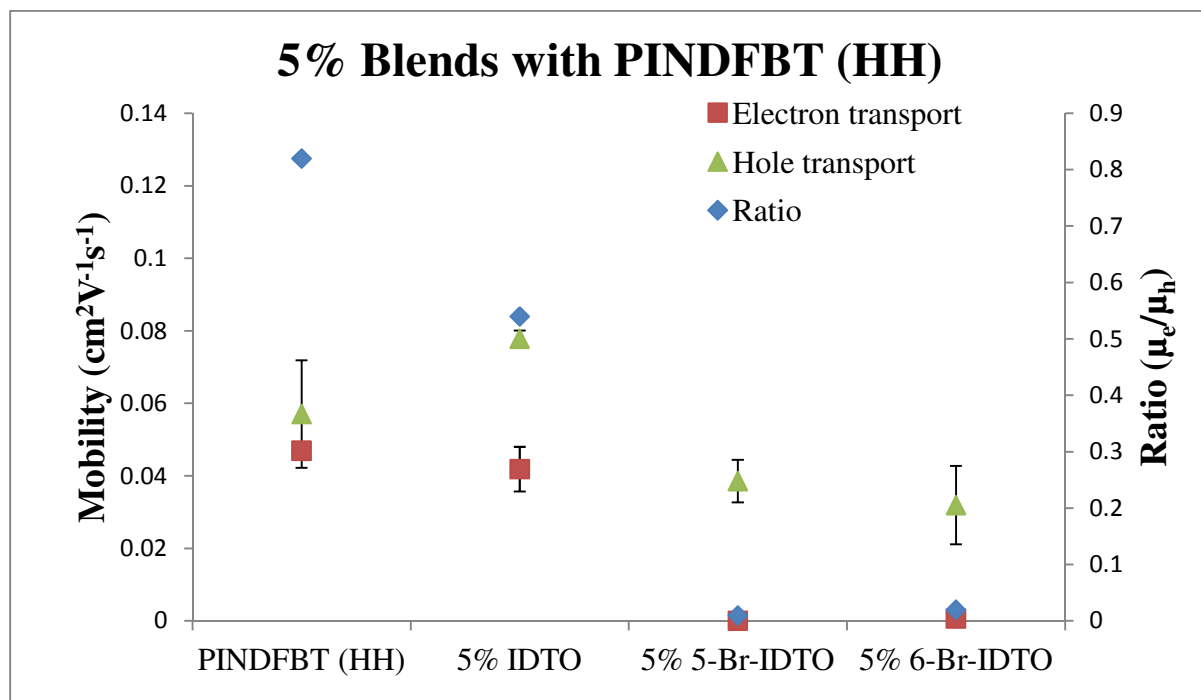


Figure D.2: Comparison of 5% blends with PINDFBT (HH).

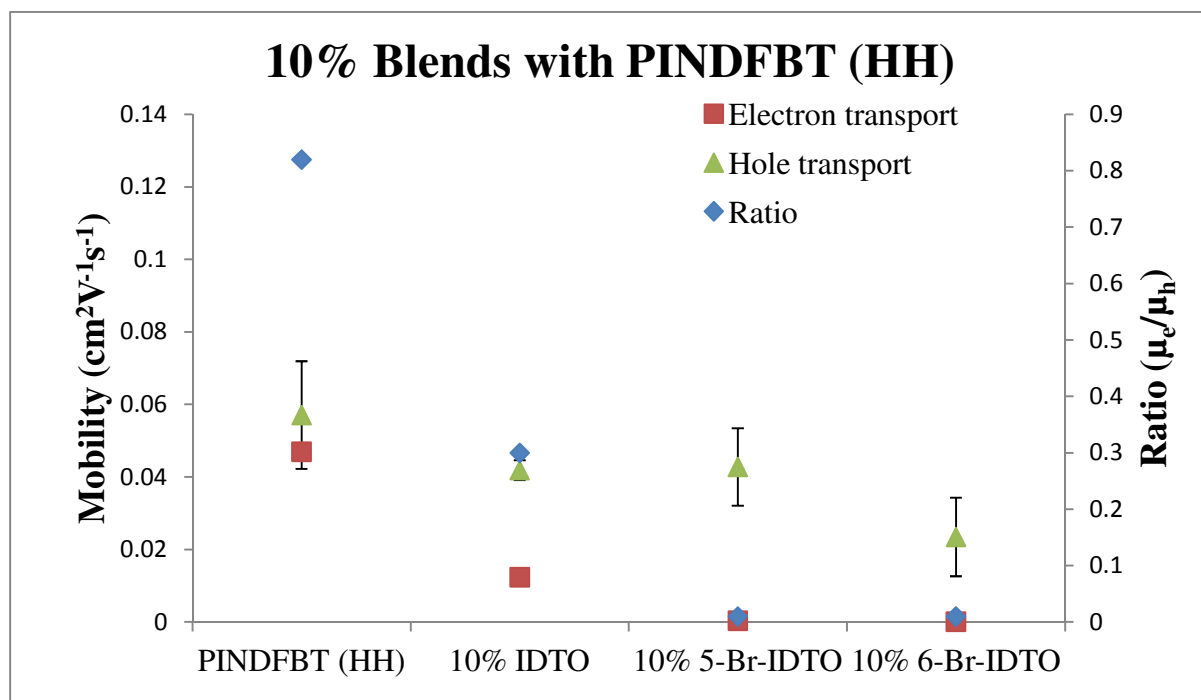


Figure D.3: Comparison of 10% blends with PINDFBT (HH).

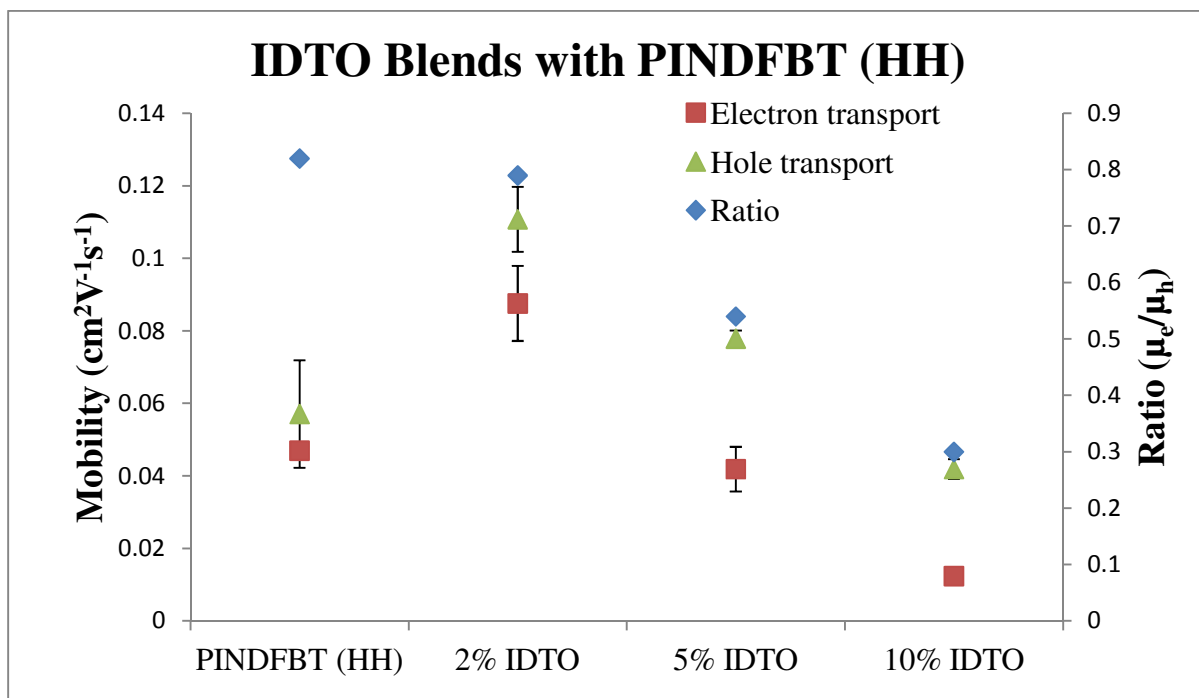


Figure D.4: Comparison of IDTO blends with PINDFBT (HH).

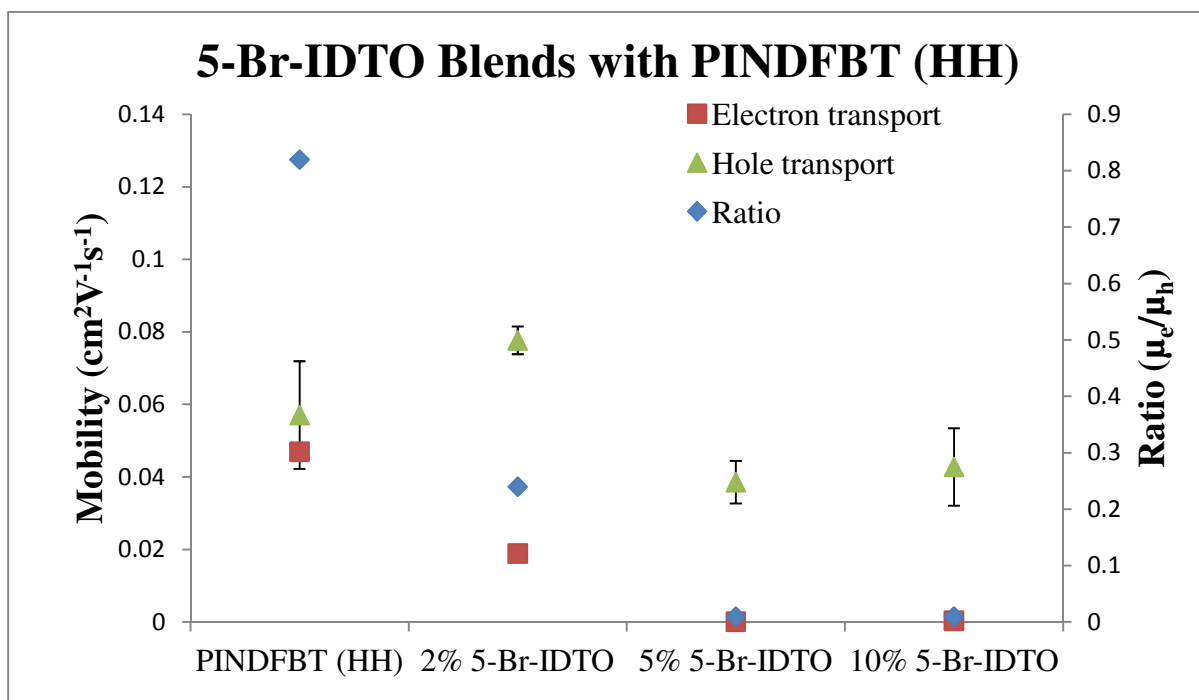
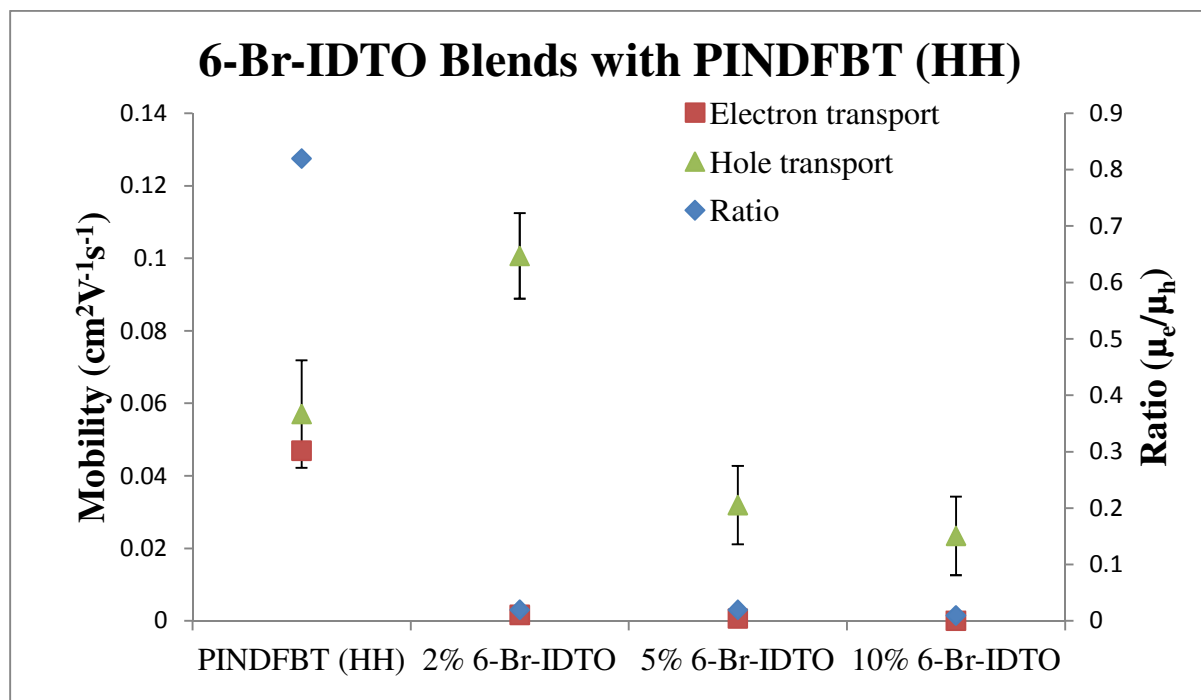


Figure D.5: Comparison of 5-Br-IDTO blends with PINDFBT (HH).



**Figure D.6: Comparison of 6-Br-IDTO blends with PINDFBT (HH).**